UNIVERSITY OF CALIFORNIA,
IRVINE

Factors Governing Information Transfer into the Primary Hippocampal Circuit

DISSERTATION

Submitted in partial satisfaction of the requirements
for the degree of

DOCTOR OF PHILOSOPHY

in Biomedical Sciences

by

Julian Quintanilla

Dissertation Committee:
Professor Gary Lynch, Chair
Professor Christine M. Gall
Associate Professor Robert Hunt
Assistant Professor Javier Diaz-Alonso

2023

DEDICATION

To my parents, grandparents,
Noel, Toby, and the
rest of my family

TABLE OF CONTENTS

LIST OF FIGURES

ACKNOWLEDGMENTS

I am very much of the belief that no one is “self-made”. With that said, several people have influenced the path I have taken to get to this position.

The culmination of my work would not be possible without the mentorship of Dr. Gary Lynch. Being mentored by a pioneer of the field has been an incredible opportunity. He has the ability to inspire scientific inquiry by describing every hypothesis and experiment with passion and enthusiasm. I always left our meetings feeling motivated and confident about the research I was conducting, a trait that is extremely appreciated within a field where the vast majority of experiments tend to fail. Furthermore, he was willing to meet with me for as much time as I needed to understand or discuss projects, meetings which admittedly had a habit of becoming history lessons.

Just as vital to my growth as a graduate student was Dr. Christine M. Gall. I would like to thank her for being an amazing mentor, giving equal praise and constructive criticism. She was always available for guidance, ranging from a brain anatomy lesson to planning a series of experiments. Thank you for challenging me and teaching me that, like a recipe, sometimes science is more of an art.

None of the work conducted here nor the work done throughout my time as a graduate student would have been possible without the help from my colleagues in the Lynch and Gall labs. Since the work that I conducted within this thesis is 90% slice electrophysiology experiments, I would like to give a special thanks to Aliza Le, my fellow cohort and graduate student colleague, as she was the person who initially taught me how to conduct the technique. She patiently answered every question I had about the process and helped with all my troubleshooting, all while conducting her own experiments. Thank you for all your help and being an amazing friend, who appreciates my many movie and television references. I would like to thank Dr. Julie Lauterborn for all her guidance in topics ranging from lab to how to navigate graduate school. I thank her for also showing me the importance of a vast vocabulary. Dr. Ben Gunn for being another amazing mentor especially with the projects that are presented here. You have brought much needed expertise into my projects and have shown me how to think about the experiments that would elevate a study, even if they result in enormous sized papers. A thank you to my fellow graduate student, Jasmine Chavez for adding a breath of rejuvenation into the lab while also being a constant reminder that life moves faster than we would like. Similarly, a thanks to Celina Yang for reminding me of the importance of the work we are conducting and that everything is “fine”. Dr. Conor Cox for always encouraging me to learn something new and fixing anything that went wrong in the lab. Dr. Brittney Cox for being instrumental in the foundation of my graduate studies. Dr. Yousheng Jia for passing on his years of electrophysiological expertise whether that be preparing, trouble shooting, or passing on superstitions/ rituals. Lucy Yao for keeping the essential day-to-day portions of the lab operating. Thanks to Ben Pruess for being an incredible collaborator and whose coding and simulation modeling experience goes above my head. Dr. Linda Palmer for troubleshooting our light-sheet microscope and being a great collaborator. Dr. Steve Mahler for being an amazing mentor, especially during the early years of my graduate school experience and being

instrumental in helping me be awarded he NSF GRFP. I also would like to thank the undergraduate students that I have had the privilege of mentoring as a graduate student Elaine Tran, Jessie Huang, Giuliana Zelaya, Amy Do Nguyen, Annie Lam, Henry Kim, Peter Vu, Tom Song.

Graduate school would not be as enjoyable as it was had it not been for the friends I made here. I would like to thank Natalie DiProspero, Elena Dominguez, Morgan Coburn, Hamsi Radhakrishnan, Caden Henningfield, Lizzy Hubbard, Taylor Nakayama, Scott Kilianski, Jess Noche, Rachael Hokenson, and Rajat Saxena. Thank you for the many distractions.

Growing up, the importance of an education was always emphasized in my household. My family provided me with every opportunity to get to this position, no matter the sacrifice and for that, I would like to thank my parents Yolanda Hilario and Ruben Quintanilla. Thank you to my brother Noel Quintanilla for the much needed study breaks; even though you are my younger brother, I hope you know I still look up to you. I would also like to thank my cousin, though more of a brother, Toby Quintanilla. I am sorry you could not see the start nor end of this journey but know that you still make me laugh when I most need it. I would also like to thank my grandparents and my extended family for always keeping me motivated to stay on this track but also ensuring to humble me on occasion. I would also like to thank my dogs throughout my life, who have always been my late night study partners: Rocks, Oso, Matley, Lizzy, Frida, and Anri. Finally, I would like to thank my partner Miki Ohata who has helped me on this journey every step of the way. I am grateful for your support during the highs and lows from undergrad to now. She is a constant source of motivation and joy in my life.

Financial Support: I thank the National Science Foundation Graduate Research Fellowship Program (GRFP) Grant No.DGE-1839285 and the Office of Naval Research (Grant No. N00014-18-1-2114 and N00014-21-1-2940) for the funding that contribute to the completion of this work.

The text from Chapter 1 is a reprint of material as it appears in Quintanilla et al., 2022, The Journal of Physiology, accessible at https://doi.org/10.1113/JP283012. The co-authors listed in this publication are Yousheng Jia, Julie C. Lauterborn, Benedict S. Pruess, Aliza A. Le, Conor D. Cox, Christine M. Gall, Gary Lynch, and Benjamin G. Gunn

The text from Chapter 2 is based on material currently under review at Science Advances. My coauthors include Yousheng Jia, Benedict S. Pruess, Christine M. Gall, Gary Lynch, and Benjamin G. Gunn

Portions of the text from Chapter 3 is based on material as it appears in Chavez et al. 2022, bioRxiv, under (CC-BY-ND 4.0) accessible at doi.org/10.1101/2022.07.29.501926. The co-authors include Jasmine Chavez, Aliza A. Le, Alex Mabou Tagne, Daniele Piomelli, Gary Lynch, and Christine M. Gall

VITA

Julian Quintanilla

Education

University of California, Irvine – 4.0 GPA — Sept. 2017- June 2023
Doctor of Philosophy, Biomedical Sciences

University of California, Irvine – 3.682 GPA — Sept. 2011- June 2015
Bachelor of Science, Neurobiology

University of Sussex, Brighton, UK — Jun. 2013- Aug. 2013
Study Abroad UCEAP Program: Physics

Current Position

Department of Anatomy and Neurobiology, University of California, Irvine — Sept. 2017-2023
Graduate Student Researcher

Past Research Experience

Department of Neurobiology and Behavior, University of California, Irvine — Jul. 2016- Sept 2017
Junior Specialist

Center for Behavioral Neuroscience, American University, Washington, D.C. — Jun. 2015- Aug. 2015
Research Assistant- Summer Intern

Beckman Laser Institute Dept. Surgery, University of California, Irvine — Jan. 2014-Jun. 2015
Research Assistant

Working Memory and Plasticity Lab, University of California- Irvine — Sept. 2014-Jun. 2015
Undergraduate researcher

Department of Ecology and Evolution- University of California, Irvine — Jan.2013- Jul. 2014
Undergraduate researcher

Publications

- **Quintanilla J**, Gunn BG, Lauterborn JC, Jia Y, Gall CM, Lynch G. Novel Types of Frequency Filtering in the Lateral Perforant Path Projections of Dentate Gyrus. J Physiol. 2022 Aug;600(16):3865-3896. doi: 10.1113/JP283012. Epub 2022 Aug 1. PMID: 35852108.
  ***Cover Image (August 2022)**
- Chavez J*, Le AA*, **Quintanilla J***, et al. Microglia Depletion Selectively Eliminates a Singular Form of Hippocampal Long-Term Potentiation. bioRxiv; 2022. DOI: 10.1101/2022.07.29.501926.
- **Quintanilla J***, Le AA*, Amani M, Piomelli D, Lynch G, Gall CM. Persistent Sexually Dimorphic Effects of Adolescent THC on Hippocampal Synaptic Plasticity and Episodic Memory in Rodents. Neurobiol Dis. 2022 Jan; 162:105565. DOI: 10.1016/j.nbd.2021.105565.
- Amani M, Lauterborn JC, Le AA, Cox BM, Wang W, **Quintanilla J**, Cox CD, Gall CM,

Lynch G. Rapid Aging in the Perforant Path Projections to the Rodent Dentate Gyrus. J. Neuroscience. 2021 Jan. DOI: 10.1523/jneurosci.2376-20.2021.

- **Quintanilla J**, Cox BM, Gall CM, Mahler SV, Lynch G. Retrograde enhancement of episodic learning by a post-learning stimulus. Learn Mem. 2021 Feb 16;28(3):82-86. doi: 10.1101/lm.052191.120. PMID: 33593926
  ***Cover Image (March 2021)**
- Santos RA, Fuertes AJC, Short G, Donohue KC, Shao H, **Quintanilla J**, Cohen-Cory S. DSCAM differentially modulates pre- and postsynaptic structural and functional central connectivity during visual system wiring. Neural Development. 2018 Sept; 13, 22. PMCID: PMC6138929
- Mahler SV, Brodnik ZD, Cox BM,... **Quintanilla J**,... Aston-Jones G. Chemogenetic Manipulations of Ventral Tegmental Area Dopamine Neurons Reveal Multifaceted Roles in Cocaine Abuse. J. Neurosci. 2018,JN-RM-0537-18

Presentations

- Quintanilla J, Gunn BG, Laughterborn JC, Le A, Gall CM, Lynch G. *Marked differences in processing across nodes of the hippocampal circuit.*
  2022 Presented as a poster at Society for Neuroscience
- Quintanilla J, Gunn BG, Laughterborn JC, Jia Y, Gall CM, Lynch G. *New rules for the transfer of information from the entorhinal cortex to hippocampus.*
  2021 UC Irvine: Department of Anatomy and Neurobiology: Progress in Neuroscience Session (*PIN*).
- Quintanilla J, Gunn BG, Laughterborn JC, Jia Y, Gall CM, Lynch G. The lateral perforant path as a low-pass filter to the dentate gyrus: substrates and LTP-related interactions.
  2021 Poster presentation at the Society for Neuroscience.
- Quintanilla J, Le AA, Amani M, Gall CG, Lynch G. *Sexually Dimorphic Effects of Adolescent THC on Long-term Potentiation in Hippocampus.*
  2021 Virtual poster presentation at Society for Neuroscience: Global Connectome
  2021 Elevator talk at UC Irvine Interdepartmental Neuroscience Program Recruitment
- Quintanilla J, Gunn BG, Lynch G. *Signal Transformation within the Hippocampus*.
  2020 Presented at UC Irvine Department of Anatomy and Neurobiology: Grad Day
- Cox BM, Quintanilla J, Le AA, Amani M, Cox CD, Gall CM, Lynch G. *Cannabinoid (THC) Exposure During Adolescence has Enduring Effects on Hippocampal Plasticity and Learning in Females.*
  2019 Presented as a poster at Society for Neuroscience: Global Connectome
- Quintanilla J, Cox BM, Le AA, Gall CM, Mahler SV, Lynch G. *Rodent Model for Flashbulb Memory*. Presented at
  2019 UC Irvine Department of Anatomy and Neurobiology: Grad Day
  2019 UC Irvine Department of Neurobiology and Behavior: Neuroblitz Session
- Quintanilla J, Cox BM, Le A, Lauterborn JC, Gall CM, Mahler SV, Lynch G (2019) *Retroactive Enhancement of Episodic Memory.* Presented at
  2019 UC Irvine: Department of Anatomy and Neurobiology: Progress in Neuroscience Session.
- Quintanilla J, Cox BM, Le A, Gall CM, Mahler SV, Lynch G. *Retroactive Enhancement of Episodic Memory Following an Environmental Cue*,
  2018 Poster session at the annual School of Medicine Graduate Student Day.
- Quintanilla J, Cox BM, Le A, Gall CM, Mahler SV, Lynch G. *Rodent Model for Flashbulb Memory*.
  2018 Presented at UC Irvine Department of Neurobiology and Behavior: Neuroblitz Session

Fellowships/ Awards/ Honors

2022 UC Irvine School of Medicine Graduate Student Travel Award
2019 National Science Foundation Graduate Research Fellowship Program (**NSF GRFP**)
2017 UC Irvine Diversity Recruitment Fellowship, University of California, Irvine.
2017 Ayala School of Biological Sciences/ School of Medicine Graduate Fellowship, University of California, Irvine.
2011-2015 Deans Honor List: 10 Academic quarters

Other Experiences

UCI Center for Neurobiology Learning and Memory Ambassador Sept. 2017- Jun. 2023
Outreach Program CNLM Ambassador

- Invited and visited local grade schools, community centers, and elderly homes to see neuroscience related demonstrations.
- Exposed underserved children to neuroscience research, scientific progress, and scientific communication.

UCI Center for Neurobiology Learning and Memory: Brain Explorer Academy Sept. 2018- Jun. 2023

- A program that is designed to foster neuroscience interest to grade school students through weekly Saturday morning meetings.
- The weekly meetings include brain anatomy lessons with real human brains, presentations on brain imaging techniques, and other neuroscience related topics; culminating in a live review presentation that is featured in the Frontiers for Young Minds Journal

California Science Center Museum, Los Angeles, CA Feb. 2016 – Oct.2016

- Welcomed and readily engaged guests, providing assistance and answering any questions they had about a variety of topics, human biology, life in ecosystems, and air and space exhibits.
- Presented guests, of all ages, with information with the goal of stimulating curiosity and inspire science learning by creating a fun and memorable experience.

Skills & Techniques

Slice electrophysiology	Optogenetics	Stereotaxic surgery (viral injections; probe implantations)	Immunohistochemistry
Confocal microscopy	Rodent behavior	Electrophysiology rig setup	GraphPad Prism

Teaching and Mentorship

Undergraduates	Year	Awards
Elaine Tran	2020-2023	UCI Summer Undergraduate Research Program (SURP), Excellence in Research
Henry Kim	2018-2019	Excellence in Research, UROP, SURP
Amy Nguyen	2019-2020	Excellence in Research
Peter Vu	2018-2021	Excellent in Research, UROP, SURP
Annie Lam	2018-2021	Excellent in Research
Kathleen Navarro	2018-2021	Excellent in Research

Huy Pham	2018-2021	Campus Honors Program
Giuliana Zelaya	2018-2021	Excellent in Research
Jeahyuk “Tom” Song	2018-2021	UROP
Lorena Torres	2018-2021	Excellent in Research
Stephanie Zhang	2019-2020	
Alex Yan (High School Volunteer	2019-2020	2nd place in Orange County Science & Engineering Fair

Relevant Course Work

University of California, Irvine- Undergraduate 2011-2015

Neurobiology & Behavior Neurobiology & Behavior
Neurobiology of Learning & Memory
Developmental Neurobiology
Functional Neuroanatomy
Neuroscience Fundamentals A, B, C
Neurobiology Laboratory
Introduction to Bio Statistics
Cellular Biology
Molecular Biology

University of California, Irvine- Graduate 2017- 2023

Foundations Neuroscience A, B, C
Systems Neuroscience
Molecular Neuroscience
Cellular Neuroscience
Cellular Neuroscience Lab
Behavioral Neuroscience
Statistics Neurobiology
Current Topics in Neuroscience
Programming for Neuroscience Research
Neural Coding, Computation, and Dynamics

ABSTRACT OF THE DISSERTATION

Substrates that Govern the Transfer of Information into the Hippocampal Circuit

By

Julian Quintanilla

Doctor of Philosophy in Biomedical Sciences

University of California, Irvine, 2023

Professor Gary Lynch, Chair

The hippocampus is critical for the acquisition and retrieval of episodic memory. Sensory information from cortical regions is conveyed to the hippocampus primarily via the lateral and medial perforant path (LPP, MPP) projections originating in the lateral and medial entorhinal cortex (LEC, MEC) respectively. The LPP projection has been shown to be involved in the transfer of information regarding cue identity, while the MPP conveys spatial information (Hargreaves et al., 2005; Reagh and Yassa, 2014). Within the hippocampus, the LPP sends its projections to both the dentate gyrus (DG) and field CA3 with evidence suggesting that these terminals can be extensions from the same axon (Yeckel and Berger, 1990; Tamamaki and Nojyo, 1993). However, comparisons between the two LPP branches, with regard to their release dynamics and synaptic plasticity mechanisms, are scarce and will thus be the focus of this dissertation.

The manner in which the two LPP branches transform (i.e., amplify, filter) incoming signals to the hippocampus at behaviorally- relevant frequencies and patterns is relatively unknown. Multiple factors regulate frequency-dependent signal transformations (e.g. vesicle release dynamics) that can result in markedly different responses to similar inputs within the same network (Trieu et al., 2015). *Chapter 1* characterizes the signal transformations at the

LPP-DG branch located at the head-stage of the circuit. These studies demonstrate that the LPP-DG synapse operates as a low-pass filter, where responses to repetitive activation at ≥50 Hz (i.e., γ–frequency) display within-train suppression. This operation appears to be governed by factors located in the presynaptic terminal associated with release probability and vesicle recycling. Indeed, the induction of a unique form of presynaptic long-term potentiation (LTP) at LPP-DG terminals increases the release probability and, as a result, enhances the low-pass filtering at this terminal.

Given that the two LPP branches originate from the same axon, it would appear plausible that the unique release dynamics and LTP mechanisms evident at the LPP-DG terminal are also present at those synapses innervating CA3 pyramidal cells. However, as described in *Chapter 2*, recordings from the distal apical dendrites of field CA3 reveal that responses to repetitive stimulation are radically different than those seen in the DG. Within this node, 50 Hz frequency stimulation results in a frequency following as opposed to a depression, with lower frequencies acting similarly. These differences in frequency facilitation at the two LPP terminals suggest distinctions in vesicle release and recycling at the two sites. Furthermore, while LTP is expressed at presynaptic sites at the LPP-DG synapse, a postsynaptic variant of LTP that does not require endocannabinoid signaling is evident at LPP-CA3 terminals. These observations support a target-cell specification hypothesis for the production of LTP variants and suggest the preferential routing to, and encoding by, CA3.

Finally, to emphasize the mechanistic differences in plasticity at these two terminals, a separate study, presented in *Chapter 3* was conducted in which the effects that microglia had on LTP was assessed. Removal of microglia with the Colony Stimulating Factor-1 antagonist, PLX5622, had no effects on baseline synaptic responses at either LPP termination site (i.e., LPP-DG or LPP-CA3). However, when LTP was evaluated, mice that underwent PLX treatment had severe impairments at LPP-DG but not LPP-CA3 synapses. Although, the levels of the

endocannabinoid, 2-AG, were elevated four-fold in the DG, the prevention of its breakdown fully restored LTP at these synapses. These results demonstrate that disruption of endocannabinoid signaling following microglia loss impairs LPP-DG LTP with no effect upon plasticity at LPP-CA3 terminals.

INTRODUCTION

The hippocampus as a neuronal network.

As humans traverse through their daily environment, they process an immeasurable amount of information about the context around them. The type of unsupervised learning that characterizes everyday life leads to the formation of episodic memories (the "what"," where", and "when" of an experience) and since the groundbreaking case of patient H.M., the hippocampus has been a central focus due to this regions role in episodic memory formation (Scoville & Milner, 1957; Tulving *et al.*, 1972; Tulving, 1983). Several studies have shown that the hippocampus is necessary for the formation of episodic memories in humans (Nadel *et al.*, 2000; Rosenbaum *et al.*, 2000; Westmacott *et al.*, 2001; Burgess *et al.*, 2002; Dede *et al.*, 2016), and animal (O'Keefe & Nadel, 1978; Morris *et al.*, 1986; Moser *et al.*, 1993; Fortin *et al.*, 2004; McHugh *et al.*, 2007) studies have shown impairments in memory tasks through manipulation of hippocampal circuits.

At its core, the trisynaptic circuit consists of the DG, CA3, and CA1; however, the information transfer between these fields is complicated by their local connections and innate firing properties. The entorhinal cortex is the primary input into the DG through its afferents, the LPP and medial (MPP) perforant path (Witter, 1993). The LPP arising from layer II of the lateral entorhinal cortex (LEC) terminates in the outer molecular layer of the DG while the MPP, arises from the medial entorhinal cortex (MEC) and terminates in the middle third of the molecular layer (Hjorth-Simonsen, 1972; Steward,

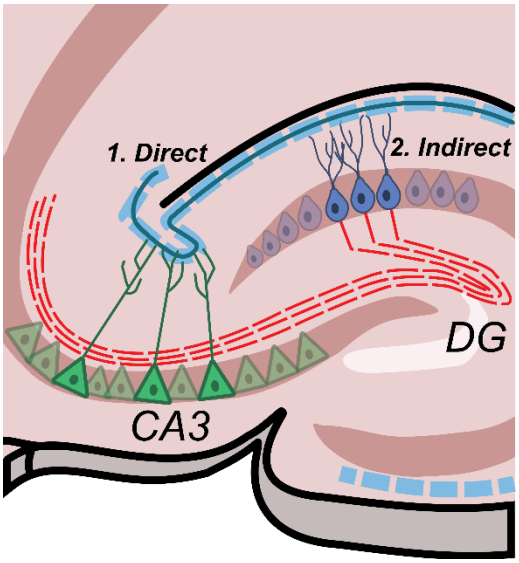

Figure 1. Schematic of the direct and indirect pathway to CA3. The lateral perforant path (blue) *directly* project to the distal end of (stratum lacunosum moleculare (1). Additionally, the lateral perforant path projects to the granule cells of DG within the outer molecular layer. Granule cells then send their mossy fiber projections (red dotted line) to the proximal end of CA3, providing an *indirect* projection from the lateral perforant path to CA3 (2).

1976; Dolorfo & Amaral, 1998). Granule cells of the DG send their sole output, the peculiar mossy fibers, to the proximal portions of the dendrites of CA3 pyramidal cells, where they form massive boutons. However, at the distal end of the apical dendrites of CA3 (stratum lacunosum moleculare), both components of the perforant path extend beyond the DG to innervate CA3 (Tamamaki & Nojyo, 1993; Witter, 1993). Although the LPP provides a much weaker influence over CA3, compared to mossy fibers, they nevertheless have been shown to induce CA3 firing (Yeckel & Berger, 1990; Berzhanskaya *et al.*, 1998; McMahon & Barrionuevo, 2002). Thus, field CA3 receives both a direct (monosynaptic; LPP-CA3) and indirect (disynaptic; LPP-DG-CA3) projection from the entorhinal cortex (Amaral *et al.*, 1990; Amaral, 1993). Functions for these parallel pathways have been proposed. In particular, work with computational models has given rise to the hypothesis that direct projections carry sensory information that serves to initiate the retrieval/recall of memories that were once established through the indirect projection (Treves & Rolls, 1992; Lee & Kesner, 2004). Projections arising from the CA3 pyramidal cells terminate in the stratum radiatum layer of both field CA1, referred to as the S-C projections, and CA3. The CA3-CA3 commissural/associational (C/A) system provides both positive feedback both onto itself and onto contralateral CA3. Field CA1 then sends a 'cascading' connection (a direct and indirect through the subicular complex) to the entorhinal cortex. Thus, the hippocampal circuit can be thought of as a loop, with the DG and CA1/subiculum acting as entry and exit points, respectively.

The elegance in the anatomical organization of the hippocampus makes it an ideal location for electrophysiological recordings. The density of cells within each subregion, alignment of dendritic arbors, and lamination of principal afferents allows for optimal recording of local field potentials (LFPs) and synchronized activity from a group of neurons (Freund & Buzsaki, 1996; Lein *et al.*, 2011). Based on studies conducted in human and animal models, the entorhinal cortex and its major output target, the hippocampus, is characterized by rhythmic oscillations with specific frequencies, during different behaviors, in the range of theta (5-10Hz),

beta (20-40Hz), and gamma (≥40Hz). It is thus not surprising that these frequencies have been correlated with learning behaviors, such as exploration of a novel environment or odor (Bragin *et al.*, 1995; Martin *et al.*, 2007; Colgin *et al.*, 2009; Igarashi *et al.*, 2014; Colgin, 2015, 2016). Responses to trains of stimuli aligned with these frequencies typically give rise to frequency facilitation, as first described within the NMJ (Eccles *et al.*, 1941), and more recently in the mossy fibers (Nicoll & Schmitz, 2005; Trieu *et al.*, 2015) and the S-C projections from CA3 to CA1 (Trieu *et al.*, 2015; Jackman & Regehr, 2017; Amani *et al.*, 2021). Nevertheless, we have identified different responses within the LPP connections to the DG. At lower frequencies (5- 40 Hz), responses tend to facilitate briefly but fall back down to near baseline levels. With stimulation in the low gamma range (50Hz) there is a brief facilitation that is followed by a rapid depression in response (Wang *et al.*, 2018b; Amani *et al.*, 2021). The synaptic mechanisms, such as those initially investigated within the NMJ (i.e., release probability, vesicle recycling, etc.), that are responsible for this unusual low-pass filtering at LPP-DG will be the focus of *Chapter 1*.

This aberrant response profile raises the question as to how higher frequency activity, as is typical for output of the entorhinal cortex, is transferred across the DG node and through the hippocampal network. One conceivable explanation is that the direct pathway to CA3, processes high frequency inputs differently. If there are differences in the response to inputs between the indirect and direct projections to CA3, then depending on the frequency of an incoming signal, the hippocampus may use different subnetworks (direct projections used during high frequency stimulation; indirect projections used during low frequency stimulation). This notion will be further explored in *Chapter 2*.

Understanding the mechanisms and optimal frequencies at which each subregion operates may prove to be essential for understanding the network dynamics of hippocampus and is vital in constructing representative models of hippocampal circuit function. In other words, how does a specific sensory signal that enters the circuit from the entorhinal cortex transform as

it traverses each circuit node and how the full circuit transforms the input signal to generate the output of the hippocampal network.

Long-term synaptic plasticity within the lateral perforant path projections to hippocampus.

As previously mentioned, the LEC (layer II) sends projections to not only the DG, but also CA3 via the LPP (Hjorth-Simonsen, 1972; Steward, 1976). Recently, the LPP has been shown to transfer information about cue identity into the DG, while MPP projections from the MEC transfer information about spatial location (Suzuki *et al.*, 1997; Knierim *et al.*, 2014; Reagh & Yassa, 2014; Cox *et al.*, 2019). Early physiological studies assumed that the perforant path, including the LPP and the MPP, were part of a homogeneous structure. It was not until 1980 that physiological differences between the two pathways were observed (McNaughton, 1980). The LPP and MPP express paired pulse facilitation (PPF) and paired pulse depression (PPD), respectively. These variations in short-term dynamics were due to differences in the initial release probability wherein the LPP expresses a low release probability and the MPP expresses a high release probability (McNaughton, 1980, 1982). Additionally, in 1994 Brian Christie and Wycliffe Abraham found changes in these short-term plasticity mechanisms in response to earlier activity. A decrease in the PPF at LPP-DG synapses was found 30 min after long-term potentiation (LTP) induction, going from ~40% to ~20% facilitation (Christie & Abraham, 1994). These findings suggested that LTP changed the probability of release within the LPP, because a decrease within the PPF would indicate increases in initial transmitter release. These experiments were among the first to identify highly unusual mechanisms at the LPP-DG synapse and raised questions as to how LTP, that was thought to be expressed postsynaptically, could influence short-term presynaptic dynamics.

At LPP-DG synapses, the mechanisms of LTP have only recently been found to differ significantly from all other brain regions thus far evaluated. Briefly, at these synapses high frequency activity leads to activation of post-synaptic NMDARs and mGluR5s, and the

associated increase in post-synaptic calcium triggers the production of the endocannabinoid, 2-arachindonoyl-sn-glycerol (2-AG), through activation of DGL-α (Jung *et al.*, 2005; Jung *et al.*, 2007; Jung *et al.*, 2012). 2-AG acts as a retrograde signal, traversing back across the synaptic junction to bind presynaptic CB_1 receptors. Then, in distinction from other CNS synapses that have been studied (Castillo *et al.*, 2012), the receptors work cooperatively with presynaptic integrins to elicit signaling to the presynaptic actin cytoskeleton leading to a CB_1-, integrin-, and f-actin-dependent increase in glutamate release (Wang *et al.*, 2018b). Thus, at LPP-DG synapses, initiation of LTP occurs post-synaptically through NMDA receptor activation but expression of LTP occurs presynaptically, through an increase in neurotransmitter release (Wang *et al.*, 2016; Wang *et al.*, 2018b). Thus, the studies conducted by Christie and Abraham nearly two and a half decades prior are retrospectively unsurprising given the context of the experiments conducted above. They found decreases in PPF (Christie & Abraham, 1994) because presynaptic modifications, associated with LTP, increased *p* and thus exaggerated the filtering of frequencies mentioned above.

Although evidence suggests that the direct and indirect pathways work in conjunction, in comparison to the more frequently studied indirect pathway, studies directed at understanding the plasticity mechanisms within the direct LPP projections to field CA3 are largely absent. Specifically, the LTP mechanisms remain largely unknown for the direct pathway. For these synapses, the role of NMDA receptors in LTP initiation is still debated. Findings of NMDA receptor independent LTP in the mossy fiber projections to CA3 (Harris & Cotman, 1986) inspired studies of the LPP-CA3 connections. These studies, conducted in the early 1990s, observed a dependence on NMDAR activation(Barrionuevo & Brown, 1983; Yeckel & Berger, 1990; Zalutsky & Nicoll, 1990; McMahon & Barrionuevo, 2002). However, other work gave rise to the opposite results which paralleled the NMDAR independence observed for the mossy fibers (Do *et al.*, 2002). Proposed explanations for these discrepancies are that the studies differentially involved a contribution of both perforant path systems (medial and lateral) as these

are in close proximity and reportedly express different forms of short (McNaughton, 1980, 1982; Christie & Abraham, 1994) and long term plasticity (Wang *et al.*, 2016; Wang *et al.*, 2018b). Of relevance are reports that LPP-CA3 LTP within this pathway can be modified by activity of the C/A- CA3 system (Do *et al.*, 2002). Specifically, tetanization of the C/A system was found to produce a robust potentiation at LPP-CA3 synapses when paired with weak stimulation of the LPP-CA3 pathway. Recent work within the Lynch lab has shown that patterns of activity in the C/A system can be modified by stimulation of the mossy fiber projections resulting in reverberating C/A activity lasting several minutes (Cox *et al.*, 2019). Thus, it is possible that something like reverberating C/A activity could cause an additional depolarization of the CA3 pyramidal cells and facilitate the induction of LTP at LPP-CA3 synapses. Still, the location of LTP expression at the LPP-CA3 synapses has yet to be resolved. Given the unique form of LTP at LPP-DG synapses and evidence that single LPP axons form connections with dendrites of both the DG granule cells and CA3 pyramidal cells (Tamamaki & Nojyo, 1993), it is surprising that the expression has not been characterized. Using slice electrophysiology and pharmacological approaches, we will characterize the loci of LTP expression within *Chapter 2*.

Influencing endocannabinoid signaling within the lateral perforant path.

The dependence of LPP-DG LTP on endocannabinoid signaling may allow for unintended disruptions within DG with no effects on other hippocampal subregions. For example, in Fragile-X mice (FMR1 KO), LPP-DG LTP was disrupted to near baseline levels compared to their control counterparts (Wang *et al.*, 2018a). This deficit was likely due to issues in 2-AG signaling since manipulation that either increased production of 2-AG, slowed the breakdown of 2-AG, or directly stimulated target receptors (CB_1R), effectively increased potentiation to baseline levels. Furthermore, these FMR1 KO mice also had an associated impairment on their performance on episodic memory tasks that are dependent on LPP-LTP (Wang *et al.*, 2018a). A more recent instance looked at the effects that adolescent Δ9-

tetrahydrocannabinol (THC) exposure had on hippocampal LTP, specifically at S-C terminals of CA1 and the LPP-DG projection (Le *et al.*, 2022). No effects were found on baseline transmission at either of the two sites nor in the frequency facilitation profiles when compared to control animals. Instead, THC caused a depletion in LTP stabilization at LPP-DG synapses while CA1 LTP was unaffected (Le *et al.*, 2022). One would infer that endocannabinoid levels, specifically 2-AG, or CB_1 receptor levels were altered as a result of this exposure, but no lasting effects of either have been reported (Rubino *et al.*, 2008; Rubino *et al.*, 2015; Silva *et al.*, 2015; Bara *et al.*, 2021). One potential mechanism that THC exposure influenced was the endocannabinoid signaling within microglia. In particular, microglia transcription of the 2-AG degrading enzyme, MGL, was suppressed. Such manipulations to endocannabinoid signaling have been reported to influence LPP-DG LTP (Wang *et al.*, 2018a). As a result, THC may be influencing LPP-DG LTP through the dysregulation of microglia endocannabinoid signaling. Because there have also been reports of differences in microglia density across the hippocampal subregions, in particular very few in *stratum lacunosum-moleculare* of CA3 compared to DG, and the most expressed in CA1, the degree to which microglia influence plasticity in each of these regions would be of interest (Jinno *et al.*, 2007; Choi & Won, 2011). Thus, in *Chapter 3*, by using slice hippocampal physiology from microglial deleted mice, we will investigate the role, if any, microglia have on synaptic plasticity across each node of the hippocampal circuit.

References

Amani M, Lauterborn JC, Le AA, Cox BM, Wang W, Quintanilla J, Cox CD, Gall CM & Lynch G. (2021). Rapid Aging in the Perforant Path Projections to the Rodent Dentate Gyrus. *J Neurosci* **41,** 2301-2312.

Amaral DG. (1993). Emerging principles of intrinsic hippocampal organization. *Curr Opin Neurobiol* **3,** 225-229.

Amaral DG, Ishizuka N & Claiborne B. (1990). Neurons, numbers and the hippocampal network. *Prog Brain Res* **83,** 1-11.

Bara A, Ferland JN, Rompala G, Szutorisz H & Hurd YL. (2021). Cannabis and synaptic reprogramming of the developing brain. *Nat Rev Neurosci* **22,** 423-438.

Barrionuevo G & Brown TH. (1983). Associative long-term potentiation in hippocampal slices. *Proc Natl Acad Sci U S A* **80,** 7347-7351.

Berzhanskaya J, Urban NN & Barrionuevo G. (1998). Electrophysiological and pharmacological characterization of the direct perforant path input to hippocampal area CA3. *J Neurophysiol* **79,** 2111-2118.

Bragin A, Jando G, Nadasdy Z, Hetke J, Wise K & Buzsaki G. (1995). Gamma (40-100 Hz) oscillation in the hippocampus of the behaving rat. *J Neurosci* **15,** 47-60.

Burgess N, Maguire EA & O'Keefe J. (2002). The human hippocampus and spatial and episodic memory. *Neuron* **35,** 625-641.

Castillo PE, Younts TJ, Chavez AE & Hashimotodani Y. (2012). Endocannabinoid signaling and synaptic function. *Neuron* **76,** 70-81.

Choi JH & Won MH. (2011). Microglia in the normally aged hippocampus. *Lab Anim Res* **27,** 181-187.

Christie BR & Abraham WC. (1994). Differential regulation of paired-pulse plasticity following LTP in the dentate gyrus. *Neuroreport* **5,** 385-388.

Colgin LL. (2015). Theta-gamma coupling in the entorhinal-hippocampal system. *Curr Opin Neurobiol* **31,** 45-50.

Colgin LL. (2016). Rhythms of the hippocampal network. *Nat Rev Neurosci* **17,** 239-249.

Colgin LL, Denninger T, Fyhn M, Hafting T, Bonnevie T, Jensen O, Moser MB & Moser EI. (2009). Frequency of gamma oscillations routes flow of information in the hippocampus. *Nature* **462,** 353-357.

Cox BM, Cox CD, Gunn BG, Le AA, Inshishian VC, Gall CM & Lynch G. (2019). Acquisition of temporal order requires an intact CA3 commissural/associational (C/A) feedback system in mice. *Commun Biol* **2,** 251.

Dede AJ, Frascino JC, Wixted JT & Squire LR. (2016). Learning and remembering real-world events after medial temporal lobe damage. *Proc Natl Acad Sci U S A* **113,** 13480-13485.

Do VH, Martinez CO, Martinez JL, Jr. & Derrick BE. (2002). Long-term potentiation in direct perforant path projections to the hippocampal CA3 region in vivo. *J Neurophysiol* **87,** 669-678.

Dolorfo CL & Amaral DG. (1998). Entorhinal cortex of the rat: topographic organization of the cells of origin of the perforant path projection to the dentate gyrus. *J Comp Neurol* **398,** 25-48.

Eccles JC, Katz B & Kuffler SW. (1941). Nature of the "endplate potential" in curarized muscle. *Journal of Neurophysiology* **4,** 362-387.

Fortin NJ, Wright SP & Eichenbaum H. (2004). Recollection-like memory retrieval in rats is dependent on the hippocampus. *Nature* **431,** 188-191.

Freund TF & Buzsaki G. (1996). Interneurons of the hippocampus. *Hippocampus* **6,** 347-470.

Harris EW & Cotman CW. (1986). Long-term potentiation of guinea pig mossy fiber responses is not blocked by N-methyl D-aspartate antagonists. *Neurosci Lett* **70,** 132-137.

Hjorth-Simonsen A. (1972). Projection of the lateral part of the entorhinal area to the hippocampus and fascia dentata. *J Comp Neurol* **146,** 219-232.

Igarashi KM, Ito HT, Moser EI & Moser MB. (2014). Functional diversity along the transverse axis of hippocampal area CA1. *FEBS Lett* **588,** 2470-2476.

Jackman SL & Regehr WG. (2017). The Mechanisms and Functions of Synaptic Facilitation. *Neuron* **94,** 447-464.

Jinno S, Fleischer F, Eckel S, Schmidt V & Kosaka T. (2007). Spatial arrangement of microglia in the mouse hippocampus: a stereological study in comparison with astrocytes. *Glia* **55,** 1334-1347.

Jung KM, Astarita G, Zhu C, Wallace M, Mackie K & Piomelli D. (2007). A key role for diacylglycerol lipase-alpha in metabotropic glutamate receptor-dependent endocannabinoid mobilization. *Mol Pharmacol* **72,** 612-621.

Jung KM, Mangieri R, Stapleton C, Kim J, Fegley D, Wallace M, Mackie K & Piomelli D. (2005). Stimulation of endocannabinoid formation in brain slice cultures through activation of group I metabotropic glutamate receptors. *Mol Pharmacol* **68,** 1196-1202.

Jung KM, Sepers M, Henstridge CM, Lassalle O, Neuhofer D, Martin H, Ginger M, Frick A, DiPatrizio NV, Mackie K, Katona I, Piomelli D & Manzoni OJ. (2012). Uncoupling of the endocannabinoid signalling complex in a mouse model of fragile X syndrome. *Nat Commun* **3,** 1080.

Knierim JJ, Neunuebel JP & Deshmukh SS. (2014). Functional correlates of the lateral and medial entorhinal cortex: objects, path integration and local-global reference frames. *Philos Trans R Soc Lond B Biol Sci* **369,** 20130369.

Le AA, Quintanilla J, Amani M, Piomelli D, Lynch G & Gall CM. (2022). Persistent sexually dimorphic effects of adolescent THC exposure on hippocampal synaptic plasticity and episodic memory in rodents. *Neurobiol Dis* **162,** 105565.

Lee I & Kesner RP. (2004). Encoding versus retrieval of spatial memory: double dissociation between the dentate gyrus and the perforant path inputs into CA3 in the dorsal hippocampus. *Hippocampus* **14,** 66-76.

Lein PJ, Barnhart CD & Pessah IN. (2011). Acute hippocampal slice preparation and hippocampal slice cultures. *Methods Mol Biol* **758,** 115-134.

Martin C, Beshel J & Kay LM. (2007). An olfacto-hippocampal network is dynamically involved in odor-discrimination learning. *J Neurophysiol* **98,** 2196-2205.

McHugh TJ, Jones MW, Quinn JJ, Balthasar N, Coppari R, Elmquist JK, Lowell BB, Fanselow MS, Wilson MA & Tonegawa S. (2007). Dentate gyrus NMDA receptors mediate rapid pattern separation in the hippocampal network. *Science* **317,** 94-99.

McMahon DB & Barrionuevo G. (2002). Short- and long-term plasticity of the perforant path synapse in hippocampal area CA3. *J Neurophysiol* **88,** 528-533.

McNaughton BL. (1980). Evidence for two physiologically distinct perforant pathways to the fascia dentata. *Brain Res* **199,** 1-19.

McNaughton BL. (1982). Long-term synaptic enhancement and short-term potentiation in rat fascia dentata act through different mechanisms. *J Physiol* **324,** 249-262.

Morris RG, Anderson E, Lynch GS & Baudry M. (1986). Selective impairment of learning and blockade of long-term potentiation by an N-methyl-D-aspartate receptor antagonist, AP5. *Nature* **319,** 774-776.

Moser E, Moser MB & Andersen P. (1993). Spatial learning impairment parallels the magnitude of dorsal hippocampal lesions, but is hardly present following ventral lesions. *J Neurosci* **13,** 3916-3925.

Nadel L, Samsonovich A, Ryan L & Moscovitch M. (2000). Multiple trace theory of human memory: computational, neuroimaging, and neuropsychological results. *Hippocampus* **10,** 352-368.

Nicoll RA & Schmitz D. (2005). Synaptic plasticity at hippocampal mossy fibre synapses. *Nat Rev Neurosci* **6,** 863-876.

O'Keefe J & Nadel L. (1978). *The hippocampus as a cognitive map*. Clarendon Press; Oxford University Press, Oxford, New York.

Reagh ZM & Yassa MA. (2014). Object and spatial mnemonic interference differentially engage lateral and medial entorhinal cortex in humans. *Proc Natl Acad Sci U S A* **111,** E4264-4273.

Rosenbaum RS, Priselac S, Kohler S, Black SE, Gao F, Nadel L & Moscovitch M. (2000). Remote spatial memory in an amnesic person with extensive bilateral hippocampal lesions. *Nat Neurosci* **3,** 1044-1048.

Rubino T, Prini P, Piscitelli F, Zamberletti E, Trusel M, Melis M, Sagheddu C, Ligresti A, Tonini R, Di Marzo V & Parolaro D. (2015). Adolescent exposure to THC in female rats disrupts developmental changes in the prefrontal cortex. *Neurobiol Dis* **73,** 60-69.

Rubino T, Vigano D, Realini N, Guidali C, Braida D, Capurro V, Castiglioni C, Cherubino F, Romualdi P, Candeletti S, Sala M & Parolaro D. (2008). Chronic delta 9-tetrahydrocannabinol during adolescence provokes sex-dependent changes in the emotional profile in adult rats: behavioral and biochemical correlates. *Neuropsychopharmacology* **33,** 2760-2771.

Scoville WB & Milner B. (1957). Loss of recent memory after bilateral hippocampal lesions. *J Neurol Neurosurg Psychiatry* **20,** 11-21.

Silva L, Harte-Hargrove L, Izenwasser S, Frank A, Wade D & Dow-Edwards D. (2015). Sex-specific alterations in hippocampal cannabinoid 1 receptor expression following adolescent delta-9-tetrahydrocannabinol treatment in the rat. *Neurosci Lett* **602,** 89-94.

Steward O. (1976). Topographic organization of the projections from the entorhinal area to the hippocampal formation of the rat. *J Comp Neurol* **167,** 285-314.

Suzuki WA, Miller EK & Desimone R. (1997). Object and place memory in the macaque entorhinal cortex. *J Neurophysiol* **78,** 1062-1081.

Tamamaki N & Nojyo Y. (1993). Projection of the entorhinal layer II neurons in the rat as revealed by intracellular pressure-injection of neurobiotin. *Hippocampus* **3,** 471-480.

Treves A & Rolls ET. (1992). Computational constraints suggest the need for two distinct input systems to the hippocampal CA3 network. *Hippocampus* **2,** 189-199.

Trieu BH, Kramar EA, Cox CD, Jia Y, Wang W, Gall CM & Lynch G. (2015). Pronounced differences in signal processing and synaptic plasticity between piriform-hippocampal network stages: a prominent role for adenosine. *J Physiol* **593,** 2889-2907.

Tulving E. (1983). *Elements of episodic memory*. Clarendon Press; Oxford University Press, Oxford Oxfordshire, New York.

Tulving E, Donaldson W, Bower GH & United States. Office of Naval Research. (1972). *Organization of memory*. Academic Press, New York,.

Wang W, Cox BM, Jia Y, Le AA, Cox CD, Jung KM, Hou B, Piomelli D, Gall CM & Lynch G. (2018a). Treating a novel plasticity defect rescues episodic memory in Fragile X model mice. *Mol Psychiatry* **23,** 1798-1806.

Wang W, Jia Y, Pham DT, Palmer LC, Jung KM, Cox CD, Rumbaugh G, Piomelli D, Gall CM & Lynch G. (2018b). Atypical Endocannabinoid Signaling Initiates a New Form of Memory-Related Plasticity at a Cortical Input to Hippocampus. *Cereb Cortex* **28,** 2253-2266.

Wang W, Trieu BH, Palmer LC, Jia Y, Pham DT, Jung KM, Karsten CA, Merrill CB, Mackie K, Gall CM, Piomelli D & Lynch G. (2016). A Primary Cortical Input to Hippocampus Expresses a Pathway-Specific and Endocannabinoid-Dependent Form of Long-Term Potentiation. *Eneuro* **3**.

Westmacott R, Leach L, Freedman M & Moscovitch M. (2001). Different patterns of autobiographical memory loss in semantic dementia and medial temporal lobe amnesia: a challenge to consolidation theory. *Neurocase* **7,** 37-55.

Witter MP. (1993). Organization of the entorhinal-hippocampal system: a review of current anatomical data. *Hippocampus* **3 Spec No,** 33-44.

Yeckel MF & Berger TW. (1990). Feedforward excitation of the hippocampus by afferents from the entorhinal cortex: redefinition of the role of the trisynaptic pathway. *Proc Natl Acad Sci U S A* **87,** 5832-5836.

Zalutsky RA & Nicoll RA. (1990). Comparison of two forms of long-term potentiation in single hippocampal neurons. *Science* **248,** 1619-1624.

CHAPTER 1: Novel Types of Frequency Filtering in the Lateral Perforant Path Projections to Dentate Gyrus

Summary

Despite its evident importance to learning theory and models, the manner in which the lateral perforant path (LPP) transforms signals from entorhinal cortex to hippocampus is not well understood. The present studies measured synaptic responses in the dentate gyrus (DG) of adult mouse hippocampal slices during different patterns of LPP stimulation. Theta (5Hz) stimulation produced a modest within-train facilitation that was markedly enhanced at the level of DG output. Gamma (50Hz) activation resulted in a singular pattern with initial synaptic facilitation being followed by a progressively greater depression. DG output was absent after only two pulses. Reducing release probability with low extracellular calcium instated frequency facilitation to gamma stimulation while long-term potentiation (LTP), which increases release by LPP terminals, enhanced within-train depression. Relatedly, per terminal concentrations of VGLUT2, a vesicular glutamate transporter associated with high release probability, were much greater in the LPP than in CA3-CA1 connections. Attempts to circumvent the potent gamma filter using a series of short (3-pulse) 50 Hz trains spaced by 200msec were only partially successful: composite responses were substantially reduced after the first burst, an effect opposite that recorded in field CA1. The interaction between bursts was surprisingly persistent (> 1.0 second). Low calcium improved throughput during theta/gamma activation but buffering of postsynaptic calcium did not. In all, presynaptic specializations relating to release probability produce an unusual but potent type of frequency filtering in the LPP. Patterned burst input engages a different type of filter with substrates that are also likely to be located presynaptically.

Introduction

The lateral perforant path (LPP), which arises in the superficial layers of lateral entorhinal cortex, is the principal conduit through which the hippocampus receives information about cue identity (Witter, 1993; Hargreaves *et al.*, 2005; Yoganarasimha *et al.*, 2011; Tsao *et al.*, 2013; Reagh & Yassa, 2014). Accordingly, the manner in which the synaptic connections formed by the projection transform (i.e., amplify, filter) incoming signals is of considerable importance for the construction of hippocampal theories and models. The entorhinal cortex-hippocampal system, along with other sites in the cortical telencephalon, typically operates at three rhythms – Θ (5Hz), β (20Hz), and γ (>40Hz) -- during behavior. Interleaving of Θ and γ rhythms, resulting in 'Θγ' bursts, is a prominent feature of local field potentials and cell spiking during learning (Bragin *et al.*, 1995; Chrobak & Buzsaki, 1998; Chrobak *et al.*, 2000; Jensen & Colgin, 2007; Colgin *et al.*, 2009; Tort *et al.*, 2009; Colgin, 2015). Signal transformation thus involves the production of enhanced or depressed responses to repetitive inputs arriving at these frequencies or patterns. Such operations are known from work at diverse sites in the brain to require rapid adjustments on both sides of the synapse but how they interact to produce LPP filtering is not clear.

Evidence for presynaptic modifications during repetitive stimulation was first obtained in the peripheral nervous system with the demonstration that facilitation or suppression of the second response of closely paired stimuli is dependent on initial release probability (*p*) (Eccles *et al.*, 1941). Later work found that a train of afferent stimulation typically elicits frequency facilitation at those synapses showing paired pulse facilitation, whilst within train responses progressively decrease in those synapses displaying paired pulse depression (Thomson, 2000). Considerable progress has been made in identifying presynaptic variables responsible for the two phenomena. These include mechanisms required for the mobilization and release of vesicles including Ca^{2+} entry to the terminal, detection of the cation and subsequent vesicle release, as well as those responsible for vesicle recycling and refilling (Edwards, 2007; Jackman *et al.*,

2016; Jackman & Regehr, 2017; Nanou & Catterall, 2018). The residual Ca^{2+} hypothesis, first posited in the peripheral nervous system (Katz & Miledi, 1968), has been expanded by the identification of synaptotagmin 7 (Syt7) as a secondary high affinity, slow activating Ca^{2+} sensor in the presynaptic terminal. Genomic manipulations confirmed that Syt7 is critical for frequency facilitation in hippocampal and thalamo-cortical synapses (Jackman *et al.*, 2016).

Complementing these findings are results showing that the type of vesicular glutamate transporter (i.e., VGLUT1 or VGLUT2) expressed at a synapse correlates with the initial release probability, a factor that as noted plays a central role in determining if contacts facilitate or depress when repetitively stimulated. The two transporters have different expression profiles within the brain (Fremeau *et al.*, 2001) with VGLUT1 largely confined to the cortex and VGLUT2 expressed elsewhere. Terminals with high levels of VGLUT2 depress during high rates of input while those containing VGLUT1 generally exhibit frequency facilitation. Although some evidence suggests a potential role for VGLUT isoform-specific interactions with factors governing exocytosis (Weston *et al.*, 2011), the primary role of these proteins is in vesicle refilling (Edwards, 2007).

The CA3-CA1 (i.e., Schaffer-commissural) connections of hippocampus exhibit robust facilitation across theta to gamma frequencies (Trieu *et al.*, 2015; Amani *et al.*, 2021) but there are inconsistencies between reports for the LPP (Jackman *et al.*, 2016; Wang *et al.*, 2018b). Given the significance of the issue the aim of the present study was to re-examine responses elicited in the outer molecular layer (OML) of the dentate gyrus (DG) to short trains of Θ, β, or γ frequency stimulation. Using electrophysiological approaches, we performed a detailed analysis of the operations occurring at the LPP-DG synapses and describe a potent form of low pass filtering. The contribution of pre- and postsynaptic factors to this LPP-DG filter, and how they may differ from the CA3-CA1 synapse was then investigated using selective pharmacological agents, immunocytochemistry and computational approaches. Additional studies then evaluated

responses to a sequence of brief γ frequency bursts (3 pulses) spaced apart by the period of the Θ wave (the above noted 'theta/gamma' bursts). A large body of work shows that such bursts undergo a marked facilitation in CA1 but comparable studies are lacking for LPP-DG synapses. Results show profound differences between the two hippocampal synapses and suggest a novel type of filtering in the LPP. In all, specialized features of LPP-DG synapses lead to a marked transformation of afferent input from the entorhinal cortex and, as a result, the signal transfer to the pyramidal cell fields of hippocampus.

Materials and Methods

Ethical Approval and Animals.

All studies used male C57/BL6 mice from 2-4 months of age. Animals were group housed in cages of 5 with access to water and food ad libitum and maintained on a 12 h light/dark cycle. Electrophysiology experiments were initiated from 8-10 AM. All procedures were in accordance with the Institutional Animal Care and Use Committee at the University of California, Irvine and the National Institute of Health Guidelines for the Care and Use of Laboratory Animals. For all electrophysiology studies, mice were anesthetized with isoflurane and euthanized by decapitation. Experiments complied with the animal ethics checklist and guidelines laid down by *The Journal of Physiology.*

Extracellular field recordings.

Hippocampal slices were prepared from adult (3-4 mo old) male C57BL6 mice as previously described (Gunn *et al.*, 2017; Cox *et al.*, 2019). Briefly, brains were rapidly removed and placed in ice cold, oxygenated (95% O_2/ 5% CO_2) high Mg^{2+} artificial cerebrospinal fluid (aCSF) containing (in mM): 87 NaCl, 26 $NaHCO_3$, 25 glucose, 75 sucrose, 2.5 KCl, 1.25 NaH_2PO_4, 0.5 $CaCl_2$, 7 $MgCl_2$, (320-335mOsm). Horizontal sections (350-400µm) were cut using a Leica Vibrotome (model VT1000s, Leica) at 4°C. Slices were rapidly transferred to an interface

recording chamber maintained at 31±1°C with constant perfusion (60-70 ml/hr) of oxygenated (95% O_2/ 5% CO_2) aCSF containing (in mM): 124 NaCl, 3 KCl, 1.25 KH_2PO_4, 1.5 $MgSO_4$, 26 $NaHCO_3$, 2.5 $CaCl_2$, and 10 dextrose, (300-310 mOsm, pH 7.4). Recordings began ~1.5-2 hrs later. A stimulating (twisted nichrome wire) electrode was placed within the outer third of the DG molecular layer (OML) targeting the LPP, and glass (2M NaCl, 2-3MΩ) recording electrodes were placed in the OML (dendritic responses) or within the granule cell layer (population spike responses) of the DG. Paired-pulse stimulation (40ms interval) was used to confirm facilitation, as is characteristic of the LPP (Christie & Abraham, 1994; Wang *et al.*, 2016). Stimulation strength was adjusted to elicit a field excitatory post synaptic potential (fEPSP) that was 50% of the maximum population spike free response; responses to 0.05Hz stimulation were recorded thereafter. For cell layer recordings, stimulation was adjusted to achieve population spike amplitudes of 1-2 mV with responses similarly evoked at a frequency of 0.05Hz. The effect of repetitive stimulation was tested by delivering 10 pulse trains at 5Hz (Θ), 20Hz (β), or 50Hz (γ) after 10 minutes of stable baseline. Delivery of the different trains was randomized, with no difference in responses to order and each train was separated by a minimum of 10 mins to prevent potentiation or depression in responses. A subset of experiments investigated the effect of stimulating the LPP-DG synapse with a physiologically relevant pattern of activity consisting of five high frequency bursts (50Hz; 3 pulses) separated by 200ms (Θγ). The effect that the inter-burst interval had upon the burst response was tested by increasing the duration to 1 second and then to 5 seconds to establish a time course for the different forms of synaptic filtering that occurred.

In a number of experiments, responses were additionally recorded from the CA3-CA1 synapse. Field EPSPs were elicited from CA1b stratum radiatum as previously described (Le *et al.*, 2022), and the effect of repetitive γ frequency stimulation and Θγ bursts assessed as described above.

Inhibition of MPP-DG synapses: A subset of experiments tested the specificity of our LPP stimulation paradigm by pharmacologically inhibiting transmission at the MPP-DG synapse with the mGluR II/III agonist DCG IV (1μM). A stimulating electrode and a glass recording electrode (2M NaCl, 2-3MΩ) were placed in the middle third of the DG molecular layer, separated by ~500-600 μm, to record MPP-evoked dendritic fEPSPs. Paired-pulse suppression (40ms interval) and the frequency-dependent depression of responses to brief stimulation trains (5Hz, 20Hz, and 50Hz), characteristic of MPP synapses (McNaughton, 1980, 1982; Christie & Abraham, 1994), were used to confirm placement. Responses to brief (10 pulses) stimulation trains delivered at Θ, β or γ frequencies (separated by >10 minutes) were obtained prior to recording a stable baseline period of at least 20 minutes (0.05Hz stimulation). DCG IV was then applied to the chamber via a second perfusion line (6ml/hr) for at least 40 minutes to confirm the inhibitory effect upon baseline responses. A second set of experiments investigated the effect of DCG IV upon LPP-evoked dendritic responses. Responses to brief stimulation trains (10 pulses; Θ, β or γ frequencies at 10 minute intervals) were obtained prior to recording a stable baseline period (0.05Hz stimulation; 20 minute). DCG IV was then infused (> 40 minutes) to assess the effect upon baseline responses before repeating the stimulation trains (at 10 minute intervals) in the presence of the agonist.

Treatment with selective antagonists: A subset of experiments tested the effect that bath application of picrotoxin (PTX: 1μM) or apamin (200nM), to inhibit $GABA_AR$-mediated inhibition and SK channel function respectively, had upon LPP-evoked baseline transmission and the responses to both repetitive (20Hz and/ or 50Hz) and burst patterns (Θγ) of stimulation. Responses to stimulation trains (either repetitive or bursts) were obtained prior to recording a stable baseline period of at least 20 minutes (0.05Hz stimulation). Stimulation trains were separated by >10 minutes. PTX or apamin was then applied to the chamber via a second perfusion line for at least 40 minutes to assess the effect upon baseline responses before

repeating the stimulation trains (at 10 minute intervals) in the presence of the antagonist. As a positive control, the effects of apamin upon baseline responses and repetitive γ frequency (50Hz) stimulation were tested in field CA1.

Low external Ca^{2+} experiments: The effect that lowering the release probability (*p*) had upon the responses to repetitive LPP stimulation (i.e., 10 pulse trains at 5Hz, 20Hz or 50Hz) as well as to $\Theta\gamma$ bursts was tested in a subset of experiments, where slices were perfused with a low Ca^{2+} aCSF (in mM): 124 NaCl, 3 KCl, 1.25 KH_2PO_4, 3 $MgSO_4$, 26 $NaHCO_3$, 1 $CaCl_2$, and 10 dextrose immediately following slice preparation.

LTP experiments: In separate experiments we investigated how induction of LTP at the LPP-DG synapse influenced synaptic filtering. Responses to stimulation trains delivered to the LPP at 5Hz, 20Hz and 50Hz (each separated by >10mins) were collected prior to recording a 20 min period of stable baseline responses. LPP-LTP was then induced using a single, 1 second train of high frequency 100Hz stimulation (HFS) with pulse duration doubled and intensity increased by 1.5X relative to baseline stimulation. Stimulation trains (i.e., 5Hz, 20Hz and 50Hz) were repeated 60 min after HFS stimulation and the responses collected. As a control for temporal drift of the evoked responses, stimulation trains were delivered at each of the frequencies as described above with slices being left for 60 minutes (no LTP induction) before repeating the stimulation trains.

Responses to set-frequency stimulations trains were collected using NACGather 2.0 (Theta Burst Corp.) and then analyzed offline using NACShow 2.0 (Theta Burst Corp.). Slopes (20-80%) of the leading edge of the fEPSPs were measured across the train and were normalized as the percentage ratio of the first pulse. For $\Theta\gamma$ trains, the slope of each fEPSP was measured. The slope of fEPSPs were normalized (as the percentage ratio) to 1) the slope of the initial fEPSP in the first burst response (to test for overall facilitation across the burst train) and 2) the

first response of their respective burst. This enabled a comparison of the overall facilitation across the burst train, as well as the magnitude of within burst facilitation across successive bursts. For drug treatment studies (i.e., PTX, apamin), stable baseline responses, collected over a 20 min period, were analyzed with regard to peak amplitude, rising slope, and half width of the fEPSP. The decay phase of a digitally averaged fEPSP (20 events) was described using a single exponential equation. The fEPSP slope in response to stimulation trains (repetitive or burst patterns) in the absence and presence of the specific agonist/antagonist were normalized as described above. The magnitude of LTP was determined by comparing the fEPSP slope of responses collected during the last 5 minutes of a 20 minute, pre-HFS baseline period with those obtained during the last 5 minutes of the recording (i.e., 55-60 minute post LTP induction). The paired pulse ratio (40ms interval) was analyzed before and 60 minutes after LTP induction.

Whole-cell recordings.

Hippocampal slices for whole-cell electrophysiology were prepared as previously described (Wang *et al.*, 2018b). Briefly, the brain was rapidly removed and placed in ice cold oxygenated (95% O_2/ 5% CO_2) aCSF containing (in mM): 124 NaCl, 3 KCl, 1.25 KH_2PO_4, 3 $MgSO_4$, 26 $NaHCO_3$, and 10 dextrose, (300-310 mOsm, pH 7.4). Transverse sections (350μm) were cut using a Leica Vibrotome (model VT1000s, Leica) at 4°C. Slices were transferred to a holding chamber and incubated at room temperature in oxygenated (95% O_2/ 5% CO_2) aCSF containing (in mM): 124 NaCl, 3 KCl, 1.25 KH_2PO_4, 1.5 $MgSO_4$, 26 $NaHCO_3$, 2.5 $CaCl_2$, and 10 glucose, (300-310 mOsm, pH 7.4). At least 1 hour after preparation, slices were transferred to the recording chamber where they were continuously perfused in oxygenated aCSF (above).

A small diameter (1μm) bipolar stimulating electrode (World Precision Instruments Inc., USA), placed with the DG OML adjacent to the fissure and overlying the recorded granule cell, was used to evoke LPP-specific responses. Patch pipettes (5-8MΩ) were pulled from thick-

walled borosilicate glass (1.5mm outer diameter; 0.86 mm inner diameter; Sutter Instruments, USA) and filled with an internal solution containing (in mM): 130 $CsCH_3SO_4$, 8 CsCl, 8 NaCl, 10 HEPES, 0.2 EGTA, 2 Mg-ATP, 0.3 Na-GTP and 2 QX-314 (Sigma, USA). Under these conditions, the calculated (pClamp 10) and experimentally verified reversal potentials for glutamate ($E_{glutamate}$) and GABA (E_{GABA}) were 0 and -55mV respectively. LPP evoked excitatory postsynaptic currents (eEPSCs) were recorded from DG granule cells (30 ± 1°C) at a holding potential of -70mV in aCSF that additionally contained the $GABA_AR$ antagonist PTX (50μM). Paired pulse stimulation (40ms interval) was used to confirm the characteristic facilitation at the LPP-DG synapse (McNaughton, 1980, 1982; Christie & Abraham, 1994). Stimulation trains (10 pulses) were delivered at Θ, β and γ frequencies with a 3 minute interval between trains. In a subset of experiments evoked excitatory postsynaptic currents (eEPSCs) were recorded (30 ± 1°C) from granule cells at a holding potential of -50mV in aCSF (above) that additionally contained the NMDAR and $GABA_AR$ antagonists AP-5 (50μM) and bicuculline (20μM), respectively. Responses to brief γ frequency bursts (3 pulses; 50Hz) separated by 200ms (5 bursts; Θγ) were recorded either with or without the Ca^{2+} chelator, BAPTA (10mM) in the internal solution (above). Finally, LPP evoked inhibitory postsynaptic currents (eIPSCs) were recorded from DG granule cells (30 ± 1°C) at a holding potential of 0mV in the absence of glutamate receptor antagonists. Stimulation trains (10 pulses) were delivered at 5Hz, 20Hz and 50Hz with each train separated by 3 minutes. Currents were filtered at 2Hz using an 8-pole Bessel filter. Only those cells with a stable access resistance were used, and recordings were aborted if >20% change in series resistance occurred. Recordings for both sets of experiments were performed using an Axopatch 200A and pClamp 10 and stored directly to a PC (4kHz digitization) using a Digidata 1550A.

All recordings were analyzed offline using the Strathclyde Electrophysiological Software (WinEDR and WinWCP; Dr J Dempster, University of Strathclyde). Ensemble averages (3

events) of a single eIPSC generated for each cell were analyzed with regard to peak amplitude, and decay time course. The decay phase was best described by the single exponential function $Y(t)=A*exp(-1/\tau)$. The peak amplitude of eEPSCs and eIPSCs were measured across the train and then normalized as the percentage ratio of the first pulse. The decay phase of the final inhibitory response of each stimulation train was described using the above single exponential function. For $\Theta\gamma$ stimulation, the eEPSCs (in the presence or absence of BAPTA) were analyzed with regard to peak amplitude and responses were then normalized (as the percentage ratio) to 1) the initial eEPSC in the first burst response (to test for overall changes across the burst train) and 2) the first response of their respective burst. This enabled a comparison of the overall facilitation across the burst train and the magnitude of within burst facilitation across successive bursts.

Drug application.

Drugs were made fresh on day of use. For field recording studies, the $GABA_AR$ antagonist picrotoxin (PTX) was prepared as a stock solution (10mM) in DMSO, whereas the SK channel antagonist, apamin (250μM), and the mGluR II/III agonist, DCG IV (10mM) were made as stock solutions in distilled water (all from Tocris Biosciences, USA). Each was then diluted in aCSF to attain the desired final concentration; for PTX containing a final DMSO concentration at <0.1% (PTX, 1μM; apamin 200nM; DCG IV, 1μM). For whole cell recordings, the NMDAR antagonist AP-5 (HelloBio, USA) and the $GABA_AR$ antagonist bicuculline (Tocris Biosciences, USA) were made as stock solutions (50mM and 20mM respectively) in distilled water and diluted to the final concentration in aCSF. PTX was made as a stock solution (50mM) in DMSO. The Ca^{2+} chelator, BAPTA (Tocris Biosciences, USA) was made directly in the internal solution to a concentration of 10mM.

Immunofluorescence.

For analysis of VGLUT synaptic localization, adult mice (n= 5) were anesthetized with isoflurane and euthanized by decapitation. Brains were removed and quick frozen in -40ºC 2-methylbutane and then cryostat sectioned at a thickness of 25 µm on the coronal plane through hippocampus and thaw mounted onto Superfrost Slides (Fisher Scientific, USA). After fixation in 4% paraformaldehyde in 0.1M phosphate buffer pH7.2 (PB) the tissue was processed for dual immunofluorescence as described (Rex *et al.*, 2009; Seese *et al.*, 2013; Seese *et al.*, 2014) using knockout verified antisera from Synaptric Systems GmbH (Germany) including polyclonal guinea pig anti-VGLUT1 (Synaptic Systems GmbH No. 135 304, Germany; RRID AB_887878) or anti-VGLUT2 (Synaptic Systems GmbH No. 135404, Germany; RRID AB_887884) in combination with rabbit anti-Synaptotagmin-7 (Synaptic Systems GmbH No. 105137, Germany; RRID AB_887838) all at 1:1000 dilution in PB containing 0.3% Triton X 100 and 3% normal swine serum. Secondary antisera included AlexaFluor 488 goat anti-guinea pig IgG and AlexaFluor 594 goat anti-rabbit IgG (1:1000; Thermo Fisher, USA). Tissue was cover- slipped with Vectashield containing DAPI (Vector Laboratories, USA).

Entorhinal cortex lesion.

For verification of VGLUT localization in the perforant path, an additional 3 mice received unilateral electrolytic lesion of the entorhinal cortex as previous described (Lynch *et al.*, 1972; Guthrie *et al.*, 1995); the contralateral unlesioned side served as control. Mice were anesthetized with ketamine/ xylazine cocktail (100mg and 10mg/kg Intraperitoneal), and an electrode (insulated stainless steel wire) was lowered into the LEC (from lambda; AP: +1.0, ML: -4.0, DV: -4.8), unilaterally. A current was passed through the electrode at 0.8mA for 20 seconds. After surgery, mice were returned to their home cage for recovery. These mice were euthanized 4 days post-lesion with an overdose of euthasol and intracardially perfused with 4% paraformaldehyde in 0.1M PB. After cryoprotection, brains were sectioned at a thickness of 35 µm on the horizontal plane through hippocampus and the free-floating tissue sections were

processed for localization of VGLUT1 or VGLUT2 (as above) and then slide mounted and cover- slipped with Vectashield containing DAPI.

Analysis of synaptic localization / fluorescence deconvolution tomography (FDT).

For analysis of synaptic localization, image z-stacks were collected from field CA1b stratum radiatum and the OML and MML that contains the lateral (LPP) and medial perforant path (MPP) innervation respectively, using a Leica DM6000B epifluorescence microscope equipped with a Ludl stage with a BioPrecision Stepper motor driven by Volocity 4.0 software (PerkinElmer). Images were collected at 63X (1.4 NA) at 0.2 µm intervals through a depth of 3 µm for a 135 x 105 x 3µm (42,525 μm^3) sample field in CA1. For the LPP and MPP fields, two adjacent image stacks (with ~10% overlap) were collected from the internal blade of th DG molecular layer; the long edge of the first image field was adjacent to and aligned with the hippocampal fissure and the second was placed immediately proximal to this. The DAPI counterstain was used to align and digitally stitch the z-stack into one continuous image using pairwise stitching in Fiji and the larger image was stack was then segmented to quantify the synaptic labeling in the outer and middle molecular layers containing LPP and MPP innervation respectively (Wang *et al.*, 2018a). Images were collected from both CA1 and DG fields for 5 tissue sections per brain. Quantitative FDT analysis entailed processing images through restorative deconvolution (99% confidence; Volocity 4.0, Perkin Elmer) and used to construct a 3-dimensional (3D) montage of the sample field. Within that montage, immunolabeled objects were detected using threshold segmentation separately for each channel: the image was normalized for background density and objects were segmented based on connected pixels above threshold using in house software that employed C. Java, Matlab and Perl (Granger *et al.*, 1989; Rex *et al.*, 2009; Lauterborn *et al.*, 2021). Immunofluorescent elements meeting the size and eccentricity constraints of synapses, and detected across multiple intensity thresholds, were quantified using automated systems (Rex *et al.*, 2009; Wang *et al.*, 2018b; Wang *et al.*,

2018c). Elements were considered double-labeled if there was contact or overlap of fields occupied by the two fluorophores as assessed in 3D. For each z-stack these procedures identified approximately 30,000 reconstructed terminal synapses for field CA1 and 15,000 terminal synapses in each of the LPP and MPP fields. Thus, metrics were collected from approximately 150,000 and 75,000 synapses for CA1 and perforant path fields, respectively, for each animal. With this approach we have successfully identified localization to pre- and post-synaptic compartments in multiple studies (Chen *et al.*, 2010; Wang *et al.*, 2018c).

Monte Carlo simulations of a two-step release model.

We implemented a previously published (Miki et al, 2016) renewable two-step synaptic release model based upon Monte Carlo simulations (Igor Pro from Wavemetric, Lake Oswego, OR, USA) to test if the operation of factors within the presynaptic terminal could account for the LPP-DG filter. The two-step model incorporates four factors associated with the release and subsequent recycling of synaptic vesicles. These include the probability of docking site occupancy (δ) and the probability of docked vesicle release (p_v). The overall probability of release (p) is described by the product of these two factors ($p=\delta p_v$). Each docking site (N) is associated with a replacement site and the transition from an occupied replacement site to an empty docking site is described by the probability 'r.' Before stimulations the occupancy probability of the replacement site is fixed at 1, with replenishment of the replacement site occurring with a probability 's' following depletion of the replacement vesicle(s).

A parameter search was conducted to identify the combination of variables that most accurately recapitulated the experimental data recorded from LPP-DG, MPP-DG and CA3-CA1 synapses following stimulation at 50Hz (10 pulses). Simulations were conducted using a range of docking site numbers (3 to 8) and replacement pool size (up to 20 vesicles). Note that the model was constrained such that each docking site had at least one replacement vesicle drawn

from a common vesicle pool. The factors associated with release (δ, p_v) and vesicle recycling (r, s) were tested across a range of probabilities (0.2 to 0.8). When considering low and high *p* synapses, the simulated product of δp_v was constrained to $p<0.3$ and <0.6 respectively. The simulation was repeated 50 times for each combination of variables. The simulated output, mean vesicle number, was normalized to the initial response (i.e., pulse 1) and then fit to the normalized curves generated experimentally. The standard error between each individual point (i.e., pulse number) was compared and a mean value generated. The parameter search was conducted using custom code generated using Python.

Combining high and low probability of release synapses: Using the parameters found to most reliably recapitulate the MPP-DG and CA3-CA1 curves (putative high and low p synapses respectively) we tested if a weighted combination of the two synapses could reproduce the experimentally measured LPP-DG responses. Using a custom written code (Python) the optimum ratio of the two curves was established. In order to generate the best fit between the simulated and experimentally derived data, a scale factor was required. The combined output of the two curves was generated using the following equation:

$$\text{LPP-DG} \approx x(\text{CA3-CA1}) + y(\text{MPP-DG})$$

The above equation was additionally used to generate a combined curve of the electrophysiological CA3-CA1 and MPP-DG responses.

Investigating the effect of replacement pool size: Using the optimal parameters for the low (i.e., CA3-CA1) and high (MPP-DG) *p* synapses the effect of changing the number of replacement vesicles influences the simulated output was tested.

Reducing p at the simulated LPP-DG synapse: Using the single set of parameters that best described the experimentally derived LPP-DG responses, the *p* was reduced by incrementally

lowering δ and p_v values. The output was then fit to the experimentally derived LPP-DG responses recorded under conditions of reduced external Ca^{2+}. The quality of fit was assessed by generating a mean standard deviation for each point.

Statistical analysis.

All results are presented as group mean values ± SD. Statistical comparison of the properties of fEPSPs before and after drug treatment were made using paired two-tailed Student's t- test. Two-way repeated measures ANOVA (RM-ANOVA; GraphPad Prism version 6.0) were used to determine the statistical significance of drug treatment, LTP and reduced external Ca^{2+} upon normalized responses to repetitive and $\Theta\gamma$ patterns of LPP stimulation. For electrophysiology studies, the group n refers to the number of slices (extracellular recordings) or cells (whole-cell recordings) studied, from a minimum of 3 animals. For analyses of immunofluorescence frequency distribution curves, RM-ANOVA was used (GraphPad Prism version 9.1.1). Paired Student t-tests or 1-way ANOVA followed by Tukey's multiple comparison test (Tukey's) were used for comparisons of high density labeled synapses between two or three fields respectively. Each group consisted of 5 animals. For all studies, p-values < 0.05 were considered significant.

Results

1.1 & 1.2 The lateral perforant path (LPP) operates as a low-pass filter.

To assess the functional characteristics of LPP synapses, 10-pulse trains were delivered to the LPP at three frequencies -- Θ (5Hz), β (20Hz), and γ (50Hz) -- known to occur in the entorhinal cortex and hippocampus during processing of spatial cues (Colgin, 2016). With 5 Hz stimulation, fEPSPs slopes recorded from the LPP-DG exhibited a modest initial facilitation that gradually decreased in magnitude over the course of the train with the last pulse producing a near baseline response (pulse 10: 97 ± 12.54%, n=21 slices/ 9 mice). β frequency stimulation produced a larger initial facilitation followed by a rapid decrease in response size over

successive pulses (pulse 10: 93 ± 15.27%, n=22 slices/ 9 mice). In accord with earlier reports (Wang *et al.*, 2018b), γ trains produced a striking within-train reduction in fEPSP slope beginning with the fourth pulse (pulse 10: 57 ± 14.68%, n=22 slices/ 9 mice. **Fig 1.1A, B**). The β and γ stimulation results for the LPP are dramatically different than those described for the CA3-CA1 link in hippocampal circuitry (Trieu *et al.*, 2015; Koutsoumpa & Papatheodoropoulos, 2019; Amani *et al.*, 2021). We confirmed that the latter connections exhibit robust facilitation throughout a 50Hz train (pulse 10: 127 ± 17.15%, n=8 slices/ 5 mice) (**Fig 1.1B**).

In a separate set of experiments, we addressed the question of how the output of the LPP target neurons (i.e., granule cell spiking) was influenced by the LPP-DG filter. Stimulation currents were increased to a level sufficient to produce a small population spike (1-2 mV amplitude) after which Θ, β, and γ trains were applied in an ascending or descending order. Results paralleled those for the dendritic fEPSPs but were more pronounced. In response to a 5Hz train, the population spike amplitude was amplified dramatically from the first to the second pulse and was then maintained across the duration of the train with responses by the tenth pulse being significantly greater than baseline (pulse 10: 256 ± 132.83%. n=7 slices/ 4 mice). In contrast, responses to LPP stimulation at β frequency were initially facilitated (pulse 2: 293 ± 88.82%, n=7 slices/ 4 mice), but successive pulses elicited progressively smaller population spikes such that the response fell to the original response by pulse #10 (pulse 10: 94 ± 70.64%, n=9 slices/ 4 mice). Stimulation at γ frequency again produced dramatic results: population spikes were undetectable from the 3rd or 4th pulse forward (**Fig 1.1C, D**).

The co-activation of medial perforant path (MPP) fibers located in the middle third of the molecular layer (Hjorth-Simonsen, 1972; Steward, 1976; Witter, 1993) could, given the previously reported frequency-dependent suppression of responses (McNaughton, 1980, 1982), contribute to the filtering operations described at the LPP-DG synapse. To explore this notion,

we tested the LPP-DG filter in the presence of DCG IV (1 μM), an mGluR II/III agonist that inhibits transmission at the MPP-DG synapse (Macek *et al.*, 1996; Bough *et al.*, 2004; Rohde *et al.*, 2012). Initial experiments confirmed that 1) MPP-evoked responses exhibited the previously described frequency-dependent suppression following brief stimulation trains (**Fig 1.2A**) and 2) DCG IV inhibited MPP-DG transmission (**Fig 1.2B, C**). Having confirmed that DCG IV significantly attenuated MPP-evoked responses, we next tested the effect that bath application of DCG IV had upon LPP-evoked dendritic responses. The agonist produced a modest yet significant decrease in the baseline fEPSP (**Fig 1.2B-D**), while no effects upon responses to brief stimulation trains in the β range and above were observed (Θ: $F_{(9,54)}$=2.075; p=0.048; β: $F_{(9,54)}$=1.533; p=0.1601; γ: $F_{(9,54)}$=1.057; p= 0.4088; n=7 slices/ 4 mice; two-way RM-ANOVA; **Fig 1.2E, F**). Whether the DCG IV-induced decrease in the baseline response and increased facilitation following LPP stimulation at Θ frequencies is a result of reduced stochastic release from MPP terminals or the direct stimulation of this pathway remains to be determined. Collectively, these findings indicate that the LPP filter is not due to partial activation of MPP inputs.

In all, the LPP-DG synapses act as low pass filters for inputs from the lateral entorhinal cortex: they follow 5Hz and 20Hz inputs but quickly depress during 50Hz γ stimulation. The latter depression does not appear to involve significant recruitment of MPP inputs. The next stage of processing – evoked spiking by the target neurons – exaggerates the signal transformation occurring in the dendrites.

1.3 & 1.4 Recruitment of GABAergic transmission is not critical for the LPP-DG low pass filter.

Feedforward GABAergic interneurons produce a strong shunting effect on AMPAR-mediated currents following activation of the CA3 inputs to field CA1 (Larson & Lynch, 1986; Pacelli *et al.*, 1989; Davies *et al.*, 1991; Mott & Lewis, 1991; Arai *et al.*, 1995; Larson &

Munkacsy, 2015). We tested for this version of postsynaptic filtering in the LPP-DG connections using bath application of the $GABA_AR$ antagonist, picrotoxin (PTX; 1μM). The compound had no significant effect on the amplitude or initial slope of fEPSPs but did produce a significant increase in the waveform half width and decay time (τ; $p<0.05$ paired Student's *t* test; **Fig 1.3A, B**). Within-train suppression of responses produced by activation of LPP inputs in the β range (20Hz) showed a modest yet significant reduction with PTX present (baseline pulse #10: 73 ± 8.37%, PTX pulse #10: 88 ± 9.50%, n=5 slices/ 2 mice. $F_{(9,36)}=2.17$, $p=0.049$; two-way RM-ANOVA. **Fig 1.3C,D**), but no significant effect of PTX was observed with γ frequency activation (baseline pulse 10: 48 ± 2.70%, PTX pulse 10: 57 ± 7.29%, n=5 slices/ 2 mice, $F_{(9,36)}=1.13$, $p=0.378$; two-way repeated measures ANOVA. **Fig 1.3E,F**). These findings suggest that repetitive stimulation results in only a modest, frequency-dependent increase in the level of $GABA_AR$-mediated inhibition on granule cells. We further explored this idea using whole-cell voltage-clamp recordings of LPP-eEPSCs from DG granule cells with GABAergic transmission completely blocked (50μM PTX). Under these conditions, a similar frequency-dependent suppression of the eEPSC amplitude was evident (**Fig 1.3G, H**). These data further support the conclusion that the low-pass filter at the LPP-DG synapse is not critically dependent upon the recruitment of feedforward GABAergic inhibition.

Although GABAergic inhibition does not appear to be heavily involved in the low pass filter at the LPP-DG synapse, the recruitment of feedforward interneurons that innervate other somato-dendritic sites may be important in modulating the DG spike output (i.e., local circuit activation). To explore this further we tested the effect of bath applied PTX (1μM) upon the granule cell output (i.e., 1-2mV population spike). Bath application of the $GABA_AR$ antagonist produced a significant increase in the baseline population spike amplitude of single responses (baseline: 1.0 ± 0.58 mV; PTX: 3.4 ± 2.35 mV, $t_5=3.10$, $p=0.027$, n= 6 slices/ 4 mice; paired Student's t-test **Fig 1.4A, B**). The amplification of the population spike observed following LPP

activation in the Θ range was not significantly influenced by PTX ($F_{(9,54)}$=0.9938, p=0.4562, n=7 slices/ 4 mice: two way RM-ANOVA; **Fig 1.4C**). The within train suppression of the population spike amplitude observed with β frequency stimulation was significantly increased on the second pulse whilst γ frequency LPP activation was unaffected by PTX (β: $F_{(9,45)}$=3.932, p=0.001,; γ: $F_{(9,45)}$=0.0231, p>0.999, n=6-7 slices/ 4 mice; **Fig 1.4D, E**). These data indicate that recruitment of GABAergic interneurons does not contribute significantly to the modulation of granule cell output following brief LPP activation at Θ, β and γ frequencies.

We further investigated the effects of $GABA_AR$-mediated inhibition using the whole-cell voltage clamp configuration to record LPP-eIPSCs and examined how these responses were influenced during repetitive stimulation in the Θ, β, and γ ranges. With the membrane voltage held at 0mV, which is the AMPAR reversal potential (E_{AMPA}), application of bicuculline (20μM) produced a complete suppression of the evoked response (**Fig 1.4F**). LPP-evoked IPSCs had a large peak amplitude (192 ± 54.23 pA, n=11 cells/ 4 mice) and relatively slow decay time course (τ= 90 ± 25.64 ms, n=11cells/ 4 mice; **Fig 1.4G**). Consistent with previous studies (Ewell & Jones, 2010), there was a marked, frequency dependent within-train suppression of eIPSCs (**Fig 1.4H-K**). At higher stimulation frequencies, the decline in eIPSC amplitude was offset by prolongation of the decay time (**Fig 1.4I-K)**. Such an effect may be indicative of "spill over" activation of perisynaptic δ-$GABA_A$Rs, a receptor isoform highly expressed in granule cells (Wei *et al.*, 2003) that is characterized by slow rates of desensitization, and is typically associated with mediating a tonic form of inhibition (Saxena & Macdonald, 1994; Nusser *et al.*, 1998) although see (Sun *et al.*, 2020) for contribution to phasic transmission. These results likely reflect a failure of interneurons to follow higher frequency input as well as the saturation of a population of slowly desensitizing receptor isoforms.

Collectively, these data suggest that the LPP-DG low pass filter observed at the levels of the synapse and the granule cell output (i.e., population spike) do not involve the significant recruitment of feedforward GABAergic transmission. The observation that LPP-eIPSCs show a pronounced frequency-dependent within train suppression indicates an inability of DG interneurons to follow high frequency LPP activation; a feature that likely underlies the circuit level phenomena.

1.5 & 1.6 Decreasing external Ca^{2+} reduces low pass filtering at the LPP-DG synapse.

The inability of LPP synapses to follow high rates of input, as described above, could involve a depletion of a readily releasable pool (RRP) of vesicles due to an initially high *p* or to a reduction in quantal size because of relatively slow neurotransmitter cycling (Thomson, 2000; Edwards, 2007). Reduced extracellular Ca^{2+} is commonly used to lower *p* and we accordingly tested its effect on LPP frequency facilitation. There was a clear enhancement of frequency facilitation produced by Θ trains in slices maintained in 1mM Ca^{2+} (**Fig 1.5A**; pulse 10: control: 98 ± 8.80%, low Ca^{2+}: 128 ± 21.72%, n=7-12 slices/ 4-5 mice/ group; $F_{(9,144)}$=9.365, p<0.0001; two way RM-ANOVA) and yet greater enhancement with β (20 Hz) stimulation (**Fig 1.5B;** pulse 10: control: 91 ± 7.34%, low Ca^{2+}: 173 ± 34.73%, n=7-12 slices/ 4-5 mice/ group. $F_{(9,144)}$=35.11, p<0.0001; two way RM-ANOVA). Within-train facilitation was also markedly increased during γ stimulation in the presence of low external Ca^{2+} and the pronounced depression of responses evident with control medium (i.e., 2.5mM Ca^{2+}) was largely eliminated (**Fig 1.5C** pulse 10: control: 54 ± 11.91%, low Ca^{2+}: 148 ± 30.33%, n=7-12 slices/ 4-5 mice/ group. $F_{(9,153)}$=38.02, p<0.0001; two way RM-ANOVA).

Although a principal effect of lowering the external Ca^{2+} concentration will be to modulate the initial *p*, additional Ca^{2+}-dependent processes within the postsynaptic site may potentially contribute to the observed synaptic filtering. In particular, activation of small conductance Ca^{2+}-

dependent K^+ (SK) channels, located in the spine head, have been implicated in shunting fEPSPs recorded from CA1 pyramidal cells (Ngo-Anh *et al.*, 2005; Wang *et al.*, 2014). The expression of SK channels in the DG molecular layer (Sailer *et al.*, 2004) raises the possibility that they may also shape responses to LPP stimulation. Bath application of the selective SK channel blocker apamin (200nM) had no effect upon amplitude, slope or decay time of single LPP-evoked fEPSPs (**Fig 1.6A-D**). However, a modest yet significant reduction in the within-train suppression of responses during γ (50Hz) activation was observed (baseline pulse #10: 52 ± 9.62%, apamin pulse #10: 63 ± 19.47%, n=8 slices/ 4 mice. $F_{(9,63)}$=2.290, p=0.027; two-way RM-ANOVA. **Fig 1.6E, F**). As a positive control, the effects of apamin were tested at the CA3-CA1 synapse. Bath application of apamin had no significant effect upon the amplitude, slope or half width of baseline responses (amplitude p=0.387; slope p=0.639; half width p=0.427. Paired Student's *t* test), although the within-train facilitation of responses during γ frequency stimulation was significantly enhanced (baseline pulse #10: 120 ± 18.40%, apamin pulse #10: 146 ± 22.40%, n=7 slices/ 5 mice. $F_{(9,54)}$=4.67, p=0.0001; two-way RM- ANOVA. **Fig 1.6G, H**). These findings suggest that repetitive activation of LPP inputs is sufficient to drive the necessary increase in local Ca^{2+} to rapidly activate SK channels (Stocker, 2004) but that this effect is only minimally involved in filtering.

1.7 LTP modifies presynaptic filtering in the LPP.

At the LPP-DG synapse, long-term potentiation (LTP) is dependent upon presynaptic modifications that result in a reduction in paired pulse facilitation (PPF) (Wang *et al.*, 2016) indicative of an increase in initial *p*. Based upon the findings described immediately above, this would be predicted to enhance within-train suppression of responses. We accordingly tested for interactions between the stable changes underlying LTP expression and the transient adjustments responsible for frequency facilitation.

Ten-pulse trains were administered to the LPP in a single slice at Θ, β and γ frequencies; this was repeated 45 to 60 minutes later with the three trains delivered in the same order (high to low or low to high frequency) as followed in the first session. LTP was induced in some cases immediately after session one (**Fig 1.7A, B**). A reduction in the PPF was observed following the induction of stable LTP, indicating an increased *p* (PPF pre-LTP: 43 ± 8.49%, PPF post-LTP: 28 ± 7.75%, n=5 slices/ 3 mice; p=0.039 paired Student's *t* test. **Fig 1.7C**). Analysis of the effects of LTP was complicated by a tendency towards an upward shift in frequency curves between sessions one and two in the control (no LTP) slices. The reasons for the between-session shifts in frequency facilitation curves are unclear. Whether the session effect reflects a modest adjustment in terminals elicited by 30 stimulation pulses or instead is due to an over time (up to 60 min) generalized change in the slice preparation is an interesting question for future work.

Because of the above observations, we assessed the effects of LTP on frequency facilitation by comparing responses to Θ, β, and γ stimulation for sessions one and two (**Fig 1.7D, E**), in control slices and in those in which stable potentiation had been induced. No differences between groups were found during session one (5Hz: $F_{(9,135)}$=1.85, p=0.065; 20Hz: $F_{(9,153)}$=0.75, p=0.704; 50Hz: $F_{(9,135)}$=1.56, p=0.135; n= 11 slices/ 7 mice, two way RM-ANOVA, **Fig 1.7D**). During session two however, there were striking differences between the facilitation curves in the LTP vs. control groups. At each stimulation frequency, LTP both blunted the initial (pulse #2) facilitation and depressed responses to subsequent pulses, resulting in a significant downward shift in the curve relative to that observed for the second session in control slices. Thus, the earlier described modest and sustained increase in fEPSPs obtained with Θ activation was reduced to near baseline levels in potentiated LPP synapses (interaction between pulse number and groups: $F_{(9,162)}$= 5.41, p<0.0001, n= 11 slices/ 7 mice). The statistically significant separation between the control and LTP curves was maintained across the full extent of the β (interaction $F_{(9,153)}$= 5.78, p<0.0001) and γ ($F_{(9,135)}$=5.85, p<0.0001) stimulation trains (**Fig 1.7E**), suggesting

that the factor(s) responsible for the initial decrement in facilitation continue to operate across successive, repetitive inputs. In all, LTP markedly augments the strength of LPP synapses while also exaggerating frequency filtering of responses to higher frequency inputs.

1.8 Relative concentrations of synaptotagmin-7 and VGLUTs in LPP terminals.

Vesicular glutamate transporters (VGLUTs) are essential for vesicle recycling, with evidence suggesting that VGLUT2 kinetics are slower than those for VGLUT1 (Nakakubo *et al.*, 2020). Broadly speaking, VGLUT1 is found throughout the cortical telencephalon including all subfields of hippocampus and is associated with low *p* synapses, while VGLUT2 predominates in subcortical structures that have synapses with a high *p* (Fremeau *et al.*, 2001; Fujiyama *et al.*, 2001). As such these transporters may provide a qualitative marker for the release properties of a given synapse.

Both VGLUT2 and VGLUT1 have been localized to the outer two thirds of the DG molecular layer (ML) field (Bellocchio *et al.*, 1998; Kaneko *et al.*, 2002), the terminal zone for the LPP and MPP projections that account for ~90% of all synapses in these laminae (Steward, 1976; Witter, 1993; Dolorfo & Amaral, 1998). We confirmed this observation using immunofluorescence. VGLUT2 immunoreactivity (-ir) was concentrated in the supragranular region and outer two thirds of the DG molecular layer; modest VGLUT2-ir was evident in stratum lacunosum-moleculare of the hippocampus proper whereas other regions including the stratum radiatum field of CA3-CA1 termination had very low immunoreactivity. In contrast, VGLUT1-ir was more evenly distributed across fields (**Fig 1.8A**), consistent with previous descriptions (Herzog *et al.*, 2004). Next, we used the Fluorescence Deconvolution Tomography (FDT) to quantify levels of synaptic VGLUT immunoreactivity associated with the presynaptic marker synaptotagmin 7 (Syt7; **Fig 1.8B**) and thereby test if the disparity in frequency facilitation curves for LPP-DG vs. CA3-CA1 synapses is associated with marked differences in the relative presynaptic

concentrations of VGLUT1 and VGLUT2. FDT performs 3-dimensional reconstructions of image z-stacks and supports quantification of tens of thousands of single- and double-immunolabeled elements within the size constraints of synapses per image field. Results can be summarized as immunolabeling intensity frequency distributions which plot target protein immunolabeling densities in ascending bins on the X-axis and percent double-labeled elements (target co-localized with the presynaptic marker Syt7) on the Y-axis. The regional differences in VGLUT2 were dramatic: the intensity frequency curve for VGLUT2 in the DG OML (LPP field) was strikingly right shifted towards denser concentrations relative to that for terminals in CA1 sr ($F_{(50,400)}$=63.52; p<0.0001; **Fig 1.8C**). As expected, the percentage of terminals with high levels of the VGLUT2-ir (>100 on the intensity scale) was 2-fold higher in the OML vs CA1 (p = 0.0001, Tukey's; **Fig 1.8D**); the percentage of terminals with very high levels of VGLUT2 was comparable between the outer and middle molecular layer fields of LPP and MPP termination (p=0.558, Tukey's).

VGLUT1 has been localized to both DG and CA1 dendritic fields in multiple studies (Bellocchio *et al.*, 1998; Fremeau *et al.*, 2001; Halasy *et al.*, 2004). Quantitative comparisons of the FDT intensity frequency distributions revealed a slight but significant difference in per terminal VGLUT1-ir between these fields ($F_{(31,248)}$= 5.533; p< 0.0001; **Fig 1.8E**) but the proportion of terminals with very high levels of VGLUT1 did not differ (p = 0.3781, Tukey's; **Fig 1.8F**). It thus appears that the balance of the two vesicle transporters in the LPP is markedly shifted in favor of VGLUT2.

As noted, residual Ca^{2+} is a key factor in frequency facilitation and computational studies concur with this conclusion. Recent work indicates that the Ca^{2+} sensor protein, Syt7 mediates the effects of residual Ca^{2+} on facilitation (Jackman *et al.*, 2016) and it was accordingly of interest to compare concentrations of this presynaptic protein in DG OML and CA1 sr fields. The density frequency distributions for Syt7-ir in bouton-sized profiles were similar between the OML

and CA1 sr ($F_{(50,400)}$= 1.358; p = 0.0602; **Fig 1.8G**), as were the high density Syt7-ir terminals in each field (p = 0.8859, paired Student's t-test; **Fig 1.8H**). These results indicate that differences in Syt7 levels do not account for differences in frequency facilitation between LPP and CA3-CA1 synapses and verify that Syt7 is an unbiased presynaptic marker for the VGLUT analysis described above.

Finally, to verify that clusters of VGLUT2-ir, in the DG OML, are indeed localized to perforant path terminals (Halasy *et al.*, 2004) we evaluated effects of unilateral electrolytic lesion of the entorhinal cortex. As this projection is virtually unilateral in mid- to temporal hippocampus the contralateral side served as the control for evaluating effects of deafferentation. As assessed 5 days after entorhinal cortex lesion placement, there was near complete elimination of VGLUT1-ir and VGLUT2-ir within the distal DG molecular layer and stratum lacunosum moleculare ipsilateral to the lesion, relative to robust labeling in these fields on the contralateral side (**Fig 1.8I**); this is consistent with localization in the perforant path and temporo-ammonic systems, respectively.

1.9 Presynaptic factors may contribute to the low pass filter at the DG-LP synapse.

The findings from our electrophysiological studies indicate that the low pass filter at the LPP-DG synapse appears to be dependent upon factors within the presynaptic terminal. Given the difficulty in investigating mechanisms that underlie release dynamics empirically we ran Monte Carlo simulations of a two-step synaptic release model (Miki et al, 2016) to test if presynaptic factors alone could recapitulate the LPP-DG filter. The two-step model incorporates factors associated with the release including the probability of vesicle docking (δ) and the release probability of a docked vesicle (p_v), as well as the probability of vesicles transitioning from the replacement pool to vacant docking sites (r) and replenishment of the replacement pool (s; **Fig 1.9A** and Methods).

Initially, we tested if Monte Carlo simulations of this two-step model were capable of recapitulating the LPP-DG low pass filter in response to γ frequency stimulation. Using a model with 3 docking sites, replacement pool size of 3 vesicles and optimized release and replenishment parameters (δ=0.6, p_v=0.55, r=0.7 and s=0.4), we were able to generate an output curve remarkably similar to our electrophysiological data (mean SD= 0.047; **Fig. 1.9B**). However, evidence that the relative expression of VGLUT1 and VGLUT2 in the dentate gyrus LPP field differs from that at the CA3-CA1 synapse (**Fig. 1.8**) raises the suggestion that the LPP-DG filter could be produced by a different combination of high and low *p* synapses. To explore this notion further we first tested if simulated low (i.e., VGLUT1) and high (i.e., VGLUT2) *p* synapses were capable of generating output profiles that resembled those recorded electrophysiologically from CA3-CA1 and MPP-DG synapses--putative low and high *p* synapses. When constrained by the overall *p* (i.e. $p_v\delta$, see Methods) and with all other variables optimized, the two-step model was capable of reliably generating the facilitation and suppression of simulated responses typically associated with low (i.e., CA3-CA1; **Fig 1.9C**, SD= 0.019) and high (i.e., MPP-DG; **Fig 1.9D**, SD= 0.066) *p* synapses. Having established that the simulation could reliably reproduce the output curve associated with low and high *p* synapses following γ frequency stimulation, we next investigated how changes in the replacement pool size could influence the nature of this curve. At the low *p* synapse, reducing the pool size caused a pronounced suppression of the within train facilitation (**Fig 1.9C**), while increasing the pool size delayed the overt depression of release at a putative high *p* synapse (**Fig 1.9D**). This indicates that the size of the replacement pool is a critical determinant of the output curve generated at both high and low *p* synapses. Next, we explored if the LPP-DG low pass filter could be generated by a mixed population of low and high *p* synapses. A parameter search revealed that combining the simulated CA3-CA1, where the pool size was reduced from 5 to 3 vesicles, and the MPP-DG curves was capable of reproducing the LPP-DG curve recorded

experimentally when fit with a scale factor (**Fig 1.9E,** SD= 0.123). The application of the scale factor indicates that an approximately 4:1 ratio of CA3-CA1 type to MPP-DG type synapses is required to recapitulate the experimentally measured LPP output curve. We next tested whether if it was possible to combine the electrophysiologically recorded CA3-CA1 and MPP-DG output curves in a similar manner (i.e., scaled) to reproduce the LPP-evoked responses. Using the same approach, we found that the empirically measured responses could be combined to recapitulate the LPP-DG curve, albeit with a different scale factor (**Fig 1.9E**, SE= 0.082). This latter point likely reflects difference between responses generated using a simulated single synapse and the factors occurring across a population of neurons that are responsible for producing the local field potential responses.

Our experimental data indicates that reducing *p* by lowering the external Ca^{2+} concentration largely attenuated the low pass filter observed at the LPP-DG synapse following γ frequency stimulation. As such we next tested if reducing *p* in the simulated LPP-DG synapse reproduced the electrophysiological data. Under conditions where only the initial *p* (i.e., δp_v) was reduced, and all other variables were maintained, the within train facilitation in response to γ frequency stimulation was maintained in a manner analogous to our electrophysiological data (**Fig 1.9F**, SD=0.616).

Collectively, these findings indicate that the interaction between factors within the presynaptic terminal that govern vesicle release and recycling could underlie the low pass filter observed at the LPP-DG synapse. While the low pass filter may be described by a single set of presynaptic parameters, a combined response of low and high *p* synapses also provides a plausible explanation. When described by a single set of parameters, the simulated two-step model indicates that, in addition to release probability, subtle changes in the likelihood of the vesicles transitioning to the docked state may be an important factor.

1.10 & 1.11 Spaced bursts of gamma stimulation engage additional filtering.

During complex behaviors it is common for entorhinal cortex neurons to emit short bursts of γ frequency activity riding on a slower Θ wave (Chrobak *et al.*, 2000). Such bursts are thought to improve the reliability of communication and to increase the signal to noise ratio (Lisman, 1997). Based on results described above, short bursts of 2-3 spikes could potentially reduce the impact of low pass filtering and exploit the initial frequency facilitation produced by Θ stimulation. Such a scenario would enable the system to follow seconds-long spike trains that include γ frequency information. To test this idea, the LPP was stimulated using a $\Theta\gamma$ pattern, involving a series of three pulse γ bursts separated by 200ms. This strategy was only partially successful as LPP responses in the OML showed a noticeable within-train diminution of the composite potentials at burst intervals of 200ms (**Fig 1.10A, B**). This stands in contrast to the behavior of CA3-CA1 synapses in which the net response to the fifth burst was larger than that to the first (**Fig 1.10C, D**). Two factors contributed to the decrease in LPP burst responses: 1) relative to the initial LPP-evoked burst, the slope of the first fEPSP in each burst became progressively smaller over the course of the train and 2) the modest within-burst facilitation seen in the initial response was replaced by a within-burst depression (**Fig 1.10B, E & F**). In CA1, the first response was enhanced rather than decreased throughout the five-burst train (**Fig 1.10D, E**). We isolated the loss of frequency facilitation by normalizing within-burst slopes to the first response in each of the successive bursts. As shown, the modest facilitation seen in the first LPP response was greatly reduced on burst two and replaced by frequency depression on subsequent bursts (**Fig 1.10F**); this occurred despite the reduction in the size of initial fEPSP in responses two through five. A loss of frequency facilitation was also evident in CA3-CA1 synapses when fEPSPs were normalized to the first (enhanced) potential in each burst (**Fig 1.10F**).

Next, we investigated the time period over which between-burst depression of the initial

response, and suppression of within-burst facilitation, operate. A burst-by-burst analysis indicated that a marked reduction in the first fEPSP slope was evident by the 3rd burst response when using 200ms intervals, but not when successive bursts were separated by either 1 or 5 seconds (**Fig 1.11A, B**). Indeed, at interburst intervals of 1 and 5 seconds, responses were maintained, or at the longer interval moderately facilitated (relative to the initial fEPSP in the first burst), across bursts (**Fig 1.11B**). However, the loss of within-burst facilitation with Θ (i.e., 200ms) interval spacing of bursts was still present when the interval between bursts was extended to 1 second, but not 5 seconds (**Fig 1.11A, C**). These results indicate that short γ bursts engage surprisingly persistent mechanisms that add a second, novel type of filtering to the LPP-DG connection.

The duration of conventional IPSCs suggests that they do not play a significant role in the depression of spaced burst responses. However, γ frequency activation of the LPP produced GABAergic currents that persist for hundreds of milliseconds (see above). We tested if these prolonged currents affect interactions between bursts using PTX at a concentration (1μM) that prolonged the decay phase (τ) of fEPSPs (122 ± 21.51%, p=0.0065 paired Student's t test) without causing after-discharges. PTX had no detectable effects on the slopes of the three fEPSPs in the first burst response but did partially offset the decrease in the first fEPSP of subsequent bursts separated by 200msec (**Fig 1.11D,E**). The compound did not however detectably affect the loss of frequency facilitation that occurs within bursts during a Θγ stimulation train (**Fig 1.11F**). In all, it appears that LPP Θγ bursts produce distinguishable effects on the initial fEPSP in subsequent bursts vs. frequency facilitation within those bursts. The first of these effects is less persistent than the second and is likely mediated by the unusual inhibition, possibly perisynaptic δ-$GABA_A$Rs, set in motion by a γ burst. The loss of frequency facilitation during a burst train is due to factors of another type.

1.12 & 1.13 Evidence that between burst depression is due to presynaptic adjustments.

Reducing extracellular Ca^{2+} had strong effects on responses to mixed frequency stimulation (i.e., $\Theta\gamma$ train). As anticipated from the earlier experiment using 10-pulse γ trains, there was a marked facilitation of the 2nd and 3rd fEPSPs in the first burst response under conditions of reduced external Ca^{2+}, whereas the composite response to the 5th burst (200ms delays) was clearly smaller (**Fig 1.12A**). As described, a reduction of the first fEPSPs in each burst was one of two effects that emerged during a train of theta bursts under control conditions. Burst-by-burst analyses showed that this did not occur with 1 mM Ca^{2+} and instead the potentials were measurably larger relative to the first burst (**Fig 1.12A, B**). This is not unexpected assuming that the lower Ca^{2+} concentration depresses LPP activation of, and subsequent release from, the GABAergic interneurons shown to contribute to the depression of first fEPSPs in PTX experiments described above. Frequency facilitation was present throughout the train, unlike the case with control Ca^{2+}, but became progressively smaller across successive bursts (**Fig 1.12C**). This effect accounts for the depression of the net response to an LPP burst that is evident by burst #5 and suggests that the variables responsible for the depression of facilitation are not determined by release probability.

The persistent nature of the depression in frequency facilitation associated with $\Theta\gamma$ stimulation suggests a mechanism with a long-time course such as activation of postsynaptic SK channels. Infusion of apamin, which blocks these channels, in the presence of control levels of extracellular Ca^{2+} (2.5 mM) had minimal effects on the first burst response or on the reduction in the relative size of the response to the fifth burst (**Fig 1.13A**). Quantitative analyses confirmed this and showed the progressive decrease in the responses during a train was still present, although modestly reduced in magnitude ($F_{(14,182)}$=2.459, p=0.003; **Fig 1.13B**). Normalizing the slopes of the fEPSPs to the first potential in each burst response indicated that the loss of within-burst frequency facilitation was only slightly changed by apamin ($F_{(14,182)}$=1.873, p=0.032;

Fig 1.13C); an effect that was in stark contrast to the CA3-CA1 synapse and consistent with previous studies (Kramar *et al.*, 2004). We conclude from this that SK channels do not make a significant contribution to the second of the carryover effects that occur between LPP Θγ bursts (i.e., the suppression of within burst facilitation).

Activation of apamin–insensitive intermediate conductance Ca^{2+}-dependent K^+ channels, (i.e. $K_{Ca}3.1$) responsible for mediating the slow after-hyperpolarization (sAHP) that persists for seconds (Tiwari *et al.*, 2018), may provide an alternative mechanism. To address this, we used the whole-cell voltage-clamp configuration to record LPP-evoked EPSCs (eEPSCs) from granule cells (V_{clamp} -50 mV) in the presence of the NMDAR and $GABA_AR$ antagonists AP-5 (50μM) and bicuculline (20μM), respectively. A potential contribution of postsynaptic Ca^{2+} to the impaired within-burst facilitation that occurs during a 5 burst Θγ train was tested by recording responses with and without the Ca^{2+} chelator, BAPTA (10mM) in the recording electrode internal solution. The suppression of responses, both across and within bursts, was largely unaffected by BAPTA in the recording electrode (**Fig 1.13D-F**). These experiments support the conclusion from field recordings that $GABA_ARs$ do not make a significant contribution to the responses generated by theta bursts delivered to the LPP. Collectively, these findings suggest that the prolonged decrease in within-burst facilitation is not dependent upon postsynaptic Ca^{2+}-dependent mechanisms, but rather involves a process in the terminal that requires increased levels of the cation.

Discussion

Communication within and across nodes in brain circuits requires afferent inputs to efficiently drive output (i.e., action potential firing) from principal cells. As such the transformation of afferent inputs (i.e., amplification, filtering) across the synapse and how the subsequent response is processed along the somato-dendritic domain of the target cell are critical for determining information flow. At the level of the synapse, signal transformations involve the

interaction between processes governing transmitter release (i.e., initial *p,* number of release sites) and those determining neurotransmitter and vesicle recycling (Thomson, 2000; Edwards, 2007; Jackman & Regehr, 2017; Nanou & Catterall, 2018). The net result being that synapses generally display facilitation or suppression of responses to inputs at behaviorally relevant frequencies (Thomson, 2000). Although there have been few planned comparisons between synaptic populations, it is evident from the literature that connections even within the same network respond in markedly different ways to the same pattern of afferent activation. For example, low frequency Θ stimulation (5Hz) is reported to produce within-train depression or various degrees of facilitation depending on where it is was applied in a seven-node circuit extending from the piriform cortex to hippocampal field CA1 (Trieu *et al.*, 2015). Results of this kind strongly suggest that synapses are frequency 'tuned' according to their location, a factor that presumably shapes network level computations.

Results reported here indicate that the LPP-DG synapse expresses an unusual set of specialized features that interact in a frequency-specific manner to produce previously unsuspected types of synaptic filtering. Theta (5Hz) LPP stimulation produced a slight degree of facilitation comparable to that recorded for CA3 to CA1 contacts, but γ (50Hz) activation elicited a pattern unlike that reported for any other site in hippocampus: an initial facilitation followed by an overt suppression of the fEPSP. Together these features generate a type of low pass filter at one of the two pathways carrying cortical information to the first stage of hippocampal circuitry.

Synchronous discharges of the DG granule cells paralleled and exaggerated the changes in dendritic fEPSPs. The weak and sustained facilitation of fEPSPs during a 5Hz train were converted into a dramatic enhancement of granule cell population spikes. In general, the number of contacts formed between any given group of axons and a population of target neurons in a sparse system (a given axon connects with a low percentage of target cells) without local topography will form a steep Poisson distribution with lowest values (fewest

synapses/neuron) to the left (Granger *et al.*, 1989). Only a small percentage of the population will thus receive sufficient excitatory input to cross spike threshold. Facilitating release will allow the same sized input to drive the much larger group of near threshold neurons and thus produce a disproportionately (relative to the increase in fEPSP) greater increase in the number of responding neurons. Absent other factors, anatomical organization alone will serve to amplify input signals. But this argument also works in the reverse direction: a steadily developing depression of release will cause a much more rapid decline in the size of the population spike than of the fEPSP. In this sense, the same factors underlying amplification will sharpen low pass filtering as was observed here for β and γ frequency stimulation of the LPP.

Activation of the LPP with short γ bursts delivered at 200ms intervals (i.e., theta burst stimulation), a behaviorally significant pattern of activity (Chrobak *et al.*, 2000; Colgin, 2016), uncovered a second and complex set of filtering operations. The first response of the second and subsequent bursts in a train of five, was depressed relative to that of the first burst. Furthermore, the within-burst facilitation declined across successive bursts. Together, these factors result in much reduced composite responses to theta bursts as a train progresses. The depression of frequency facilitation was long lasting in that it was still present when bursts were spaced apart by one second. In all, it appears that the LPP-DG connection faithfully relays, and indeed amplifies, Θ pattern signals but potently depresses γ input whether arriving as a short train or as very brief bursts. The significance of these processes to circuit function depends on the manner in which the mossy fiber projections of the DG respond to activation at the two frequencies. The mossy fiber boutons exhibit an exaggerated form of frequency facilitation (Toth *et al.*, 2000; Urban *et al.*, 2001; Nicoll & Schmitz, 2005). If, as seems likely, this effect is greater at γ than Θ frequencies, then low pass filtering by the LPP contacts could be seen as a device that prevents excessive mossy fiber activation of CA3 pyramidal neurons. These pyramidal cells generate a massive collateral feedback system capable of maintaining reverberating

activity for remarkable periods (i.e., minutes long; (Cox *et al.*, 2019)) and relatedly promote epileptiform discharges. There is also the possibility that the direct LPP input to CA3 does not follow the same rules as the LPP-DG connection (Breindl *et al.*, 1994), in which case low pass filtering in the latter could serve to emphasize the importance of the former in processing γ frequency information (**Fig 1.14**).

Postsynaptic mechanisms and the LPP-DG filter.

We conducted a number of experiments to investigate the mechanisms underlying the unusual filtering of γ trains and $\Theta\gamma$ bursts at LPP-DG synapses. The accumulation of feed forward inhibition is an obvious candidate for the depression of dendritic and somatic (i.e., population spike) responses that emerges during these patterns. Although infusion of a low dose of the $GABA_AR$ antagonist, picrotoxin (1μM), produced significant effects upon baseline responses, prolonging the fEPSP half width and increasing the population spike amplitude, the within train facilitation and suppression of both output measures remained intact. These findings indicate that feed forward inhibition is critical for shaping the unitary fEPSP waveform and spike initiation dynamics but not the depression of responses across a γ train. Whole-cell voltage-clamp experiments using a saturating dose of picrotoxin confirmed that the recruitment of feed forward GABAergic transmission is not a critical determinant of the within train suppression observed during repetitive and burst patterns of stimulation. While this result may be somewhat surprising, factors associated with 1) the ability of interneurons to follow afferent inputs, 2) how the different experimental conditions (i.e., whole-cell *vs* extracellular) influence the efficacy of $GABA_AR$-mediated inhibition, and 3) the expression profile of $GABA_ARs$ need to be considered.

A number of prior studies have demonstrated that although DG interneurons are capable of firing at high frequencies in response to a persistent depolarizing current injection, or during paired interneuron-granule cell recordings, they do not reliably fire action potentials in response

to perforant path stimulation (Ewell & Jones, 2010; Liu *et al.*, 2014). This latter observation is critical when considering the operations of the local circuit. Our single-cell voltage-clamp data support such a scenario as the amplitude of LPP evoked IPSCs (eIPSCs) decrease in a frequency-dependent manner during brief stimulation trains i.e., less interneurons spiking. Whether this is due to the LPP-interneuron synapse operating in a manner similar to the LPP-DG synapse described in the current study remains an interesting question.

The efficacy of $GABA_AR$-mediated inhibition, determined in large part by the activity of the K-Cl co-transporter 2 (KCC2), in the extracellular recordings is also an important factor. Given that under physiological conditions the estimated driving force for Cl^- in granule cells is close to zero (Barmashenko *et al.*, 2011; Goutierre *et al.*, 2019), the size of $GABA_AR$-mediated currents will be significantly smaller than eIPSCs. As the DG contains high levels of δ-containing $GABA_ARs$ within the dentate gyrus, a receptor isoform located at primarily at peri- and extrasynaptic sites that has a high affinity for GABA and very slow decay constants (Saxena & Macdonald, 1994; Sun *et al.*, 2020), it is tempting to speculate that shunting inhibition dominates under basal conditions. The observation that partial PTX –mediated inhibition of $GABA_AR$ function increased the population spike amplitude indicates that the local circuit is finely balanced and may reflect a reduction in δ-$GABA_AR$-mediated tonic inhibition (Wei *et al.*, 2003). Such a PTX-induced change in spike initiation dynamics may mask any clear recruitment of feed forward inhibition during brief periods of γ frequency activity. The transient inactivation of specific subpopulations of interneurons may be a useful approach to manipulate GABAergic transmission at this synapse.

The rapid activation (within 1ms) and decay time course (200-400ms) of SK channels (Stocker, 2004; Adelman *et al.*, 2012) lend themselves to modulating responses generated by repetitive, high frequency inputs. Indeed, in CA1 the activation of SK2 channels by NMDAR-mediated increases in Ca^{2+} (Wang *et al.*, 2014) has been shown to generate a conductance that significantly attenuates responses to CA3 inputs and elevates the threshold of LTP (Kramar *et*

al., 2004; Ngo-Anh *et al.*, 2005). Here we found inhibition of these Ca^{2+}-dependent channels, with apamin, had no significant effect upon the properties of baseline LPP-evoked fEPSPs, but did produce a small decrease in the within-train suppression of responses to γ frequency stimulation. A comparably modest effect was found for the within-train depression of $\Theta\gamma$ burst responses. Given that SK channels are localized to the DG molecular layer (Sailer *et al.*, 2004), it is tempting to postulate that the observed attenuation of responses to γ frequency stimulation are attributable to activation of these channels within the granule cell dendritic spines (Sailer *et al.*, 2004). However, intracellular administration of a Ca^{2+} chelator to DG granule cells, that would accordingly be anticipated to reduce activation of postsynaptic SK as well as the longer duration $K_{Ca}3.1$ (i.e., slow AHP) channels, had no detectable effect on within-train depression of theta burst responses. Thus, we conclude that, neither of two plausible postsynaptic mechanisms made major contributions to γ filtering at LPP synapses, suggesting the critical mechanisms are presynaptic.

The contribution of presynaptic factors to the LPP-DG filter.

When considering potential factors present in the terminal that may contribute to the observed within-train suppression of responses, the temporal constraints imparted upon the system, in this case by a 10-pulse γ train, are critical. Our data using low external Ca^{2+} levels indicate that the synaptic filtering at the LPP-DG synapse can largely be removed by reducing the initial *p*. A parsimonious interpretation of this observation is that lowering the initial *p* results in a reduction in the depletion of the readily releasable pool (RRP) that occurs during repetitive, high frequency stimulation (Thomson, 2000; Neher & Brose, 2018). Current thinking posits that vesicular release is a sequential, two-step process, wherein vesicles are either 'loosely' or 'tightly' associated with the plasma membrane, such that only the latter are primed for rapid (μs timescale) transmitter release following local elevations in Ca^{2+} (Pan & Zucker, 2009; Miki *et al.*,

2016; Doussau *et al.*, 2017; Miki *et al.*, 2018; Neher & Brose, 2018). Using Monte Carlo simulations of such a two-step model we were able to 1) investigate if presynaptic factors alone could recapitulate the experimental observations following γ frequency stimulation across three different synapses and 2) test how different factors such as release probability and RRP size influence the output curve. The two-step model, when constrained physiologically (e.g. initial *p*, number of docking sites, replacement vesicle number) was capable of recapitulating the output curves following γ frequency stimulation of CA3-CA1 (putative low *p* synapse), MPP-DG (putative high *p* synapse) and the LPP-DG synapses. The simulation indicates that interaction between the initial *p* (i.e., δp_v) and replacement pool size (i.e., "loose" vesicles) are critical determinants of the output curve. Specifically, reducing the size of the RRP decreased the simulated within train facilitation observed at a low *p* synapse and exaggerated the suppression evident at a high *p* synapse. Finally, the observation that the LPP-DG has the highest probability of vesicles transitioning to the docked state, a process that requires cytoskeletal changes (Miki *et al.*, 2016), is intriguing given that plasticity at this synapse occurs via presynaptic mechanisms (Wang *et al.*, 2016; Wang *et al.*, 2018b).

Vesicular glutamate transporters 1 and 2 (VGLUT1 and VGLUT2), the two primary brain variants are expressed in a brain-region specific manner and ensure the refilling of vesicles with glutamate (Fremeau *et al.*, 2001; Edwards, 2007). VGLUT1 is primarily found in cortex and is associated with frequency facilitation whereas VGLUT2 is enriched in subcortical and thalamocortical terminals and is typically associated with frequency depression (Fremeau *et al.*, 2001; Fujiyama *et al.*, 2001; Fremeau *et al.*, 2004). The DG is unusual among cortical structures in that its molecular layer contains high concentrations of VGLUT2 (Halasy *et al.*, 2004). Our experiments established that the transporter is present at high levels (relative to the CA3-CA1 system) in the LPP terminal field. We accordingly postulate that the LPP-DG synapse may represent a heterogeneous population of synapses, comprised of both low and high *p* synapses.

In line with this view, combining the simulated output curves for putative low (i.e., CA3-CA1) and high (i.e., MPP-DG) *p* synapses was capable of recapitulating the LPP-DG low pass filter when an additional scale factor (i.e., weighted) was introduced with a ratio of 4:1 low to high *p* synapses. Remarkably, a weighted combination of the empirically measured output curves for the CA3-CA1 and MPP-DG responses also reproduced the low pass filter observed at the LPP-DG synapse. This suggests that the LPP-DG synapse has features common to both high and low *p* synapses, whilst the apparent differences in the ratios observed in the simulated and electrophysiological data likely results from comparing single synapse responses (i.e., simulation) and population responses at the level of the field potential.

While we posit that a depletion of the RRP associated with a preponderance of VGLUT2-containing terminals may be a primary factor for the initial suppression of responses during γ frequency inputs, there are a number of additional factors that merit consideration. First, our results indicate that levels of VGLUT1 and VGLUT2 do not differ between the LPP and MPP fields in DG, suggesting that the ratio of high and low *p* synapses is unlikely to explain the functional differences observed at these two synapses. The observation that the probability of vesicles transitioning to a docked state is ~20% higher at the simulated LPP-DG synapse may provide a clue that differences in cytoskeletal mobility are involved. In addition, it remains to be determined whether the different VGLUT isoforms are expressed in separate terminals, within the same terminal or even in the same synaptic vesicle. While it may be convenient to consider two distinct populations of terminals, the two isoforms have been identified within the same vesicle at the Calyx of Held synapse (Nakakubo *et al.*, 2020) and similar biphasic responses to high frequency stimulation have been observed at that contact (Taschenberger *et al.*, 2016). A potentially important, as yet unexplored factor that may couple VGLUT isoforms with the apparent differences in synaptic filtering relates to whether the composition and spatial organization of the presynaptic active zone differs in a VGLUT-specific manner. Given the

sensitivity of *p* to small changes in Ca^{2+} levels, the location and regulation of voltage-gated Ca^{2+} channels (VGCCs) within the active zone will be critical for regulating the efficacy of synaptic transmission (Thomson, 2000; Dittman & Ryan, 2019). While multiple mechanisms have been demonstrated to regulate VGCC function (Zamponi & Currie, 2013; Nanou & Catterall, 2018; Dolphin & Lee, 2020), our low Ca^{2+} data suggests that Ca^{2+}-dependent inactivation of these channels (Forsythe *et al.*, 1998; DeMaria *et al.*, 2001) is plausible at the LPP-DG synapse during γ frequency stimulation, in a manner analogous to processes identified in field CA1 (Nanou *et al.*, 2018). Relatedly, the two-step model used here has a number of limitations when considered in the context of the current literature. First, presynaptic Ca^{2+} concentrations are not dynamic such that intra-terminal concentrations of the cation, and as a result the initial *p*, can vary across subsequent inputs. This has implications when considering that loosely associated vesicles may contribute to synaptic transmission by rapidly transitioning (1-5ms) to the primed, tightly associated state, from which neurotransmitter release can occur when presynaptic Ca^{2+} levels are high (Miki *et al.*, 2018). In addition to having a greater proportion of vesicles in the primed state initially, high *p* synapses also exhibit a prevalence to incorporate loosely associated vesicles during repetitive activation (Miki *et al.*, 2018; Neher & Brose, 2018); a feature that has significant implications for their operations during high frequency stimulation. Such a rapid transition of loosely associated vesicles will not only increase the latency to synaptic release (decreasing temporal precision), but will introduce a refractory period (30-50ms) earlier in the train as they are replenished (Thomson, 2000; Miki *et al.*, 2018; Neher & Brose, 2018). Regarding the latter point, recent evidence indicates the replenishment pool, upstream of the RRP is small in size and as such its depletion during repetitive stimulation is likely to significantly influence synaptic responses (Tran *et al.*, 2022), a factor not considered in the current simulations.

The above arguments suggest a reasonable framework for explaining the filtering of γ trains by the LPP, although it seems unlikely that they will account for the seconds long period over which theta bursts are depressed during repetitive administration. Reducing extracellular Ca^{2+} restored within-burst frequency facilitation but with a magnitude that became progressively smaller across successive bursts, suggesting that the factors responsible for eliminating facilitation under control conditions were still operative. A simplistic interpretation may be that lowering external Ca^{2+} reduces the initial *p* sufficiently at high *p* synapses (i.e., VGLUT2) such that these synapses now primarily display classic frequency facilitation and RRP depletion does not occur. However, the notion that depletion of the RRP associated with high *p* synapses could explain the suppression observed across successive bursts separated by 200ms appears unlikely given the proposed rates of vesicle trafficking to the membrane (30-50ms). An alternative explanation may relate to mechanisms thought to underlie the Ca^{2+}-dependent transition of loosely associated vesicles to replenish the primed vesicle pool that influence release dynamics. The activity of Munc13 family proteins, critical for vesicle priming, are regulated by multiple Ca^{2+}-dependent processes (Junge *et al.*, 2004; Shin *et al.*, 2010), while latrunculin-sensitive cytoskeletal changes are additionally required for this transition of vesicles to a primed state (Miki *et al.*, 2016; Miki *et al.*, 2018). The latter is intriguing as long-term potentiation at the LPP-DG synapse is expressed presynaptically, and is dependent upon atypical endocannabinoid signaling that initiates cytoskeletal changes via activation of FAK and β1 integrin signaling (Wang *et al.*, 2016; Wang *et al.*, 2018b). Although speculative, this suggests the hypothesis that the LPP terminals are highly dynamic structures where bursts of afferent inputs (i.e., Θγ bursts) are capable of initiating cytoskeletal alterations within the terminal that influences the organization of the active zone so that release is impaired. Such alterations in the presynaptic cytoskeleton would be anticipated to persist for seconds, as experimentally observed.

References

Adelman JP, Maylie J & Sah P. (2012). Small-conductance Ca2+-activated K+ channels: form and function. *Annual review of physiology* **74,** 245-269.

Amani M, Lauterborn JC, Le AA, Cox BM, Wang W, Quintanilla J, Cox CD, Gall CM & Lynch G. (2021). Rapid Aging in the Perforant Path Projections to the Rodent Dentate Gyrus. *J Neurosci* **41,** 2301-2312.

Arai A, Silberg J & Lynch G. (1995). Differences in the refractory properties of two distinct inhibitory circuitries in field CA1 of the hippocampus. *Brain research* **704,** 298-306.

Barmashenko G, Hefft S, Aertsen A, Kirschstein T & Kohling R. (2011). Positive shifts of the GABAA receptor reversal potential due to altered chloride homeostasis is widespread after status epilepticus. *Epilepsia* **52,** 1570-1578.

Bellocchio EE, Hu HL, Pohorille A, Chan J, Pickel VM & Edwards RH. (1998). The localization of the brain-specific inorganic phosphate transporter suggests a specific presynaptic role in glutamatergic transmission. *Journal of Neuroscience* **18,** 8648-8659.

Bough KJ, Mott DD & Dingledine RJ. (2004). Medial perforant path inhibition mediated by mGluR7 is reduced after status epilepticus. *J Neurophysiol* **92,** 1549-1557.

Bragin A, Jando G, Nadasdy Z, Hetke J, Wise K & Buzsaki G. (1995). Gamma (40-100 Hz) oscillation in the hippocampus of the behaving rat. *The Journal of neuroscience : the official journal of the Society for Neuroscience* **15,** 47-60.

Breindl A, Derrick BE, Rodriguez SB & Martinez JL, Jr. (1994). Opioid receptor-dependent long-term potentiation at the lateral perforant path-CA3 synapse in rat hippocampus. *Brain research bulletin* **33,** 17-24.

Chen LY, Rex CS, Sanaiha Y, Lynch G & Gall CM. (2010). Learning induces neurotrophin signaling at hippocampal synapses. *Proc Natl Acad Sci U S A* **107,** 7030-7035.

Christie BR & Abraham WC. (1994). Differential regulation of paired-pulse plasticity following LTP in the dentate gyrus. *Neuroreport* **5,** 385-388.

Chrobak JJ & Buzsaki G. (1998). Gamma oscillations in the entorhinal cortex of the freely behaving rat. *The Journal of neuroscience : the official journal of the Society for Neuroscience* **18,** 388-398.

Chrobak JJ, Lorincz A & Buzsaki G. (2000). Physiological patterns in the hippocampo-entorhinal cortex system. *Hippocampus* **10,** 457-465.

Colgin LL. (2015). Theta-gamma coupling in the entorhinal-hippocampal system. *Current opinion in neurobiology* **31,** 45-50.

Colgin LL. (2016). Rhythms of the hippocampal network. *Nature reviews Neuroscience* **17,** 239-249.

Colgin LL, Denninger T, Fyhn M, Hafting T, Bonnevie T, Jensen O, Moser MB & Moser EI. (2009). Frequency of gamma oscillations routes flow of information in the hippocampus. *Nature* **462,** 353-357.

Cox BM, Cox CD, Gunn BG, Le AA, Inshishian VC, Gall CM & Lynch G. (2019). Acquisition of temporal order requires an intact CA3 commissural/associational (C/A) feedback system in mice. *Commun Biol* **2,** 251.

Davies CH, Starkey SJ, Pozza MF & Collingridge GL. (1991). GABA autoreceptors regulate the induction of LTP. *Nature* **349,** 609-611.

DeMaria CD, Soong TW, Alseikhan BA, Alvania RS & Yue DT. (2001). Calmodulin bifurcates the local Ca2+ signal that modulates P/Q-type Ca2+ channels. *Nature* **411,** 484-489.

Dittman JS & Ryan TA. (2019). The control of release probability at nerve terminals. *Nature reviews Neuroscience* **20,** 177-186.

Dolorfo CL & Amaral DG. (1998). Entorhinal cortex of the rat: topographic organization of the cells of origin of the perforant path projection to the dentate gyrus. *J Comp Neurol* **398,** 25-48.

Dolphin AC & Lee A. (2020). Presynaptic calcium channels: specialized control of synaptic neurotransmitter release. *Nature reviews Neuroscience* **21,** 213-229.

Doussau F, Schmidt H, Dorgans K, Valera AM, Poulain B & Isope P. (2017). Frequency-dependent mobilization of heterogeneous pools of synaptic vesicles shapes presynaptic plasticity. *eLife* **6**.

Eccles JC, Katz B & Kuffler SW. (1941). Nature of the "endplate potential" in curarized muscle. *Journal of neurophysiology* **4,** 362-387.

Edwards RH. (2007). The neurotransmitter cycle and quantal size. *Neuron* **55,** 835-858.

Ewell LA & Jones MV. (2010). Frequency-tuned distribution of inhibition in the dentate gyrus. *The Journal of neuroscience : the official journal of the Society for Neuroscience* **30,** 12597-12607.

Forsythe ID, Tsujimoto T, Barnes-Davies M, Cuttle MF & Takahashi T. (1998). Inactivation of presynaptic calcium current contributes to synaptic depression at a fast central synapse. *Neuron* **20,** 797-807.

Fremeau RT, Kam K, Qureshi T, Johnson J, Copenhagen DR, Storm-Mathisen J, Chaudhry FA, Nicoll RA & Edwards RH. (2004). Vesicular glutamate transporters 1 and 2 target to functionally distinct synaptic release sites. *Science* **304,** 1815-1819.

Fremeau RT, Troyer MD, Pahner I, Nygaard GO, Tran CH, Reimer RJ, Bellocchio EE, Fortin D, Storm-Mathisen J & Edwards RH. (2001). The expression of vesicular glutamate transporters defines two classes of excitatory synapse. *Neuron* **31,** 247-260.

Fujiyama F, Furuta T & Kaneko T. (2001). Immunocytochemical localization of candidates for vesicular glutamate transporters in the rat cerebral cortex. *The Journal of comparative neurology* **435,** 379-387.

Goutierre M, Al Awabdh S, Donneger F, Francois E, Gomez-Dominguez D, Irinopoulou T, Menendez de la Prida L & Poncer JC. (2019). KCC2 Regulates Neuronal Excitability and Hippocampal Activity via Interaction with Task-3 Channels. *Cell reports* **28,** 91-103 e107.

Granger R, Ambros-Ingerson J & Lynch G. (1989). Derivation of Encoding Characteristics of Layer II Cerebral Cortex. *J Cogn Neurosci* **1,** 61-87.

Gunn BG, Cox CD, Chen Y, Frotscher M, Gall CM, Baram TZ & Lynch G. (2017). The Endogenous Stress Hormone CRH Modulates Excitatory Transmission and Network Physiology in Hippocampus. *Cereb Cortex***,** 1-17.

Guthrie KM, Nguyen T & Gall CM. (1995). Insulin-like growth factor-1 mRNA is increased in deafferented hippocampus: spatiotemporal correspondence of a trophic event with axon sprouting. *The Journal of comparative neurology* **352,** 147-160.

Halasy K, Hajszan T, Kovacs EG, Lam TT & Leranth C. (2004). Distribution and origin of vesicular glutamate transporter 2-immunoreactive fibers in the rat hippocampus. *Hippocampus* **14,** 908-918.

Hargreaves EL, Rao G, Lee I & Knierim JJ. (2005). Major dissociation between medial and lateral entorhinal input to dorsal hippocampus. *Science* **308,** 1792-1794.

Herzog E, Gilchrist J, Gras C, Muzerelle A, Ravassard P, Giros B, Gaspar P & El Mestikawy S. (2004). Localization of VGLUT3, the vesicular glutamate transporter type 3, in the rat brain. *Neuroscience* **123,** 983-1002.

Hjorth-Simonsen A. (1972). Projection of the lateral part of the entorhinal area to the hippocampus and fascia dentata. *J Comp Neurol* **146,** 219-232.

Jackman SL & Regehr WG. (2017). The Mechanisms and Functions of Synaptic Facilitation. *Neuron* **94,** 447-464.

Jackman SL, Turecek J, Belinsky JE & Regehr WG. (2016). The calcium sensor synaptotagmin 7 is required for synaptic facilitation. *Nature* **529,** 88-+.

Jensen O & Colgin LL. (2007). Cross-frequency coupling between neuronal oscillations. *Trends Cogn Sci* **11,** 267-269.

Junge HJ, Rhee JS, Jahn O, Varoqueaux F, Spiess J, Waxham MN, Rosenmund C & Brose N. (2004). Calmodulin and Munc13 form a Ca2+ sensor/effector complex that controls short-term synaptic plasticity. *Cell* **118,** 389-401.

Kaneko T, Fujiyama F & Hioki H. (2002). Immunohistochemical localization of candidates for vesicular glutamate transporters in the rat brain. *The Journal of comparative neurology* **444,** 39-62.

Katz B & Miledi R. (1968). Role of Calcium in Neuromuscular Facilitation. *J Physiol-London* **195,** 481-&.

Koutsoumpa A & Papatheodoropoulos C. (2019). Short-term dynamics of input and output of CA1 network greatly differ between the dorsal and ventral rat hippocampus. *BMC Neurosci* **20,** 35.

Kramar EA, Lin B, Lin CY, Arai AC, Gall CM & Lynch G. (2004). A novel mechanism for the facilitation of theta-induced long-term potentiation by brain-derived neurotrophic factor. *The Journal of neuroscience : the official journal of the Society for Neuroscience* **24,** 5151-5161.

Larson J & Lynch G. (1986). Induction of synaptic potentiation in hippocampus by patterned stimulation involves two events. *Science* **232,** 985-988.

Larson J & Munkacsy E. (2015). Theta-burst LTP. *Brain research* **1621,** 38-50.

Lauterborn JC, Scaduto P, Cox CD, Schulmann A, Lynch G, Gall CM, Keene CD & Limon A. (2021). Increased excitatory to inhibitory synaptic ratio in parietal cortex samples from individuals with Alzheimer's disease. *Nature communications* **12,** 2603.

Le AA, Lauterborn JC, Jia Y, Wang W, Cox CD, Gall CM & Lynch G. (2022). Prepubescent female rodents have enhanced hippocampal LTP and learning relative to males, reversing in adulthood as inhibition increases. *Nat Neurosci* **25,** 180-190.

Lisman JE. (1997). Bursts as a unit of neural information: making unreliable synapses reliable. *Trends in neurosciences* **20,** 38-43.

Liu YC, Cheng JK & Lien CC. (2014). Rapid dynamic changes of dendritic inhibition in the dentate gyrus by presynaptic activity patterns. *The Journal of neuroscience : the official journal of the Society for Neuroscience* **34,** 1344-1357.

Lynch G, Matthews DA, Mosko S, Parks T & Cotman C. (1972). Induced acetylcholinesterase-rich layer in rat dentate gyrus following entorhinal lesions. *Brain research* **42,** 311-318.

Macek TA, Winder DG, Gereau RWt, Ladd CO & Conn PJ. (1996). Differential involvement of group II and group III mGluRs as autoreceptors at lateral and medial perforant path synapses. *J Neurophysiol* **76,** 3798-3806.

McNaughton BL. (1980). Evidence for two physiologically distinct perforant pathways to the fascia dentata. *Brain Res* **199,** 1-19.

McNaughton BL. (1982). Long-term synaptic enhancement and short-term potentiation in rat fascia dentata act through different mechanisms. *J Physiol* **324,** 249-262.

Miki T, Malagon G, Pulido C, Llano I, Neher E & Marty A. (2016). Actin- and Myosin-Dependent Vesicle Loading of Presynaptic Docking Sites Prior to Exocytosis. *Neuron* **91,** 808-823.

Miki T, Nakamura Y, Malagon G, Neher E & Marty A. (2018). Two-component latency distributions indicate two-step vesicular release at simple glutamatergic synapses. *Nature communications* **9,** 3943.

Mott DD & Lewis DV. (1991). Facilitation of the induction of long-term potentiation by GABAB receptors. *Science* **252,** 1718-1720.

Nakakubo Y, Abe S, Yoshida T, Takami C, Isa M, Wojcik SM, Brose N, Takamori S & Hori T. (2020). Vesicular Glutamate Transporter Expression Ensures High-Fidelity Synaptic Transmission at the Calyx of Held Synapses. *Cell reports* **32**.

Nanou E & Catterall WA. (2018). Calcium Channels, Synaptic Plasticity, and Neuropsychiatric Disease. *Neuron* **98,** 466-481.

Nanou E, Lee A & Catterall WA. (2018). Control of Excitation/Inhibition Balance in a Hippocampal Circuit by Calcium Sensor Protein Regulation of Presynaptic Calcium Channels. *Journal of Neuroscience* **38,** 4430-4440.

Neher E & Brose N. (2018). Dynamically Primed Synaptic Vesicle States: Key to Understand Synaptic Short-Term Plasticity. *Neuron* **100,** 1283-1291.

Ngo-Anh TJ, Bloodgood BL, Lin M, Sabatini BL, Maylie J & Adelman JP. (2005). SK channels and NMDA receptors form a Ca2+-mediated feedback loop in dendritic spines. *Nature neuroscience* **8,** 642-649.

Nicoll RA & Schmitz D. (2005). Synaptic plasticity at hippocampal mossy fibre synapses. *Nature reviews Neuroscience* **6,** 863-876.

Nusser Z, Sieghart W & Somogyi P. (1998). Segregation of different GABAA receptors to synaptic and extrasynaptic membranes of cerebellar granule cells. *The Journal of neuroscience : the official journal of the Society for Neuroscience* **18,** 1693-1703.

Pacelli GJ, Su W & Kelso SR. (1989). Activity-induced depression of synaptic inhibition during LTP-inducing patterned stimulation. *Brain research* **486,** 26-32.

Pan B & Zucker RS. (2009). A general model of synaptic transmission and short-term plasticity. *Neuron* **62,** 539-554.

Reagh ZM & Yassa MA. (2014). Object and spatial mnemonic interference differentially engage lateral and medial entorhinal cortex in humans. *Proceedings of the National Academy of Sciences of the United States of America* **111,** E4264-4273.

Rex CS, Chen LY, Sharma A, Liu J, Babayan AH, Gall CM & Lynch G. (2009). Different Rho GTPase-dependent signaling pathways initiate sequential steps in the consolidation of long-term potentiation. *The Journal of cell biology* **186,** 85-97.

Rohde J, Kirschstein T, Wilkars W, Muller L, Tokay T, Porath K, Bender RA & Kohling R. (2012). Upregulation of presynaptic mGluR2, but not mGluR3 in the epileptic medial perforant path. *Neuropharmacology* **62,** 1867-1873.

Sailer CA, Kaufmann WA, Marksteiner J & Knaus HG. (2004). Comparative immunohistochemical distribution of three small-conductance Ca2+-activated potassium channel subunits, SK1, SK2, and SK3 in mouse brain. *Molecular and cellular neurosciences* **26,** 458-469.

Saxena NC & Macdonald RL. (1994). Assembly of GABAA receptor subunits: role of the delta subunit. *The Journal of neuroscience : the official journal of the Society for Neuroscience* **14,** 7077-7086.

Seese RR, Chen LY, Cox CD, Schulz D, Babayan AH, Bunney WE, Henn FA, Gall CM & Lynch G. (2013). Synaptic abnormalities in the infralimbic cortex of a model of congenital depression. *The Journal of neuroscience : the official journal of the Society for Neuroscience* **33,** 13441-13448.

Seese RR, Wang K, Yao YQ, Lynch G & Gall CM. (2014). Spaced training rescues memory and ERK1/2 signaling in fragile X syndrome model mice. *Proceedings of the National Academy of Sciences of the United States of America* **111,** 16907-16912.

Shin OH, Lu J, Rhee JS, Tomchick DR, Pang ZP, Wojcik SM, Camacho-Perez M, Brose N, Machius M, Rizo J, Rosenmund C & Sudhof TC. (2010). Munc13 C2B domain is an activity-dependent Ca2+ regulator of synaptic exocytosis. *Nat Struct Mol Biol* **17,** 280-288.

Steward O. (1976). Topographic organization of the projections from the entorhinal area to the hippocampal formation of the rat. *J Comp Neurol* **167,** 285-314.

Stocker M. (2004). Ca(2+)-activated K+ channels: molecular determinants and function of the SK family. *Nature reviews Neuroscience* **5,** 758-770.

Sun MY, Ziolkowski L & Mennerick S. (2020). delta subunit-containing GABAA IPSCs are driven by both synaptic and diffusional GABA in mouse dentate granule neurons. *The Journal of physiology* **598,** 1205-1221.

Taschenberger H, Woehler A & Neher E. (2016). Superpriming of synaptic vesicles as a common basis for intersynapse variability and modulation of synaptic strength. *Proceedings of the National Academy of Sciences of the United States of America* **113,** E4548-4557.

Thomson AM. (2000). Facilitation, augmentation and potentiation at central synapses. *Trends in neurosciences* **23,** 305-312.

Tiwari MN, Mohan S, Biala Y & Yaari Y. (2018). Differential contributions of Ca(2+) -activated K(+) channels and Na(+) /K(+) -ATPases to the generation of the slow afterhyperpolarization in CA1 pyramidal cells. *Hippocampus* **28,** 338-357.

Tort AB, Komorowski RW, Manns JR, Kopell NJ & Eichenbaum H. (2009). Theta-gamma coupling increases during the learning of item-context associations. *Proceedings of the National Academy of Sciences of the United States of America* **106,** 20942-20947.

Toth K, Suares G, Lawrence JJ, Philips-Tansey E & McBain CJ. (2000). Differential mechanisms of transmission at three types of mossy fiber synapse. *The Journal of neuroscience : the official journal of the Society for Neuroscience* **20,** 8279-8289.

Tran V, Miki T & Marty A. (2022). Three small vesicular pools in sequence govern synaptic response dynamics during action potential trains. *Proceedings of the National Academy of Sciences of the United States of America* **119**.

Trieu BH, Kramar EA, Cox CD, Jia YS, Wang WS, Gall CM & Lynch G. (2015). Pronounced differences in signal processing and synaptic plasticity between piriform-hippocampal network stages: a prominent role for adenosine. *J Physiol-London* **593,** 2889-2907.

Tsao A, Moser MB & Moser EI. (2013). Traces of Experience in the Lateral Entorhinal Cortex. *Curr Biol* **23,** 399-405.

Urban NN, Henze DA & Barrionuevo G. (2001). Revisiting the role of the hippocampal mossy fiber synapse. *Hippocampus* **11,** 408-417.

Wang K, Lin MT, Adelman JP & Maylie J. (2014). Distinct Ca2+ sources in dendritic spines of hippocampal CA1 neurons couple to SK and Kv4 channels. *Neuron* **81,** 379-387.

Wang W, Cox BM, Jia Y, Le AA, Cox CD, Jung KM, Hou B, Piomelli D, Gall CM & Lynch G. (2018a). Treating a novel plasticity defect rescues episodic memory in Fragile X model mice. *Molecular psychiatry* **23,** 1798-1806.

Wang W, Jia Y, Pham DT, Palmer LC, Jung KM, Cox CD, Rumbaugh G, Piomelli D, Gall CM & Lynch G. (2018b). Atypical Endocannabinoid Signaling Initiates a New Form of Memory-Related Plasticity at a Cortical Input to Hippocampus. *Cereb Cortex* **28,** 2253-2266.

Wang W, Le AA, Hou B, Lauterborn JC, Cox CD, Levin ER, Lynch G & Gall CM. (2018c). Memory-Related Synaptic Plasticity Is Sexually Dimorphic in Rodent Hippocampus. *The Journal of neuroscience : the official journal of the Society for Neuroscience* **38,** 7935-7951.

Wang WS, Trieu BH, Palmer LC, Jia YS, Pham DT, Jung KM, Karsten CA, Merrill CB, Mackie K, Gall CM, Piomelli D & Lynch G. (2016). A Primary Cortical Input to Hippocampus Expresses a Pathway-Specific and Endocannabinoid-Dependent Form of Long-Term Potentiation. *eNeuro* **3**.

Wei W, Zhang N, Peng Z, Houser CR & Mody I. (2003). Perisynaptic localization of delta subunit-containing GABA(A) receptors and their activation by GABA spillover in the mouse dentate gyrus. *The Journal of neuroscience : the official journal of the Society for Neuroscience* **23,** 10650-10661.

Weston MC, Nehring RB, Wojcik SM & Rosenmund C. (2011). Interplay between VGLUT isoforms and endophilin A1 regulates neurotransmitter release and short-term plasticity. *Neuron* **69,** 1147-1159.

Witter MP. (1993). Organization of the Entorhinal Hippocampal System - a Review of Current Anatomical Data. *Hippocampus* **3,** 33-44.

Yoganarasimha D, Rao G & Knierim JJ. (2011). Lateral entorhinal neurons are not spatially selective in cue-rich environments. *Hippocampus* **21,** 1363-1374.

Zamponi GW & Currie KP. (2013). Regulation of Ca(V)2 calcium channels by G protein coupled receptors. *Biochimica et biophysica acta* **1828,** 1629-1643.

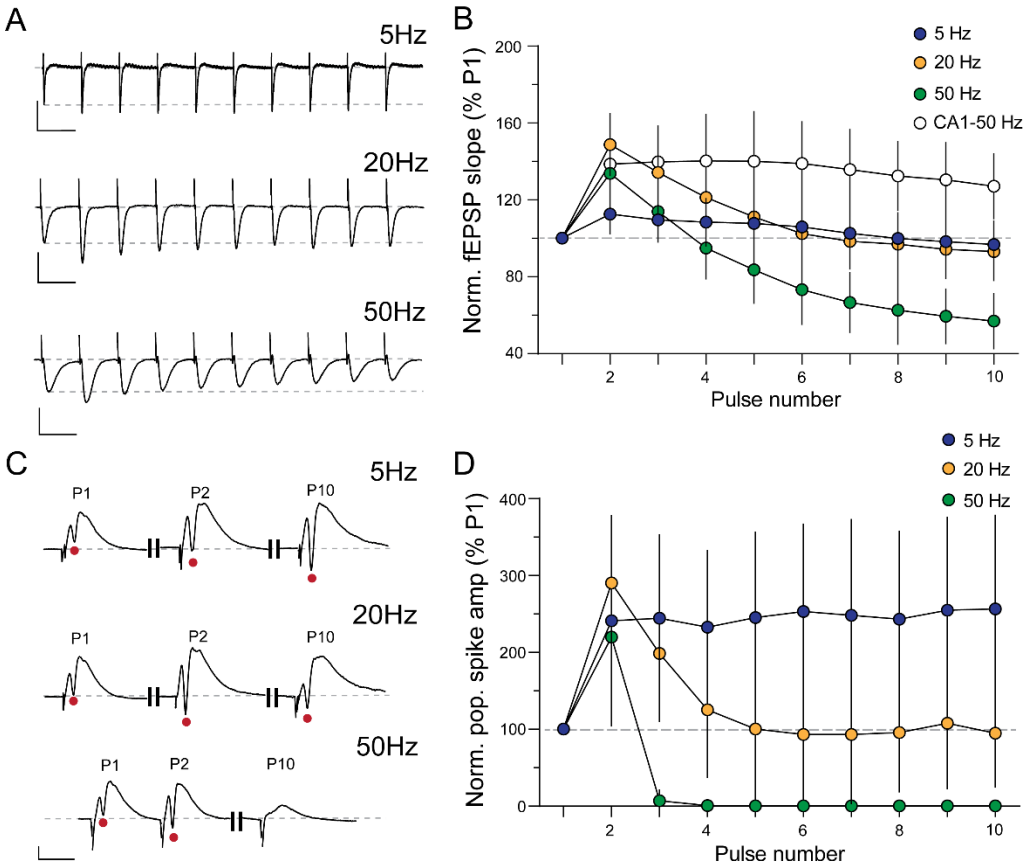

Figure 1.1. The LPP-DG synapse operates as a low pass filter. A. Representative traces recorded from the DG OML in response to LPP stimulation with 10 pulse trains delivered at 5, 20, and 50 Hz (Scale bars: 5Hz: y=1mV, x=200ms; 20Hz: y=1mV, x=50ms; 50Hz: y=1mV, x=20ms). **B.** Graph summarizing the within-train facilitation of the fEPSP slope for each stimulation frequency. Note the striking difference in the nature of the responses generated at LPP-DG (green circles) and CA3-CA1 (white circles) synapses following stimulation at 50Hz (For all frequencies, n= 21-22 slices/ 9 animals). **C.** Representative traces show the first two and final responses recorded from the granule cell layer with a 10-pulse stimulation train delivered to the LPP at 5, 20, and 50Hz. The stimulation intensity was increased to generate a small population spike (red circles; scale bars: y=1mV, x=10ms). **D.** Graph summarizing the within-train facilitation of the population spike amplitude for each stimulation frequency (5 and 20Hz, n=7 slices; 50Hz, n=10 slices; n=4 mice per frequency). Note the extreme filtering of spike output at frequencies in the γ (50Hz) range.

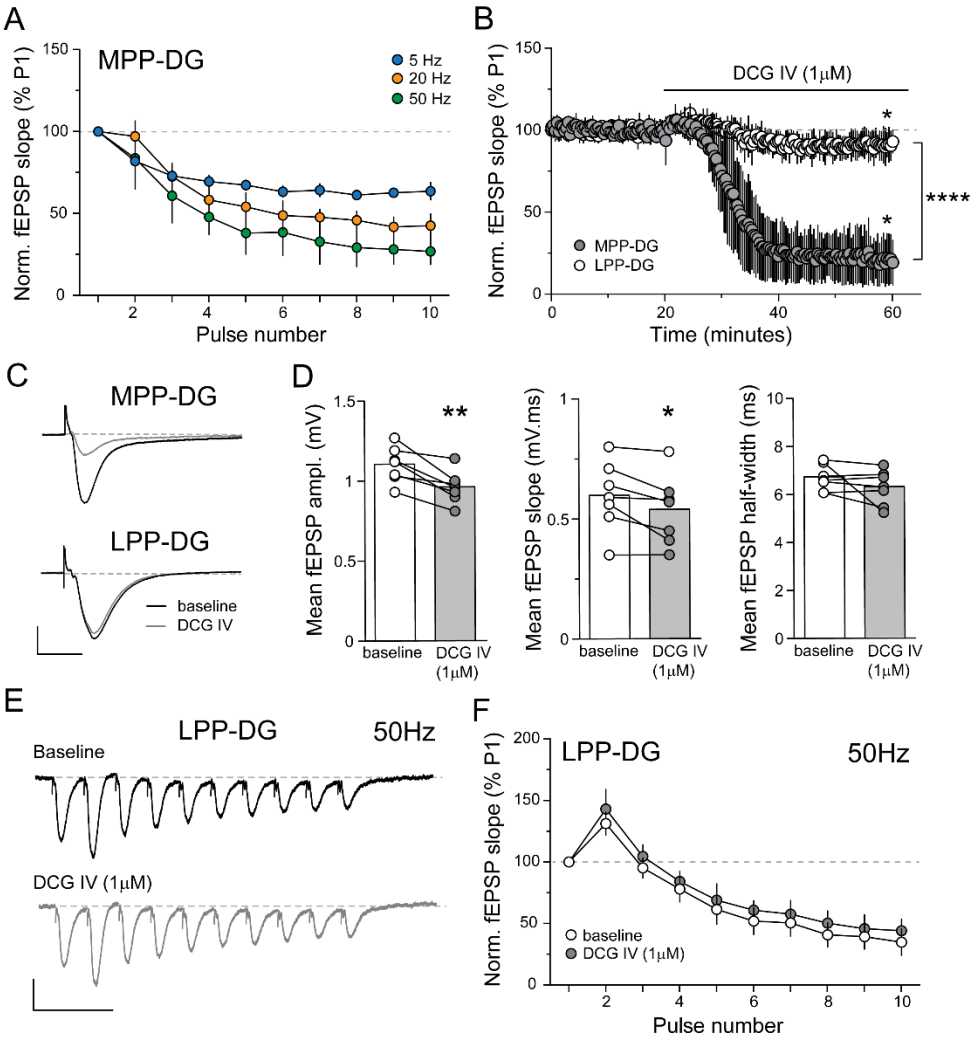

Figure 1.2. Low pass filtering at the LPP-DG synapse is independent of MPP inputs. A. Graph summarizing the fEPSP slope responses of the MPP reveals a depression across all three frequency trains (5Hz; 20Hz; 50Hz). **B.** Infusion of the mGluRII agonist DCG IV (1μM) markedly depressed baseline MPP fEPSPs (MPP: t_2=9.88, *p=0.01, average of the last 5 min before and after infusion). DCG IV infusion has much smaller effects on LPP-DG fEPSPs (LPP: t_6=3.18, *p=0.02; MPP vs LPP: t_8=9.6, ****p<0.0001; LPP n=7 slices/ 5 mice; MPP=3 slices/ 2 mice, unpaired Student's t-test of the average of the last 5 min). **C.** Representative traces of MPP (top) and LPP (bottom) -DG responses before (black) and after (grey) DCG IV infusion. **D.** Summary graphs showing the effects of DCG IV on LPP-DG fEPSP amplitude (**p=0.004, paired t-test), slope (*p=0.028), and half width (p=0.209) for individual slices (n=7 slices/ 5 mice). **E**. Representative traces recorded from the OML of the DG in response to LPP stimulation with a 10 pulse 50Hz train before (black) and 40 min after (grey) bath application of DCG IV (1μM). **F.** The within-train depression of fEPSP slopes of LPP-DG synapses at 50Hz was not influenced by 40 min DCG IV infusion ($F_{(9,54)}$=1.06, n=7 slices/ mice per group, p=0.41, two way RM ANOVA).

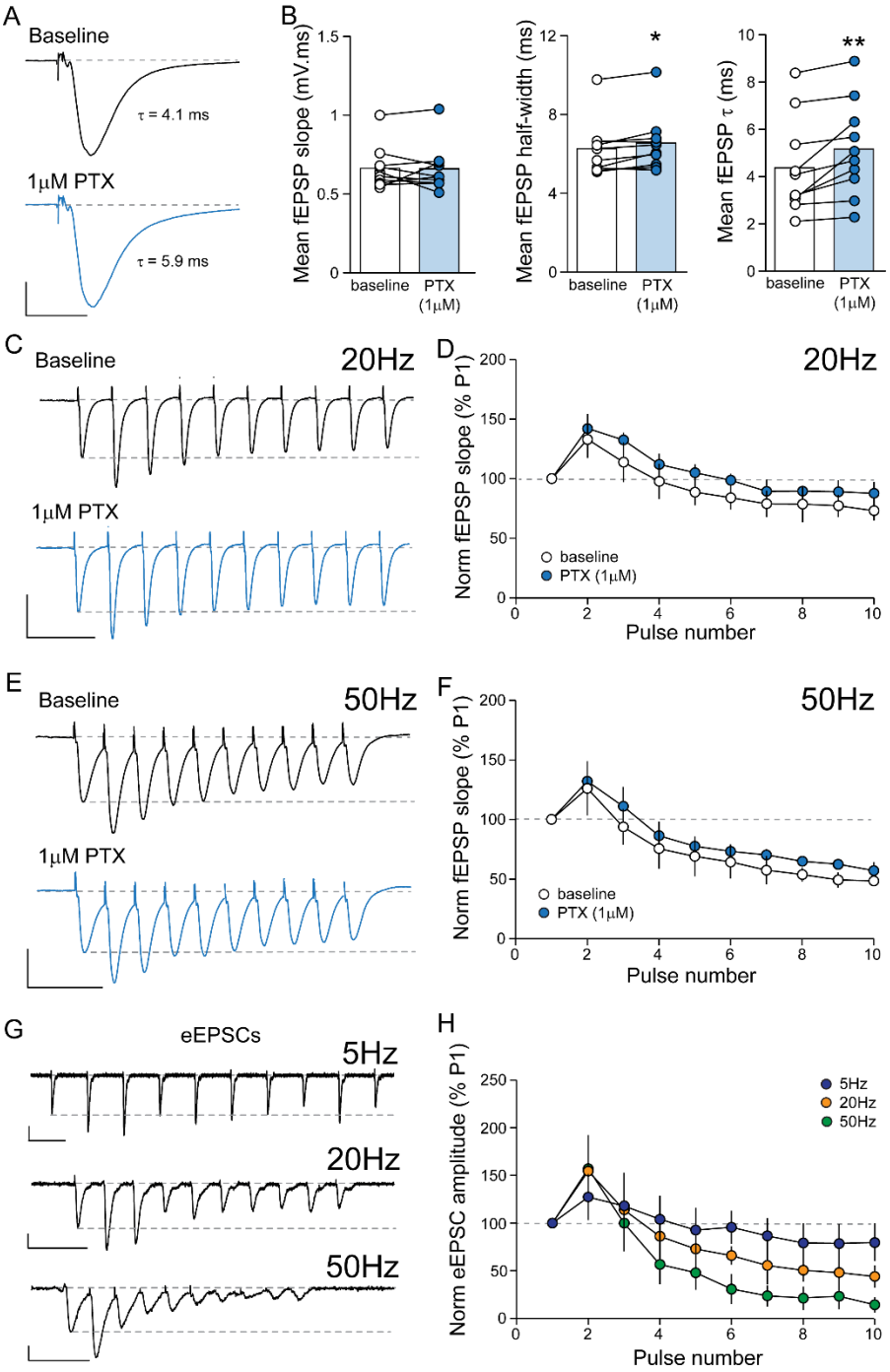

Figure 1.3. The LPP-DG low pass filter is not dependent upon GABAergic inhibition. A. Ensemble averages of LPP fEPSPs recorded from a representative slice in the absence (top) and presence (bottom) of picrotoxin (PTX; 1μM) (Scale bars: y = 0.5 mV, x = 10 ms). **B.** Summary graphs show the effect of PTX on the mean slope, half width and decay τ of the LPP fEPSPs. Note that PTX significantly increased the fEPSP duration and decay time (*p=0.012; **p=0.007; baseline vs PTX paired Student's t-test; n=10 slices/ 5 mice). **C.** Representative

traces recorded from the DG OML with stimulation (10 pulses) of the LPP at 20Hz before (black) and after (blue) PTX infusion (Scale bars: y=1mV, x=100ms). **D.** Graph showing the within-train facilitation of the fEPSP slope with 20Hz LPP stimulation in the absence and presence of bath PTX (*p=0.049, $F_{(9, 36)}$=2.167 two-way RM-ANOVA pulse number vs PTX; n=5 slices/ 2 mice). **E.** Representative traces show fEPSP responses to LPP stimulation (10 pulses) at 50Hz before (black) and after (blue) bath application of PTX (Scale bars: y=1mV, x=50ms). **F.** Graph shows the within-train facilitation of the fEPSP slope with 50Hz LPP stimulation in the absence and presence of PTX (p=0.371, $F_{(9, 36)}$=1.125 two-way RM- ANOVA pulse number vs PTX; n=5 slices/ 2 mice). **G**. Representative eIPSCs recorded from an exemplar granule cell in response to LPP stimulation at 5Hz, 20Hz, and 50Hz (Scale bars: y=50pA, x=200ms, 100ms & 50ms). **H.** Graph shows the within-train facilitation of the eEPSC for each stimulation frequency (n= 7 cells/ frequency / 4 mice).

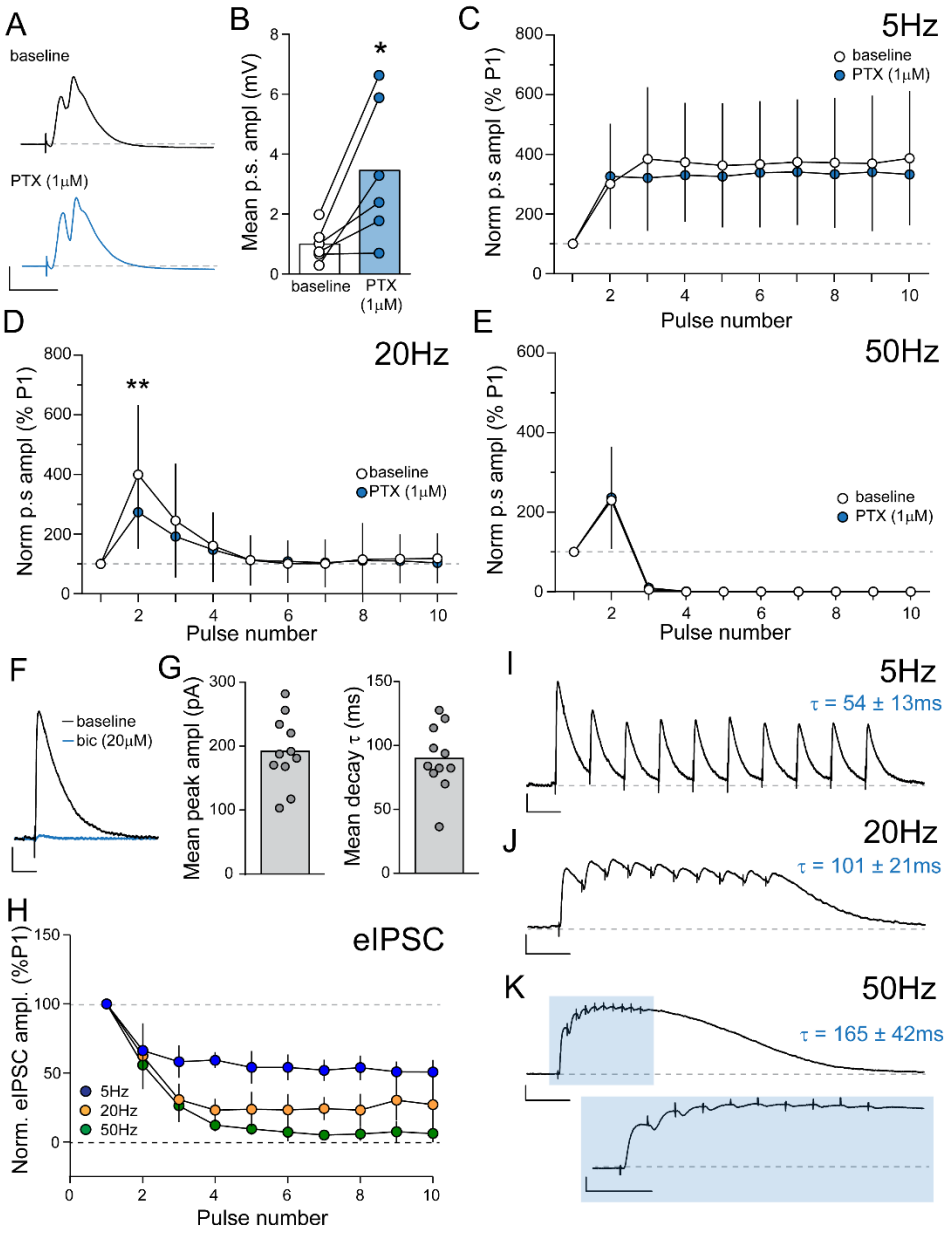

Figure 1.4. GABAergic inhibition does not shape granule cell output with LPP activation at Θ, β, and γ frequencies. A. Ensemble average LPP-evoked fEPSP recorded from a representative slice in the absence (black) and presence (blue) of picrotoxin (PTX) shows an increase in population spike (p.s) amplitude with PTX infusion (Scale bars: y=1mV, x=10ms). **B.** Bar graph summarizing the mean population spike amplitude before (white) and following (blue) PTX infusion (t_5=3.10, p=0.027, n= 6 slices/ 4 mice; paired Student's t-test). **C.** Plot of DG normalized population spike amplitude across a 10-pulse, 5Hz train, shows that the facilitation of response amplitude is unaffected by PTX ($F_{(9,54)}$=0.9938, p=0.4562, two-way RM-ANOVA; n=7 slices/ 4 mice). **D.** At 20Hz, PTX infusion significantly decreased amplitude of DG population-spike elicited by the second pulse only of a 10 pulse train ($F_{(9,45)}$=3.392, **p=0.001, n=6 slices/ 4 mice) **E.** PTX did not influence population spike responses to a 10-pulse, 50Hz train; In both cases there was no detectible population spike by pulse 4 ($F_{(9,45)}$=0.0231, p>0.999,

n=7 slices/ 4 mice). **F.** Representative eIPSCs recorded from an exemplar dentate gyrus granule cell in response to stimulation of the LPP. Bath application of bicuculline (bic; blue) completely blocked the evoked response (Scale bars: y=50pA, x=100ms). **G.** Bar graphs summarizing the mean peak amplitude and decay time) of eIPSCs recorded from dentate gyrus granule cells. **H**. Graph summarizing the normalized within-train suppression of eIPSC amplitude in response to stimulation at 5Hz, 20Hz and 50Hz frequencies (n=7 cells/ 4 mice). Note that suppression of the eIPSC although evident at all frequencies shows frequency-dependence. Representative eIPSCs recorded from an exemplar dentate gyrus granule cell in response to stimulation of the LPP at 5Hz (**I**), 20Hz (**J**) and 50Hz (**K**). The evoked responses to 50Hz stimulation are illustrated on an expanded time scale. Scale bars: 5Hz: y=50pA, x=200ms; 20Hz: y=100pA, x=100ms; 50Hz: y=100pA, x=100ms (top) & 50ms (bottom).

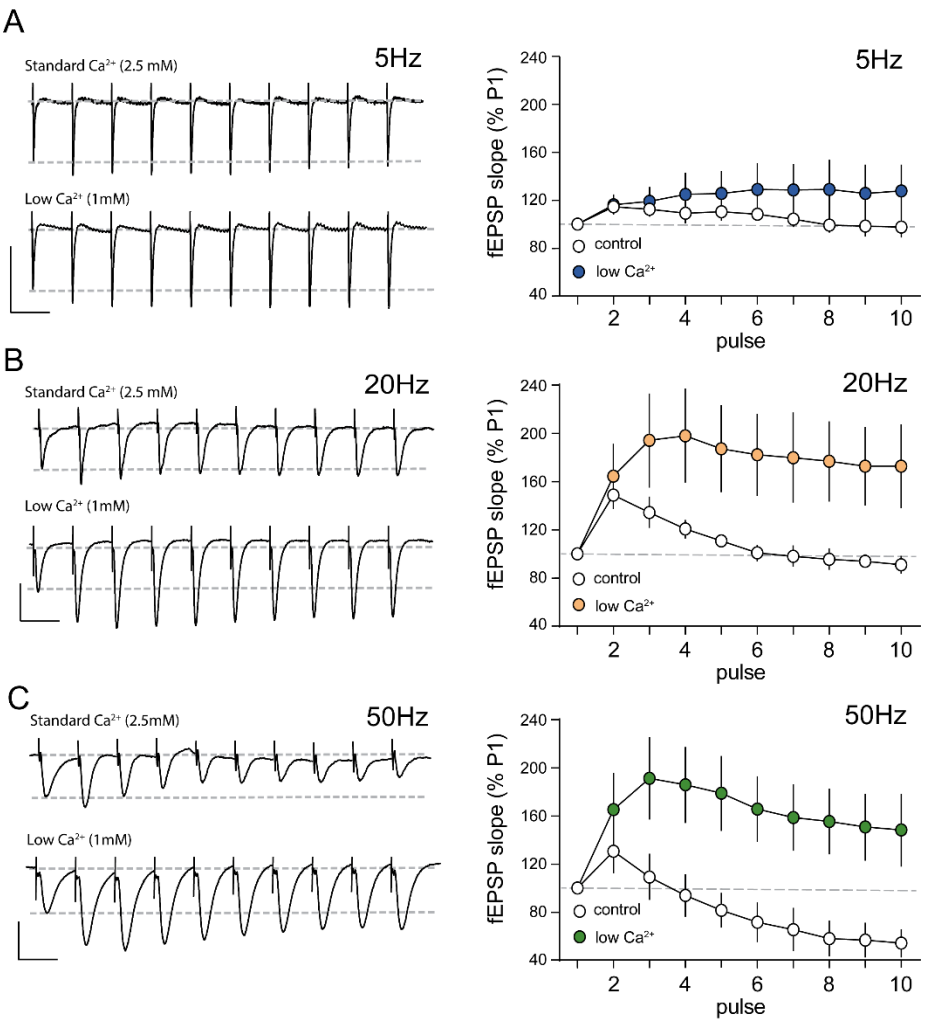

Figure 1.5. The low pass filter at the LPP-DG synapse is removed by reducing release probability. Representative traces show LPP responses to stimulation trains (10 pulses) delivered at Θ (5Hz) (**A**), β (20Hz) (**B**) and γ (50Hz) (**C**) frequencies under high (2.5mM; top) and low (1mM; bottom) Ca^{2+} conditions. Corresponding line graphs (right) illustrate the nature of within-train facilitation and suppression under the different Ca^{2+} conditions (n=7-12 slices/ group; n=4-5 mice/ group). Note the marked increase in facilitation, particularly at higher stimulation frequencies, when external Ca^{2+} is reduced. Scale bars: 5 Hz: y=1mV, x=200ms; 20Hz: y=1mV, x=50ms; 50Hz: y=1mV, x=20ms.

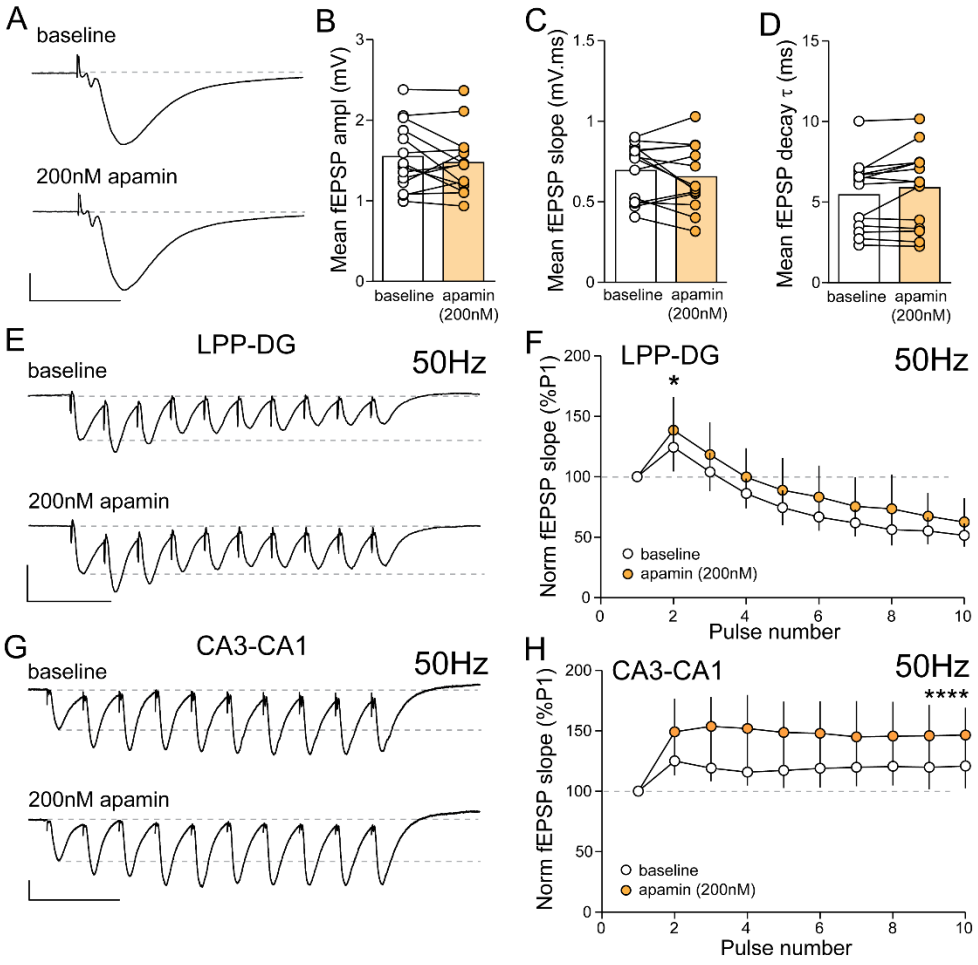

Figure 1.6. The LPP-DG low pass filter does not require activation of Ca2+-dependent SK channels. A. Ensemble averages of fEPSPs recorded from a representative slice in the absence (top) and presence (bottom) of the SK channel antagonist apamin (200nM; scale bars: y = 0.5 mV, x = 10 ms). **B-D.** Graphs show the effect of apamin upon the mean amplitude (**B**), slope (**C**), and decay τ (**D**) of LPP-evoked fEPSPs (bars show group means; points show individual slice measures). Apamin had no significant effect on any of the fEPSP parameters (amplitude: p=0.309; slope: p=0.267; τ: p=0.053 baseline vs apamin paired Student's t test; n=14 slices/ 7 mice). **E.** Representative traces show LPP responses to 10 pulse stimulation trains delivered at 50Hz before (top) and after (bottom) apamin infusion (Scale bars: y=1mV; x=50ms). **F.** Graph summarizing the within-train facilitation of fEPSP slope with and without apamin present. The inhibitor significantly increased facilitation only during the second pulse (*p=0.027 at pulse 2, $F_{(9,63)}$=2.290 two- way RM- ANOVA, n=8 slices/ 4 mice). **G.** Representative traces show fEPSP responses to field CA3-CA1 Schaffer-commissural stimulation at 50Hz (10-pulse trains) before (top) and after (bottom) apamin infusion. **H.** The within train facilitation was enhanced 40 min after apamin infusion onset through the duration of the train ($F_{(9,54)}$= 4.67, ****p<0.0001, n=7 slices/ 5 mice, two- way RM- ANOVA).

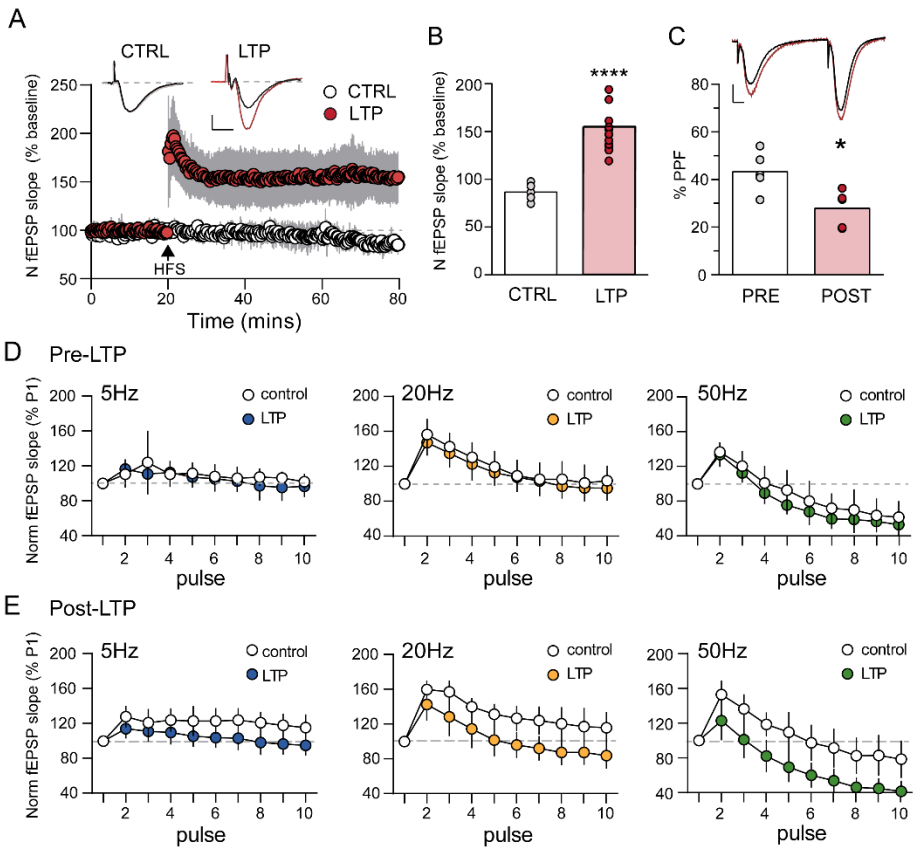

Figure 1.7. LTP modifies synaptic filtering at the LPP-DG synapse. A. LTP was induced in the LPP-DG synapses via high frequency stimulation (HFS, at upward arrow) that resulted in a 50% increase in response compared to slices that did not receive HFS. Representative traces show LPP responses before and 60 min after HFS (right) or control low frequency stimulation (left) (Scale bars: y=0.5mV, x=5ms) (n= 12 slices/ 7 mice). **B.** The mean response (fEPSP slope) recorded 55-60 min post-HFS, normalized to same-slice baseline, was markedly potentiated relative to similarly normalized measures from control slices ($t_{(17)}$=6.14, ****p<0.0001, paired t-test of the average of the last 5 min). **C.** *Top:* Representative traces of paired-pulse stimulation of the LPP-DG (40ms between pulses) before (black) and 60 min after (red) LPP-LTP induction. *Bottom:* PPF of the fEPSP slope was reduced 60 min after inducing LPP-LTP relative to baseline levels (t_4=3.02, n=5 slices/ 3 mice, *p=0.039; scale bars: y=0.5mV, x=5ms). **D.** Responses to trains of 5, 20 and 50 Hz stimulation applied to the LPP before HFS (or control LFS), reveal no differences between the groups (5Hz: $F_{(9,135)}$=1.85, p>0.05; 20Hz: $F_{(9,153)}$=0.75, p>0.05; 50Hz: $F_{(9,135)}$=1.56, p>0.05, two- way RM- ANOVA). **E.** Responses to stimulation trains applied to the LPP 45-60 min after LTP induction, revealed striking differences in the pattern of frequency facilitation for slices that were potentiated compared to those (control) that were not. At 5 Hz, facilitation is sustained throughout the train in control slices but was absent in slices that had been potentiated (Interaction between pulse number and groups: $F_{(9,162)}$= 5.41, ****p<0.0001). The frequency facilitation profiles are also significantly different between control and LTP slices in response to 20 Hz stimulation (interaction $F_{(9,153)}$= 5.78, ****p<0.0001) and 50 Hz ($F_{(9,135)}$=5.85, ****p<0.0001). For all figures n= 11 slices/ 7 mice, unless otherwise specified.

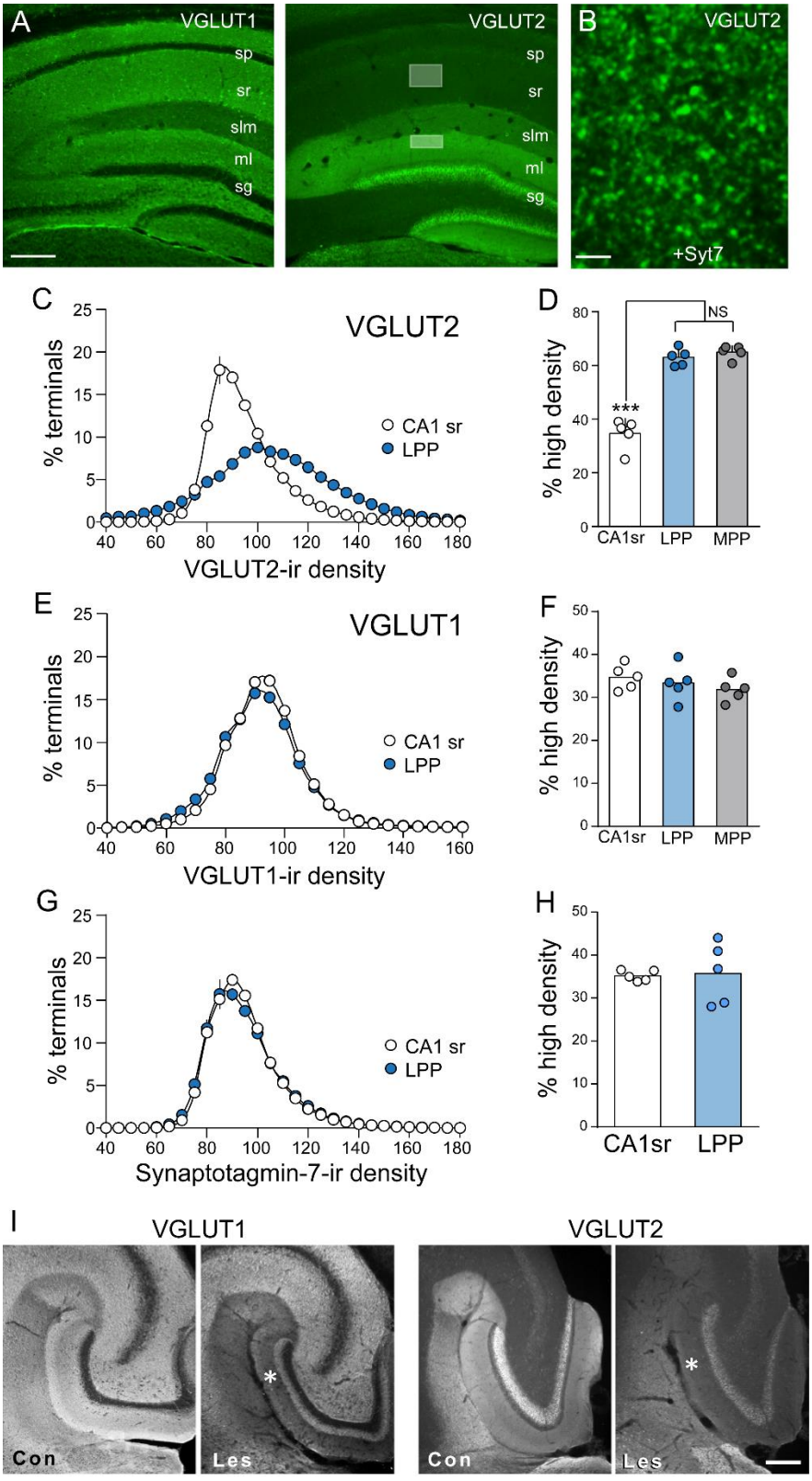
A
VGLUT1
sp
sr
slm
ml
sg
VGLUT2
sp
sr
slm
ml
sg
B
VGLUT2
+Syt7
C
VGLUT2
% terminals
CA1 sr
LPP
VGLUT2-ir density
D
NS
***
% high density
CA1sr
LPP
MPP
E
VGLUT1
% terminals
CA1 sr
LPP
VGLUT1-ir density
F
% high density
CA1sr
LPP
MPP
G
% terminals
CA1 sr
LPP
Synaptotagmin-7-ir density
H
% high density
CA1sr
LPP
I
VGLUT1
VGLUT2
Con
Les
Con
Les

Figure 1.8. VGLUT2 is selectively concentrated in LPP terminals. A. Representative photomicrographs of VGLUT1- and VGLUT2-immunoreactivity (ir) in mouse hippocampal subfields. The shaded boxes illustrate the sample fields used for FDT analyses of terminals in the DG OML for the LPP and CA1 stratum radiatum (sr) for CA3-CA1 terminals. Calibration bar, 200 µm. sp, stratum pyramidale; slm, stratum lacunosum-moleculare; ml, molecular layer of the DG; sg, stratum granulosum. **B.** Photomicrograph of VGLUT2-ir in the LPP field. Inset shows double-labeling for both VGLUT2 (green) and Syt7 (red) in the LPP field; double-labeled profiles are seen as either touching or overlapping (yellow). Calibration bar, 1 µm; 0.6 µm for inset. **C.** Intensity frequency distribution curves for VGLUT2-ir in Syt-7 positive terminals in CA1 sr and the LPP ($F_{(50,400)}$=63.52; ***p<0.0001; n = 5 mice/group); plots show group mean ± SEM values throughout (note, some error bars are short and covered by symbols for panels C,E and G). **D.** Bar graph shows there is a greater percentage of terminals with high density VGLUT2-ir in the LPP field as compared to CA1 sr ($F_{(2,12)}$= 84.56, p < 0.0001, 1-way AVOVA; ***p < 0.0001, Tukey's; high density is ≥100 in panel C, E) Note that percentage of synapses with high density VGLUT2-ir is not significantly different between the LPP and MPP fields (p=0.558, Tukey's). **E.** Intensity frequency distribution curves for VGLUT1-ir in Syt-7 positive presynaptic terminals in CA1 sr and the LPP ($F_{(31,248)}$= 5.533; ***p< 0.0001; n= 5 mice/group). **F.** Bar graph shows the percentage of terminals with high density (≥100) levels of VGLUT1-ir ($F_{(2,12)}$= 1.056, p = 0.3781). **G.** Intensity frequency distribution curves for Syt7-ir in CA1 sr and the LPP ($F_{(50,400)}$= 1.358; p = 0.0602). **H.** Bar graph shows the percentage of terminals with high density (≥100) levels of Syt7-ir (p = 0.8859, paired Student's t-test). **I.** Photomicrographs of VGLUT1-ir and VGLUT2-ir in the DG molecular layer ipsilateral to an entorhinal cortex lesion (Les) and on the contralateral, control (Con) side; asterisks denote the loss of immunolabeling in the perforant path terminal fields. Calibration bar, 200 µm.

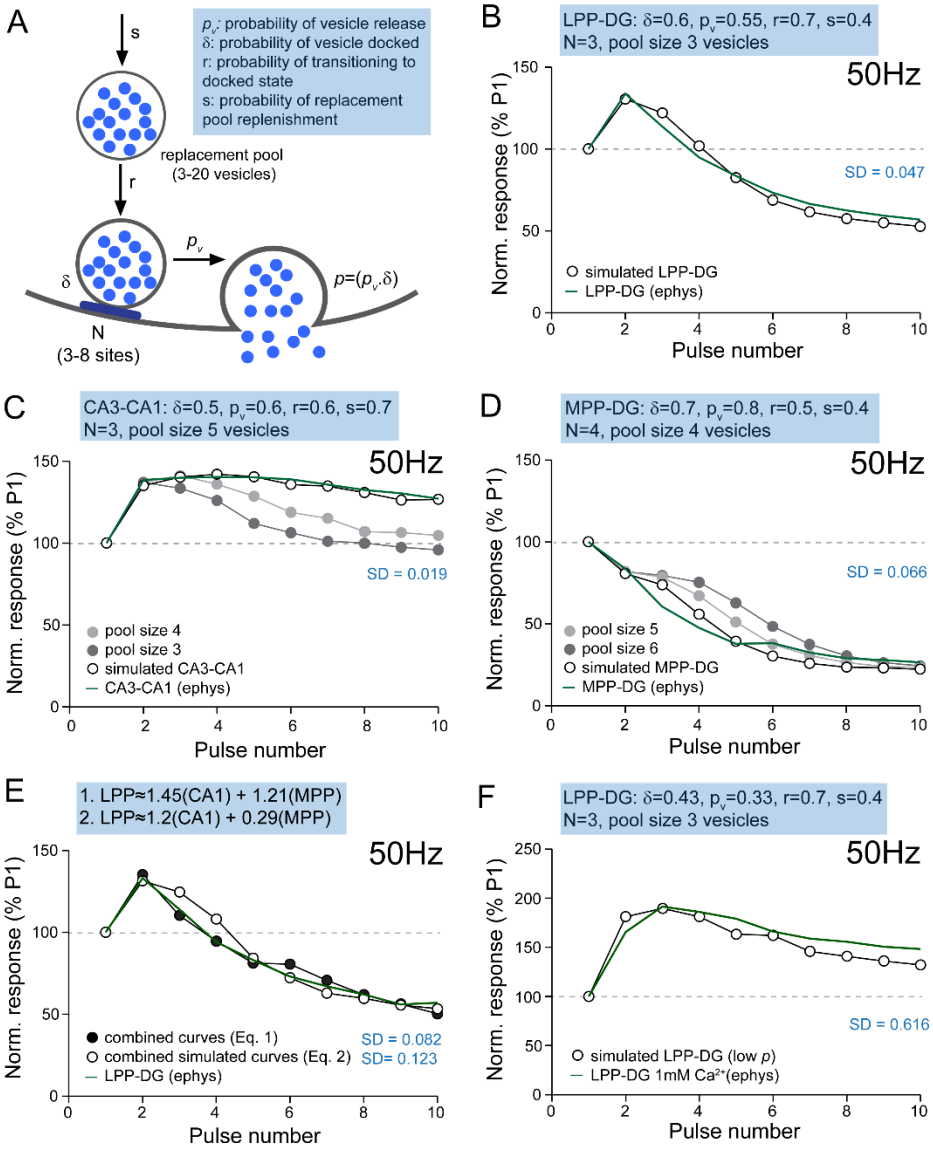

Figure 1.9. Monte Carlo simulations of a two-step release model recapitulate the output curves across three different types of synapse. A. Schematic illustrating the variables within the two-step model. **B.** Using physiologically constrained parameters, the two-step model (white circles) reliably recapitulates the electrophysiologically recorded responses (green line) following γ frequency stimulation of the LPP. When constrained by initial *p*, the two-step model reliably recapitulates the low *p* CA3-CA1 synapse (**C**) and high *p* MPP-DG synapse (**D**). Note that the simulated output at both of these synapses was highly sensitive to the pool size. **E**. The LPP-DG output curve (green line) could be replicated by combining either the simulated (white circles) or empirically measured (black circles) CA3-CA1 and MPP-DG curves when weighted appropriately. The equations used to generate each curve are given above. **F.** Reducing the initial *p* prevented the simulated within train suppression of responses (white circles), producing an output curve similar to that recorded electrophysiologically under conditions of low external Ca^{2+} (green line).

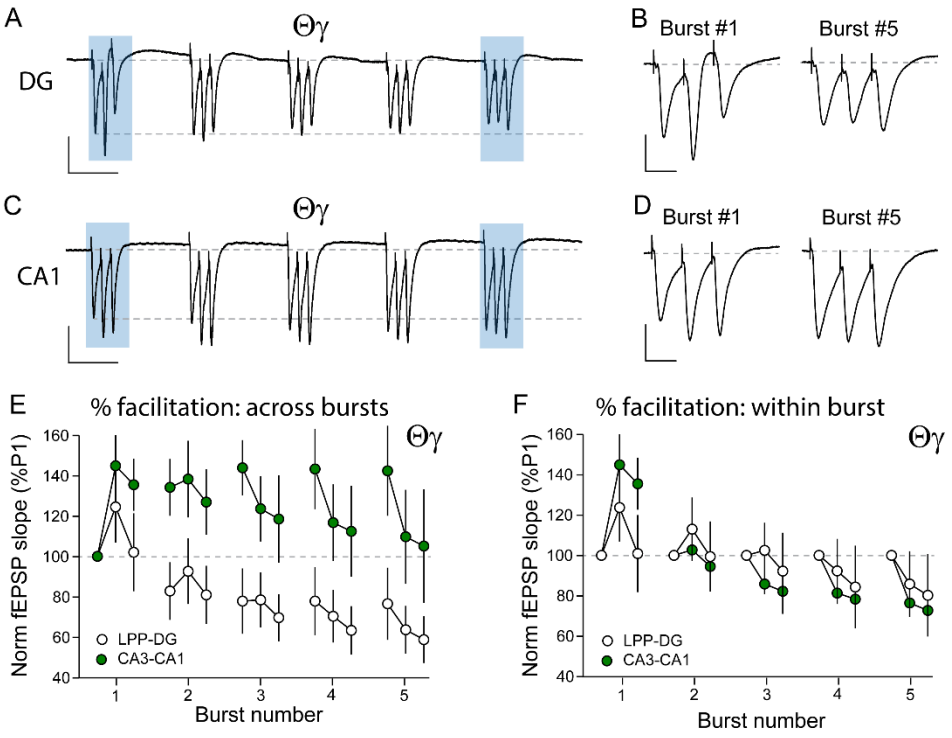

Figure 1.10. Processing short bursts of g frequency information occurs differently at LPP-DG and CA3-CA1 synapse. Representative traces recorded from the OML of the DG (**A, B**) and str. radiatum of CA1 (**C, D**) in response to five γ frequency bursts (3 pulses) delivered at intervals of 200ms (i.e.Θγ) via the LPP and Schaffer-commissural (CA3-CA1) projections, respectively (LPP-DG: n=39 slices/ 13 mice; CA3-CA1: n=7 slices/ 4 mice). The responses to pulse 1 and pulse 5 (shaded areas) are illustrated on an expanded time scale for LPP-DG (**B**) and CA3-CA1 (**D**); scale bars: y=1 mV, x=100 ms (A,C) or 20ms (B,D). **E**. Graph summarizing the change in fEPSP slopes (relative to the initial response of the first burst) during Θγ stimulation (5 bursts) at LPP-DG and CA3-CA1 synapses. Note that CA3-CA1 exhibit facilitation that is maintained across successive bursts whereas suppression occurs at LPP-DG synapses. **F.** Graph summarizing the decline in within-burst facilitation that occurs across successive bursts delivered at Θγ patterns at CA3-CA1 and LPP-DG synapses. Other than the marked difference in facilitation of the first burst, both synapses show a similar decline across successive bursts.

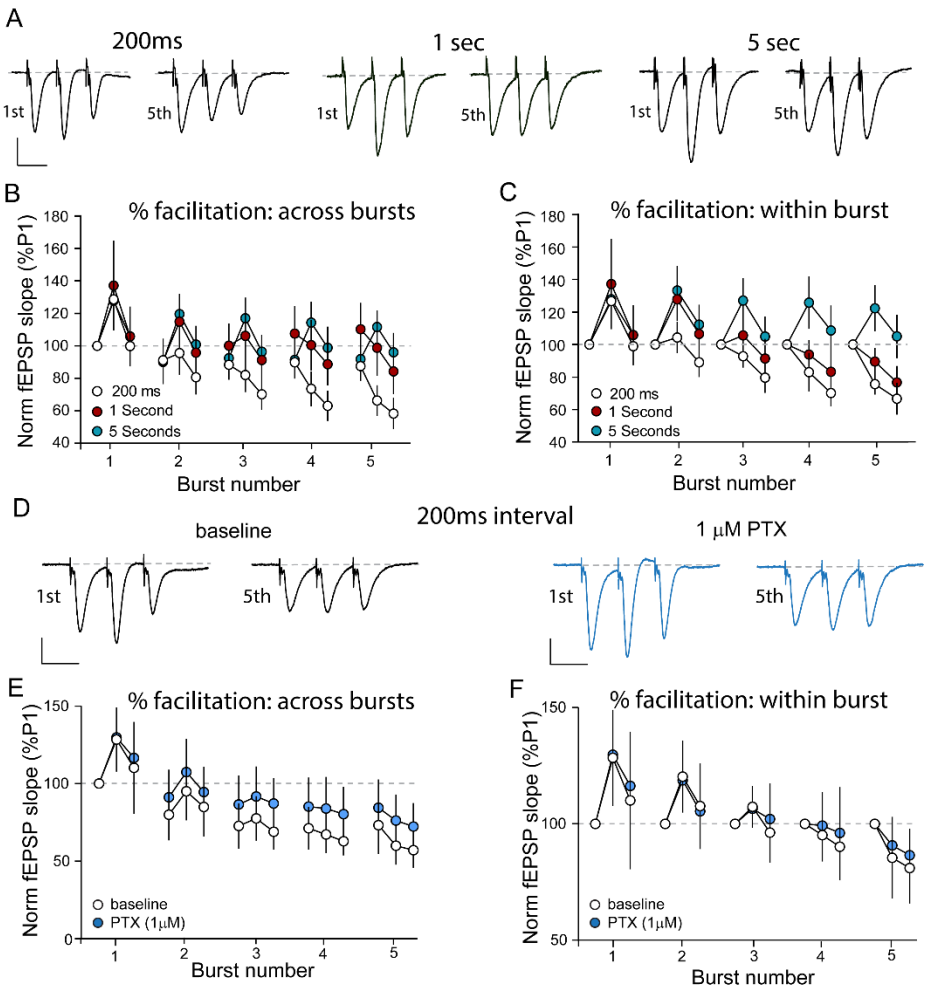

Figure 1.11. Suppression of within-burst facilitation persists for a prolonged period and does not involve enhanced GABAAR-mediated inhibition. A. Illustrated are representative responses of the LPP to the 1st and 5th burst recorded from the OML of the DG evoked during a train of five γ frequency bursts (3 pulses) delivered to the LPP with intervals of 200ms, 1 second and 5 seconds (scale bars: y=0.5mV, x= 20ms). **B.** Graph summarizing the change in fEPSP slopes (relative to the initial response of the first burst) during stimulation of the LPP with γ frequency bursts (5 bursts) separated by intervals indicated (200ms: n=19 slices/ 8 mice; 1 sec: n=11 slices/ 5 mice; 5 sec: n=14 slices/ 3 mice). **C.** Graph summarizing the within-burst facilitation that occurs across successive bursts delivered at intervals indicated. Note that the within-burst facilitation is maintained when bursts are separated by intervals of 5 sec (blue symbols) (200ms: n=19 slices/ 8 mice; 1 sec: n=11 slices/ 5 mice; 5 sec: n=14 slices/ 3 mice). **D.** Representative responses to the 1st and 5th burst recorded from the OML evoked during a train of five γ frequency bursts (3 pulses) delivered to the LPP at intervals of 200ms before (black) and after (blue) bath application of PTX (scale bars: y=0.5mV, x=20ms). **E**. Graph summarizing the change in fEPSP slopes (relative to the initial response of the first burst) during Θγ stimulation (5 bursts) before (white circle) and after (blue circle) bath application of PTX. Treatment with PTX results in a modest enhancement of responses across bursts ($F_{(14-112)}$=1.964, p=0.0269, n=9 slices/ 4 mice per group, two- way RM- ANOVA). **F.** Graph showing

the similar decline in within-burst facilitation that occurs across successive bursts delivered at Θγ patterns before (white circle) and after (blue circle) PTX ($F_{(14,112)}$=0.5098, p=0.9232, n=9 slices/ 4 mice per group, two- way RM- ANOVA).

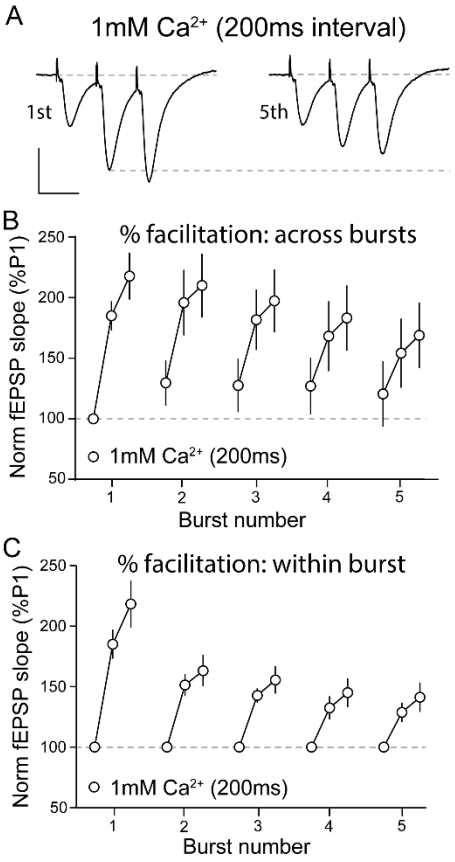

Figure 1.12. Reducing the initial release probability (p) removes the filter associated with brief γ frequency bursts at the LPP-DG synapse. A. Representative responses to the 1st and 5th burst recorded in low Ca^{2+} (1mM) aCSF from the OML of the DG evoked during a train of five γ frequency bursts (3 pulses) delivered to the LPP at intervals of 200ms (scale bars: y=0.5mV, x=20ms). **B**. Graph summarizing the change in fEPSP slopes (relative to the initial response of the first burst) during Θγ stimulation (5 bursts, 200ms interval) under low external Ca^{2+} (n=8 slices/ 4 mice). **C.** Graph summarizing the within-burst facilitation that occurs across successive bursts delivered at Θγ patterns. Under low external Ca^{2+}, both initial response and within-burst facilitation is maintained across bursts, although the latter declines across successive bursts (n=8 slices/ 4 mice).

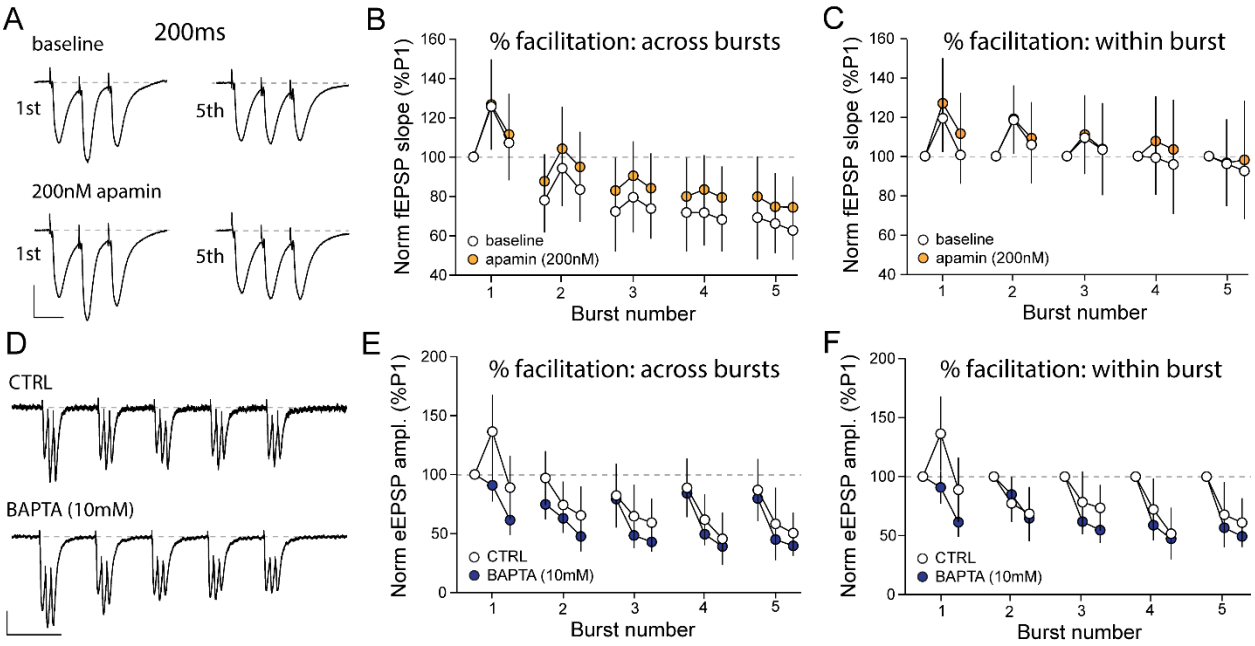

Figure 1.13. Postsynaptic Ca2+-dependent mechanisms do not contribute to the prolonged suppression of within burst facilitation. A. Representative responses to the 1st and 5th burst recorded from the DG OML evoked during a train of five γ frequency bursts (3 pulses) delivered to the LPP at intervals of 200ms before (top) and during (bottom) bath application of the SK channel antagonist apamin (200nM; scale bars: y=0.5mV, x=20ms). **B**. Graph summarizing the change in fEPSP slopes (relative to the initial response of the first burst) during Θγ stimulation (5 bursts) before (white circle) and after (orange circle) bath application of apamin. Apamin caused a modest enhancement of responses across bursts ($F_{(14\text{-}182)}$=2.459, p=0.003, n=13 slices/ 4 mice; two- way RM-ANOVA;). **C.** Graph summarizing the decline in within-burst facilitation that occurs across successive bursts delivered at Θγ patterns before (white circle) and with (orange circle) apamin present. Note the marked decline in the within-burst facilitation occurring across bursts during Θγ stimulation is modestly enhanced by apamin ($F_{(14\text{-}182)}$=1.873, p=0.032, n=13 slices/ 4 mice; two- way RM- ANOVA). **D**. Exemplar eEPSCs recorded from DG granule cells following Θγ stimulation of the LPP without (top) and with (bottom) the Ca^{2+} chelator BAPTA in the electrode's internal solution (scale bars: y=50pA, x=200ms). **E. F.** Graphs summarizing the relative change in the amplitude of eEPSC across bursts (**E**), and the decline in within-burst facilitation (**F**) that occurs following the activation of the LPP with Θγ patterns of input. Note that BAPTA does not attenuate these responses (CTRL: n=7 cells; BAPTA: n=4 cells/ 3-4 mice).

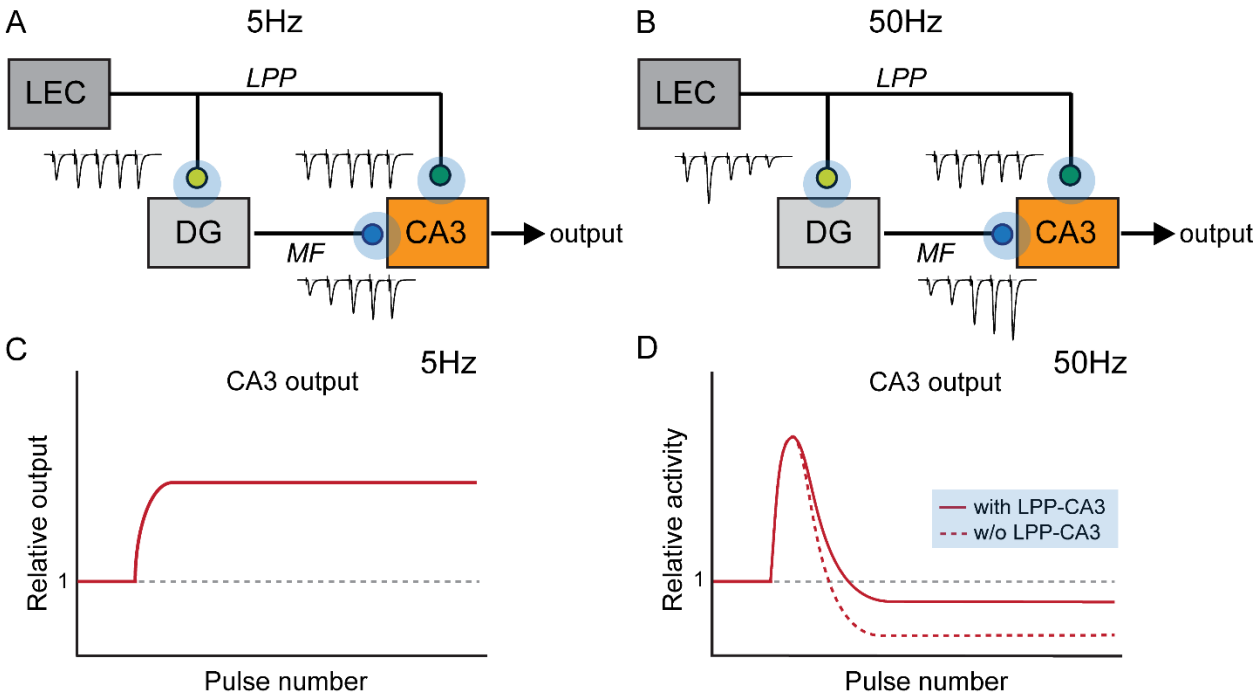

Figure 1.14 Schematic of direct and indirect inputs to CA3 with predicted outputs to activation at 5Hz and 50Hz. A. B. Schematic illustration of the proposed responses at the LPP-DG (yellow), LPP-CA3 (green) and MF-CA3 synapses in response to afferent inputs firing at 5Hz (**A**) and 50Hz (**B**); LEC, lateral entorhinal cortex. **C. D.** Graphs depicting the predicted output (red) from field CA3 following activation at 5Hz (**C**) and 50Hz (**D**) based upon the synaptic transformations that occur across the three synapses within the circuit at each frequency. At 5Hz modest frequency facilitation at both LPP-DG and LPP-CA3 synapses is accompanied by pronounced facilitation of responses at the MF-CA3 synapse (**A**). However, the predicted CA3 output (**C**) is not simply the sum of the facilitation across the three synapses as the MF-CA3 preferentially promotes robust feed forward inhibition *via* activation of the interneuron network at 5Hz. As such, one would predict that feed forward inhibition will dampen the output from CA3. At higher stimulation frequencies (50Hz), the output from CA3 will be largely determined by the balance between suppression of responses at the LPP-DG synapse and the robust frequency facilitation occurring at the MF-CA3. In **D,** the hypothetical outputs with and without a contribution from the direct LPP-CA3 input is shown. We propose that at γ frequencies (i.e. 50Hz) activation of the LPP-CA3 will, due to its ability to largely follow inputs in this frequency range, increase the CA3 output. One should note that the proposed model does not account for the manner in which different frequencies of afferent stimulation may shape output from CA3 such that throughput is enhanced or suppressed.

CHAPTER 2: Two Branches of the Same Hippocampal Afferent Express Different Forms of LTP.

Summary

Whether target-cell type or input characteristics determine the pre- vs. post-synaptic locus of memory related plasticity is poorly understood. Here we report that axons of the lateral perforant path (LPP), a primary hippocampal input, uses presynaptic Long-Term Potentiation (LTP) in their synapses with dentate gyrus (DG) granule cells, but postsynaptic LTP in terminals innervating CA3 pyramidal cells. In contrast to LPP-DG synapses, stabilization of LTP at LPP-CA3 terminals did not require endocannabinoid signaling and had no effect upon LPP release probability. Furthermore, postsynaptic inhibition of actin stabilization with intracellular latrunculin-A blocked LTP at LPP-CA3 synapses. Differences in frequency facilitation suggests distinctions in vesicle release and recycling at the two sites, and that the transfer of information at the different branches is differentially frequency dependent. These observations support a target-cell specification hypothesis for the production of LTP variants and suggests preferential routing of gamma frequency information to, and encoding by, CA3.

Introduction

The perforant path arises from the entorhinal cortex and densely innervates both the outer 2/3rds of the dentate gyrus (DG) molecular layer and the distal apical dendrites (*stratum moleculare*) of field CA3 (Amaral *et al.*, 1990; Amaral, 1993; Witter, 1993). Given that the sole output of the DG targets CA3, the entorhinal cortex has strong direct (monosynaptic) and indirect (di-synaptic) routes to influence the latter region. There has been considerable interest in the functional implications of this arrangement. The direct route will plausibly provide a more reliable representation of cue identity and spatial information conveyed respectively by the lateral (LPP) and medial (MPP) segments of the perforant path (Eichenbaum & Fortin, 2005; Hargreaves *et al.*, 2005; Eichenbaum *et al.*, 2012; Hunsaker *et al.*, 2013; Petersen *et al.*, 2013; Reagh & Yassa, 2014), especially in light of the massive convergence of the DG projection to CA3 (Henze *et al.*, 2002; Rollenhagen *et al.*, 2007; Rebola *et al.*, 2017). However, the direct LPP-CA3 route terminates on the most distal segment of the apical dendrites of CA3 and thus at a considerable distance from the spike initiation zone whereas the DG axons (mossy fibers) generate massive, extremely potent terminals located immediately proximal to CA3 cell bodies (Salin *et al.*, 1996; Henze *et al.*, 2002; Nicoll & Schmitz, 2005). A possible interpretation is that the direct route activates discrete populations of CA3 neurons that provide representations of the cortical information while the indirect path mobilizes a temporally extended response that amplifies and/or promotes encoding of that information (Cox *et al.*, 2019).

Largely missing from the discussion of functional consequences is a consideration of the possibility that the two branches of the LPP have different physiological properties. Such differences in, for example, frequency facilitation by the LPP-DG vs. LPP-CA3 synapses would have profound implications for hypotheses about information flow from cortex into hippocampus. The likelihood that two synaptic populations formed by the same LPP axon (Tamamaki & Nojyo, 1993; Witter, 1993) are functionally distinct might seem remote but such effects have been

described for same fiber innervation of interneurons vs. principle cells in cerebellum (Bao *et al.*, 2010), hippocampus (Scanziani *et al.*, 1998; Toth *et al.*, 2000; Lawrence & McBain, 2003; Lawrence *et al.*, 2004; Sun *et al.*, 2005; Aldahabi *et al.*, 2022), and neocortex (Reyes *et al.*, 1998; Rozov *et al.*, 2001). If target specification also differs between subtypes of glutamatergic (projection) neurons – a point that has yet to be tested – then the radically different cell types found in the DG vs. field CA3 might impose very different properties on their shared input from LPP axons. We tested this by comparing frequency facilitation, an effect that is firmly linked to transmitter release probability and thus presynaptic mechanisms, at the two termination sites of the LPP.

The above issues are also relevant to the question of whether axon terminals or dendritic spines specify the form of long-term potentiation (LTP) expressed by a given population of synapses. Within hippocampus, LTP in the pyramidal cell to pyramidal cell (Py–Py) connection between fields CA3 and CA1 is induced, expressed, and stabilized in the postsynaptic compartment (Kauer *et al.*, 1988; Muller & Lynch, 1988; Granger & Nicoll, 2014). In contrast, the lateral entorhinal cortex fan cell to DG granule cell (Fn-Gc) projection uses a presynaptic form of LTP (Wang *et al.*, 2016; Wang *et al.*, 2018b). The Fn-Py synapses generated by the CA3 extension of the LPP thus bring together axons and spines that are each capable of expressing LTP. An analysis of LTP at this synapse could therefore provide insights about which element dominates in determining the locus of potentiation. If target cells specify LPP operations, then we would expect to find more conventional, CA1 types of memory-related plasticity (and signal processing) in LPP-CA3 than in LPP-DG connections. The studies reported here tested this prediction.

Materials and Methods

Animals

All studies used male C57/BL6 mice (Charles River) from 2-4 months of age. Animals were

group housed (5 per cage) with access to food and water *ad libitum* and were on a 12-h light/dark cycle, with lights on at 6:30AM. Experiments were conducted in accordance with the Institutional Animal Care and Use Committee at the University of California, Irvine and the National Institute of Health Guidelines for the Care and Use of Laboratory Animals. For all electrophysiology studies, mice were anesthetized with isoflurane and euthanized by decapitation.

Extracellular hippocampal field recordings

Hippocampal slices were prepared as previously described (Cox *et al.*, 2019; Quintanilla *et al.*, 2022). Experiments were initiated from 8-10AM. Upon removal from the cranium, brains were placed in ice cold, oxygenated (95% O_2/ 5% CO_2) high Mg^{2+}, artificial cerebrospinal fluid (HM-aCSF) containing (in mM): 87 NaCl, 26 $NaHCO_3$, 25 glucose, 75 sucrose, 2.5 KCl, 1.25 NaH_2PO_4, 0.5 $CaCl_2$, 7 $MgCl_2$, (320-335 mOsm). Horizontal sections were cut at a thickness of 360µm using a Leica Vibrotome (model VT1000s, Leica) into cold HM-aCSF and rapidly transferred to an interface recording chamber containing a constant perfusion (60-70 ml/hr) of oxygenated (95% O_2/ 5% CO_2) aCSF containing (in mM): 124 NaCl, 3 KCl, 1.25 KH_2PO_4, 1.5 $MgSO_4$, 26 $NaHCO_3$, 2.5 $CaCl_2$, and 10 dextrose (300-310 mOsm, pH 7.4, 31±1°C). Recordings began 1.5- 2h later. For all hippocampal field studies, recordings were digitized at 20kHz using an AC amplifier (A-M Systems, Model 1700) and collected using NacGather 2.0 (Theta burst Corp.).

For field recordings of LPP-CA3 synapses, a stimulating (twisted nichrome wire) electrode was placed in the outer third of the DG molecular layer at the edge of the internal blade and a recording electrode was positioned in *stratum moleculare* of field CA3. Paired-pulse stimulation (40 msec interpulse interval) was used to verify a positive PPR, as is characteristic of the LPP (McNaughton, 1980; Christie & Abraham, 1994; Berzhanskaya *et al.*, 1998). Single-pulse baseline stimulation was applied at 0.05 Hz (i.e., every 20 seconds), with intensity set at

~50% of the maximum population-spike free fEPSP. For studies of LTP, baseline responses were recorded for 20 min after which LTP was induced. For LPP-CA3 synapses, LTP was induced with two trains of TBS separated by 30 sec (each TBS train included 10 bursts of 4 pulses at 100 Hz with 200 msec between bursts) with pulse duration doubled relative to baseline stimulation. For the LPP-DG system, LTP was induced with a 1 sec, 100 Hz train (HFS) with pulse duration doubled and intensity increased by x1.5 relative to baseline stimulation. For both regions, recordings of responses to baseline stimulation resumed for 60 min. In a subset of animals, LPP-CA3 LTP was induced using HFS, as described above. For studies evaluating the PPR before and after LTP, five paired stimuli (40 or 120 msec interpulse interval; 5 min between pairs) were given during the 20 min baseline period and a second set of 5 paired pulses were given 60 min after LTP induction. To evaluate short-term plasticity, responses to ten pulse trains at 5, 20, and 50 Hz were recorded. Trains at the different frequencies were delivered in randomized order and spaced by at least 10 minutes of stable baseline recording. In separate cases, identical stimulation trains were applied to slices in which a single knife cut was made from the external to internal blade of the DG, severing MF projections (DG-CA3; **Fig 2.3D**). To confirm the MF cut, a stimulating electrode was placed in the hilus proximal to the granule cell layer at the apex of the two blades of the DG. A recording pipette was then placed in the pyramidal cell layer of CA3b and responses to a 20 Hz train recorded (**Fig 2.3D**).

Pharmacological treatments:

A subset of experiments tested the role of endocannabinoid signaling at the LPP-CA3 synapse. Following a period of stable baseline (20 minutes), the CB1 receptor antagonist AM251 (5 μM) was applied to the chamber via a second infusion line (6 ml/ hour) for 40 minutes prior to LTP induction with TBS (as above). A second set of experiments tested the effect that 1-hour infusion of the CB1 receptor agonist, WIN55-212-2 (WIN55; 5μM) had upon baseline

transmission. In a separate set of experiments, the $GABA_AR$ antagonist PTX (1 μM) was bath applied for 1 hour to test the contribution that GABAergic transmission makes to responses evoked by single and paired stimulation pulses.

All extracellular recordings were analyzed offline using NACShow 2.0 (Theta Burst Corp, Irvine, CA, USA). For LTP experiments, the fEPSPs rising slopes (20-80%) were measured across the entire recording and then normalized to a stable 20-minute baseline period. The magnitude of LTP was determined by comparing the slope of fEPSPs collected during the last 5 minutes of the pre-LTP baseline period with those obtained during the last 5 minutes of the recording (i.e., 55-60 minutes post LTP induction). The fEPSP decay τ was described using a mono-exponential equation ($Y(t)=A*exp(-1/\tau)$) and measured across an 5 min baseline period and the last 5 minutes of recording (i.e., 55-60 mins). The fEPSP waveform evoked by paired-pulse stimulation were analyzed with regard to rising slope and decay τ. The effect of pharmacological treatment (e.g., AM251, WIN55, PTX) were assessed upon the baseline fEPSP waveform, which was analyzed with regard to peak amplitude, rising slope (20-80%) and decay τ, before any effects upon paired-pulse stimulation and/ or LTP were assessed (as above).

Whole-Cell Recordings

For whole-cell patch-clamp experiments, hippocampal slices were prepared as previously described (Gunn *et al.*, 2017). Briefly, the brain was rapidly removed and placed in ice-cold oxygenated (95% O_2 - 5% CO_2) aCSF containing (in mM): 124 NaCl, 3 KCl, 1.25 KH_2PO_4, 3 $MgSO_4$, 26 $NaHCO_3$, and 10 dextrose (300-310 mOsm, pH 7.4). Horizontal slices (370 μm) were cut using a Leica Vibratome (model VT1000s, Deer Park, IL, USA) at 4°C and then transferred to a holding chamber where they were incubated at room temperature in oxygenated (95% O_2 - 5% CO_2) aCSF containing (in mM): 124 NaCl, 3 KCl, 1.25 KH_2PO_4, 1.5

$MgSO_4$, 26 $NaHCO_3$, 2.5 $CaCl_2$ and 10 dextrose (300-310 mOsm, pH 7.4). Following at least 1hr incubation slices were transferred to the recording chamber as required, where they were continuously perfused in oxygenated aCSF (above) maintained at 30 ± 1°C.

A small diameter (1 μm) bipolar stimulating electrode (World Precision Instruments Inc, Sarasota, FL, USA) placed in the CA3 *lacunosum moleculare* was used to evoke LPP-specific eEPSC. LPP-eEPSCs were recorded from visually identified CA3 pyramidal cells (30 ± 1°C) at a holding potential of -70mV in aCSF that additionally contained the PTX (50 μM). Patch pipettes (5-8 MΩ) were pulled from thick-walled borosilicate glass (1.5 mm outer diameter; 0.86 mm inner diameter; Sutter Instruments Co, Novato, CA, USA) and filled with an internal solution containing (in mM): 130 $CsCH_3SO_4$, 8 CsCl, 8 NaCl, 10 HEPES, 0.2 EGTA, 2 Mg-ATP, 0.3 Na-GTP, 2 QX-314 (Sigma, St Louis, MO, USA). Alexa 594 (0.3 μM; Thermoscientific, USA) was included in the internal solution to enable visualization of the recorded cells dendrites and confirm proximity of the stimulating electrode. Paired pulse stimulation (40 ms) was used to confirm the characteristic facilitation at the LPP-CA3 synapse (McNaughton, 1980; Christie & Abraham, 1994; Berzhanskaya *et al.*, 1998). Single-pulse baseline stimulation was applied at 0.5 Hz. Baseline eEPSCs were recorded for 5 minutes before applying two trains of TBS separated by 30 seconds (each TBS train included 10 bursts of 4 pulses at 100 Hz with 200 msec between bursts) to induce LTP. In a subset of experiments, Lat- (400 nM) was included within the recording pipette to determine if reorganization of the postsynaptic actin cytoskeleton was required for LTP at the LPP-CA3 synapse. Currents were filtered at 2 kHz using an 8-pole Bessel filter. Only those cells with a stable access resistance were used, with recordings being aborted if >20% change in series resistance occurred. All recordings were made using an Axopatch 200A (Molecular Devices, San Jose, CA, USA) and pClamp 10. Recordings were stored directly to a PC (4 kHz digitization) using a Digidata 1550A (Molecular Devices, San Jose, CA, USA).

All recordings were analyzed offline using the Strathclyde Electrophysiological Software (WinEDR and WinWCP; Dr J Dempster, University of Strathclyde, UK). Individual eEPSCs were detected in WinEDR using a method based on a rate of rise threshold that targeted the stimulation artifact and was specific for individual cells. Detected events were visually inspected and any traces containing noise or multiple synaptic responses were removed from the analysis. Accepted events were analyzed with regard to peak amplitude, rise time and decay τ (T50% values: the time taken to for the amplitude of each event to decay to 50% of peak). Ensemble average eEPSCs (minimum 10 events) were generated for each cell before and following expression of stable LTP for each cell. Averaged synaptic currents were analyzed with regard to their decay τ, which was best described by the single exponential function $Y(t) = Ae^{-1/T}$. The magnitude of LTP was determined by comparing the peak amplitude of eEPSCs collected during a 10-minute pre-LTP baseline period with those obtained during the last 10 minutes of the recording, 40-50 minutes post LTP induction. The effect of LTP upon the decay τ of eEPSCs was assessed across the same baseline and post-LTP periods.

Drug Application

Compounds used in hippocampal slice experiments were introduced to the bath via a second, independent perfusion line (6ml/h). The cannabinoid receptor 1 (CB1R) inverse agonist, AM251, the CB1R agonist WIN55, 212-2 mesylate, and the $GABA_AR$ antagonist PTX were prepared as concentrated stock solutions in dimethyl sulfoxide (DMSO). Each was then diluted in aCSF to achieve the desired final concentration (AM251: 5 μM; WIN55: 5 μM; PTX: 1 μM) ≤0.01% DMSO in aCSF bath. For whole cell-recordings the $GABA_AR$ antagonist was made as a stock solution (50mM) in DMSO and diluted to the final concentration (50μM) in aCSF. Latrunculin-A (Tocris, Minneapolis, MN, USA) was made directly in the internal solution to a concentration of 400nM.

Monte Carlo simulations of a two-step release model.

To test if factors within the presynaptic terminal may be critical determinants of the short-term operations occurring at the LPP-CA3 synapse, we used a previously published (Miki *et al.*, 2016; Quintanilla *et al.*, 2022) renewable two-step release model based upon Monte Carlo simulations using Igor Pro (Wavemetrics, Lake Oswego, OR, USA). Briefly, the two-step release model incorporates four factors associated with the release and subsequent replenishment of synaptic vesicles. These include the probability of docking site occupancy (δ) and the probability of docked vesicle release (p_v). The product of these two factors (i.e., δp_v) describes the overall probability of release (p). Each synapse has a number of docking sites (N) that are supplied from a pool of replacement vesicles. The movement of replacement vesicles to empty docking sites is described by the probability '*r*'. The replacement vesicle pool has an occupancy probability of 1 prior to stimulation, with replenishment of this replacement pool occurring with a probability '*s*' following replacement vesicle depletion associated with repetitive activation.

Our previous studies conducted a parameter search to identify the combination of variables that most reliably recapitulated the experimental data recorded from the LPP-DG synapse following 50Hz (10 pulses) stimulation (Quintanilla *et al.*, 2022). Simulations used a modified version of the original model by Miki et al, with a common replacement pool (Miki *et al.*, 2016). To identify factors that may differ between the two LPP branches, simulations used variants of the previously published model where parameters were optimized to describe the LPP-DG output profile following 50Hz stimulation (Quintanilla *et al.*, 2022). Specifically, δ = 0.6, p_v = 0.55, r = 0.7, s = 0.3, N = 3, pool size = 3 vesicles. The variables within the model had been constrained to generate this optimized set of parameters as follows: docking site number ≥3 and ≤8; replacement pool size ≤20 vesicles; δ >0.2 and <0.8; p_v >0.2 and <0.8; r >0.2 and <0.8; s >0.2 and <0.8. Values for δ and p_v were separated by a probability of <0.1. The simulation was

repeated 50 times with each combination of variables to an accuracy of 0.05 probability. The simulated output (i.e., vesicle number) was normalized to the initial response (i.e., pulse #1) and then fit to the normalized LPP-CA3 curves generated from the electrophysiological data. The standard error between each individual point (i.e., pulse number) was compared and a mean value generated. Under such conditions a parameter space was then computed using a modified version of the original code (Miki *et al.*, 2016) generated using Python 3.8.

The effect of reducing p: Initial experiments tested if reducing only *p* in the optimized LPP-DG synapse (above) could recapitulate the output profile recorded from the LPP-CA3 synapse. The initial *p* (i.e., δp_v) of 0.33 was incrementally decreased (0.25, 0.2 and 0.15) and the effects upon the output profile determined. A parameter search, using the modified code, was conducted to identify the optimal value for *p* to most reliably reproduce the electrophysiological data recorded from the intact and MF-cut slices when all other parameters were unchanged.

Selectively reducing the individual components of release; δ and p_v*:* To test the contribution that δ and p_v make to the simulated output curve we next ran the model in two different configurations that produced the same overall *p* of 0.22. To do this the model was unconstrained such that δ and p_v could be separated by a probability of >0.1. In the first configuration δ=0.4 and p_v=0.55, while the values for these parameters in the second version were reversed (i.e., δ=0.55 and p_v=0.4). The simulated output curve following 50Hz stimulation was generated for each configuration of the model. In a second set of simulations a parameter search was conducted to identify the optimal vesicle recycling parameters (i.e., *r* and *s*) to reproduce the 50Hz LPP-CA3 curve when only δ was reduced.

Statistical analysis.

All results are presented as group means values ± SEM. Statistical comparisons of the PPR,

and LTP used either paired or unpaired Student's t-tests (GraphPad Prism version 6.0), as indicated in the text. For all studies the group N refers to the number of slices for extracellular field recordings or cells for whole-cell recordings, with a minimum of 3 animals per group. For all studies, p-values of <0.05 were considered significant.

Results

2.1 & 2.2 The two branches of the LPP express different forms of LTP.

Single pulse stimulation delivered to the outer molecular layer of the DG inner leaf, near the junction with CA3, elicited a large field excitatory post-synaptic potential (fEPSP) in CA3 *stratum moleculare*. This was accompanied by a positive going potential in the CA3 cell body layer. A comparable response was obtained with stimulation electrodes located closer to the hinge of the DG (**Fig 2.1A**). In both cases, the evoked potentials expressed a conventional facilitatory paired-pulse ratio (PPR) (pulse interval of 40 msec). However, the degree of enhancement from pulse 1 (P1) to pulse 2 (P2) with a 40 msec delay was substantially larger in CA3 (100.3 ± 5.1%, n=12. **Fig 2.1B**) than that at the LPP-DG connection (46.4 ± 5.0%, n=15) (t_9=6.45, p<0.0001, unpaired student's t-test) or reported for CA3-CA1 projections (Muller & Lynch, 1988; Milior *et al.*, 2016). As expected, the PPR was reduced in both branches of the LPP when pulses were separated by longer intervals (120 msec interval; *LPP-CA3*: 64.0 ± 2.0%, n= 5; *LPP-DG*: 40.7 ± 4.2%, n= 8; p= 0.002. **Fig 2.1C**).

The magnitude of paired pulse facilitation provides a simple test of whether a given manipulation enhances synaptic responses by increasing evoked transmitter release (Del Castillo & Katz, 1954; Jackman & Regehr, 2017). Original tests for such effects in CA3-CA1 projections proved negative: a robust LTP did not measurably affect PPR (Muller & Lynch, 1989). This, together with other lines of evidence led to the conclusion that stable expression of potentiation was due to postsynaptic modifications (Kim & Lisman, 1999; Krucker *et al.*, 2000;

Kramar *et al.*, 2006; Chen *et al.*, 2007; Lauterborn *et al.*, 2017). More recent work found that LTP in the LPP-DG connection is accompanied by a marked reduction in the PPR, as expected for a presynaptic variant of potentiation (Wang *et al.*, 2016; Wang *et al.*, 2018b). We conducted similar tests on LPP-CA3 synapses and obtained surprising results. Induction of LTP with theta burst stimulation (TBS) reliably depressed the PPR when the twin pulses were separated by 40 msec (baseline: 99.3 ± 5.6%; LTP: 76.9 ± 5.5%; n= 11, p= 0.0002, paired student's t-test) but had little if any effect with a 120 msec delay (baseline: 64.0 ± 2.01%; LTP: 60.1 ± 2.9%; n= 5, p= 0.070, paired student's t-test; **Fig 2.1D**). The change in PPR for the 40 msec interval (-22.4 ± 3.2%) was much larger than that for the 120 msec condition (-6.3 ± 2.7%) (p= 0.0074, unpaired student's t-test; **Fig 2.1F**). The pronounced effect of inter-pulse interval on LTP related changes in PPR was not evident in LPP-DG synapses. There was a substantial, statistically robust decrease in the ratio from baseline to 60 min after LTP induction as assessed with 40 msec (58.4 ± 3.8% to 45.5 ± 3.8%, n=6, p=0.004) or 120 msec (40.7 ± 4.2% to 31.2 ± 4.4%, n= 8, p=0.003) delays (**Fig 2.1E**). The change in PPR was not reliably different for the 40 msec vs. 120 msec intervals (-20.3 ± 4.3% vs. -26.6 + 8.5%, respectively; p= 0.565, unpaired student's t-test; **Fig 2.1F**).

The LPP-DG data were collected after LTP induction with a conventional high frequency stimulation (HFS, 100Hz) train whereas those for CA3 involved TBS-induced potentiation. We accordingly repeated the study using the same stimulation protocol used for the DG branch. The slope of fEPSPs recorded from CA3 *stratum moleculare* 60 min after HFS increased by 60.7 ± 12.2%, a value that was not statistically different than that obtained with TBS (t_{16}=1.49, p=0.156, unpaired student's t-test; **Fig 2.1G**). Surprisingly, the magnitude of the PPR (40 msec inter-pulse interval) was not significantly different before vs. after induction of LTP (baseline: 104.7 ± 2.0%; LTP: 99.7 ± 3.5%), with a mean change of 5.3 ± 2.0% (n= 7, t_6= 2.31, p= 0.060; paired t-

test; **Fig 2.1H**). Collectively, the results indicate that changes in release are not a major component of LTP in the CA3 extension of the LPP.

There remains the question of why TBS affected the 40 msec PPR in LPP-CA3 synapses. One possibility is that an event set in motion by the first pulse affects the waveform of the second fEPSP, including its initial slope, and thereby alters the measured PPR. Relatedly, the decay tau (τ) of the second fEPSP was more rapid than that of the first, when the two pulses were separated by 40 msec (P1= 5.17 ± 0.36 msec, P2= 3.47 ± 0.15 msec; n=8, t_7= 4.38, p=0.003; paired students t-test; **Fig 2.2A, B**). This was not the case for inter-pulse intervals of 120 msec (P1= 5.02 ± 0.35 msec, P2= 5.0 ± 0.35 msec; n=10, t_9=0.55, p=0.592; **Fig 2.2A, B**), suggesting that the first potential affects the shape of the second only when the two occur in rapid succession. There were no decay τ differences between responses to P1 and P2 in the LPP-DG projection at 40 msec (*DG*: P1= 3.24 ± 0.37 ms, P2= 3.39 ± 0.31 ms; n=10, t_9= 0.58, p=0.582), or 120 msec (P1= 3.96 ± 0.31 ms, P2= 3.68 ± 0.37 ms; n=8, t_7=1.72, p=0.130. **Fig 2.2C, D**). LTP induced by TBS caused a 45.2 ± 8.7% prolongation of the decay τ of LPP-CA3 fEPSPs, an effect that can be assumed to increase the influence of the first of two closely spaced responses on the initial slope of the second. In marked contrast to the TBS results, induction of LTP with HFS did not affect the waveform of single fEPSPs (HFS: 100.41 ± 4.36% of baseline; n=7) and the difference in the effects of TBS vs. HFS on decay τ was highly significant (t_{16}=3.88, p=0.001, unpaired t-test; **Fig 2.2E**).

Feedforward inhibition is a plausible mediator of interactions between responses 1 and 2. We tested this using the $GABA_A$ receptor ($GABA_AR$) antagonist picrotoxin (PTX) at a concentration (1µM) that increases the amplitude of the fEPSP by about 12% (p=0.03 paired t-test) without producing after-discharges. PTX did not detectably affect the accelerated decay of the second response with paired pulses separated by 40 msec (baseline: decay τ ratio = 0.61 ±

0.07; PTX: decay τ ratio = 0.70 ± 0.10; n=6, t_5=0.899, p=0.410; unpaired t-test; **Fig 2.2F,H**). It is therefore unlikely that inhibitory postsynaptic currents (IPSCs) initiated by P1 play a prominent role in distorting the response to P2. A more likely possibility is that TBS alters active properties of the target dendrites, thereby enhancing an already present physiological event that persists for ~40 msec.

2.3 Induction of LTP in the LPP-CA3 branch is not dependent on endocannabinoids.

LTP at LPP-DG synapses is markedly reduced by genomic or pharmacological suppression of cannabinoid receptor-1 (CB1R) (Wang *et al.*, 2016; Wang *et al.*, 2018a; Wang *et al.*, 2018b; Piette *et al.*, 2020). Multiple lines of evidence established that 2-arachidonylglycerol (2-AG) is the endocannabinoid used to elicit enduring LTP at this terminal. As 2-AG is synthesized postsynaptically and CB1Rs are localized to LPP terminals (Katona *et al.*, 2006; Kano *et al.*, 2009; Castillo *et al.*, 2012; Wang *et al.*, 2016), these results indicated that potentiation is initiated in spines and expressed presynaptically (Wang *et al.*, 2016; Wang *et al.*, 2018b). This accords with the above-described depression of PPR in LPP-DG synapses following induction of LTP (**Fig 2.1E**). In contrast to these results, the selective CB1R antagonist AM251 (5 μM) had no evident effect on LTP in LPP-CA3 synapses: The percent potentiation measured 55-60 minutes post-induction was 44.8 ± 4.6% and 45.7 ± 4.8% for slices treated with vehicle or AM251, respectively (n=12/group, t_{11}=0.15, p=0.88; unpaired t-test, **Fig 2.3A, B**). PPR (40 msec interval) was 95.5 ± 6.1% prior to induction of LTP and 69.2 ± 5.8% 60 min afterwards (n=13, t_{12}=5.17, p=0.0002, paired student's t-test; **Fig 2.3C**). In all, the retrograde (spine to terminal) signal used to generate presynaptic LTP in the DG does not play a role in LPP-CA3 synapses, which is in agreement with the argument that LTP in the latter is expressed postsynaptically.

The rapid onset and simple waveforms of the fEPSPs measured in the above

experiment strongly suggest that polysynaptic (DG-CA3-CA3) activation of the massive CA3 recurrent collaterals to *stratum radiatum* did not contribute to the responses. It is possible however that the CA3 collateral system contributed to the net depolarization of the target dendrites during the TBS used to induce potentiation and thereby promoted LTP. To test this, we ran a group of slices (n= 10) in which the mossy fibers (MF) from DG to CA3 were severed at the level of their exit from the hilus of the DG (**Fig 2.3D**). Percent LPP-CA3 potentiation in these cases was not reliably different from that recorded from intact slices (intact: 44.8 ± 4.6%; MF-cut: 37.9 ± 5.5%; t_{16}=0.909, p=0.377; unpaired student's t-test) and AM251 again did not measurably affect CA3 LTP (34.8 ± 4.9%; t_9=0.415, p=0.688; vs. controls, unpaired student's t-test) (**Fig 2.3E**).

CB1Rs on LPP-DG terminals exhibit an atypical form of signaling when activated by agonists or high frequency afferent stimulation (Chiu & Castillo, 2008; Wang *et al.*, 2018b). Rather than depressing glutamate release, as is the case at most sites, the treatments facilitate presynaptic actin signaling cascades (Wang *et al.*, 2018a; Wang *et al.*, 2018b). As reported for the DG, a 1 hr infusion of the CB1R agonist WIN55-212-2 (WIN55; 5 µM) had no evident effect on the decay τ (**Fig 2.3F**) or initial slope (**Fig 2.3G,H**) of the CA3 fEPSP. The slope, normalized to the 20-minute drug-free baseline response, was 104.0 ± 3.1% at the end of treatment (baseline vs. drug: t_9= 0.494, n=10, p=0.633, paired student's t-test) (**Fig 2.3H**). Thus, while LPP terminals in CA3 lack endocannabinoid-dependence for the stabilization of LTP, they nonetheless resemble those in the DG with regard to responses to CB1R agonists.

2.4 LPP-LTP stabilization in CA3 requires postsynaptic adjustments.

The absence of evidence for presynaptic LTP expression or retrograde endocannabinoid signaling in LPP-CA3 contacts strongly suggests that the events responsible for expressing and stabilizing LTP in this field are located in pyramidal cell dendrites. Thus, mechanisms could be

comparable to those at the CA3-CA1 connection in which LTP expression involves an expansion of the postsynaptic density and stabilization achieved by reorganization of the subsynaptic actin cytoskeleton (Kim & Lisman, 1999; Krucker *et al.*, 2000; Kramar *et al.*, 2006). We tested this idea by infusing latrunculin-A (Lat-A; 400nM), a toxin that blocks actin filament assembly, into CA3 pyramidal neurons before attempting to induce LPP-LTP. Delivery of the toxin via clamp electrodes blocks LTP consolidation in CA1 (Kramar *et al.*, 2006; Rex *et al.*, 2007), but has no effect on any aspect of LPP potentiation for the DG granule cells (Wang *et al.*, 2016). The latter result is consistent with a presynaptic locus for expression and stabilization of LPP-DG LTP.

We used the whole-cell voltage-clamp configuration to record LPP-evoked excitatory postsynaptic currents (eEPSCs) from CA3 pyramidal cells (V_{clamp} -70mV) evoked by an electrode localized in the distal *stratum moleculare*. The amplitude and decay time course of LPP-eEPSCs were unaffected by Lat-A within the recording pipette (**Fig 2.4A-C**): an effect consistent with previous studies of DG granule cells and CA1 pyramidal cells (Wang *et al.*, 2016). Two trains of TBS produced an immediate potentiation in control experiments that decayed over 10 minutes to a plateau at 176 ± 3.8% above the pre-TBS baseline. An initial potentiation was still present in the Lat-A cases, but responses decayed to baseline over 25-30 minutes (**Fig 2.4D**). The difference in percent LTP recorded at 45 minutes post-TBS for the two groups was highly significant (156 ± 1.8% vs. 97 ± 2.1%, $p<0.001$; unpaired student's t-test). These effects of intracellular application of Lat-A to CA3 neurons were similar to those described for CA1 and are indicative of postsynaptic LTP at this synapse.

2.5 & 2.6 Frequency facilitation differs at the two termination sites of the LPP.

The marked differences in LTP between the two sets of LPP synapses raise the question of whether distinctions are specific to the complex events required to modify synapses

or instead emerge at simpler levels of function. We therefore tested if the CA3 branch of the LPP expresses the unusual frequency facilitation described for LPP-DG contacts.

Prior studies showed that theta frequency (5 Hz) stimulation of LPP-DG synapses produces a small (~5-10%) within-train facilitation of fEPSPs (Trieu *et al.*, 2015; Quintanilla *et al.*, 2022) whereas 50 Hz stimulation generates an unusual pattern with initial facilitation followed by a marked depression (Amani *et al.*, 2021; Le *et al.*, 2022; Quintanilla *et al.*, 2022). Our recent analyses indicate that this frequency following profile is due to release dynamics with little if any contribution from postsynaptic variables (Quintanilla *et al.*, 2022). Facilitation was clearly greater in the CA3 branch of the LPP than in the DG segment. Theta (5 Hz) input produced an ~20% facilitation of fEPSP slope that persisted throughout a 10-pulse train (pulse 10: 115.2 ± 5.4%, n=14); an effect not evident at LPP-DG synapses (Quintanilla *et al.*, 2022). A somewhat larger initial facilitation was elicited by beta frequency (20 Hz) stimulation (176.61 ± 6.08% for pulse #2) but in this instance the enhancement steadily decreased from the third pulse onward (pulse 10: 126.54 ± 6.64%, n=14). A similar but considerably exaggerated pattern was produced by 50Hz input. The initial enhancement (161.81 ±6.38% for pulse #2) was comparable to that produced by 20Hz but the loss of facilitation was greater with responses falling below baseline later in the train (pulse 10: 90.89 ± 3.48%, n=13) (**Fig 2.5A, B**). These frequency curves are qualitatively similar to those described for LPP-DG synapses (Quintanilla *et al.*, 2022) but with a greater initial facilitation and a lesser within train decline.

A possible complication for the above analyses involves contributions from the CA3 collateral system to the size or waveform of LPP-elicited fEPSPs in *stratum moleculare*. This could occur if the LPP-DG stimulation engaged enough MFs to trigger spiking in a large number of CA3 pyramidal cells. The collaterals formed by CA3 terminate in *stratum radiatum* immediately below the distal dendritic targets of the LPP and might therefore generate potentials that contaminate those from the latter projection. However, severing the MF as they

exit the hilus (see **Fig 2.3**) had no reliable effect on frequency facilitation elicited by theta, beta, or gamma stimulation of the LPP (5Hz pulse 10: 113.93 ± 2.12%; 20Hz pulse 10: 119.08 ± 4.07%; 50Hz pulse 10: 80.82 ± 4.51%; n= 14; **Fig 2.5B**).

The PPR results together with the upward displacement of frequency facilitation curves in CA3, relative to the DG, constitute evidence for target specification of release properties from LPP terminals. We used Monte Carlo simulations of a two-step release model (Miki et al, 2016) to search for presynaptic variables that might underlie the differences in facilitation between the two LPP branches. The model incorporates factors associated with the release and the subsequent replenishment of synaptic vesicles including the following: probability of vesicle docking (δ), release probability of a docked vesicle (p_v), probability of a vesicle transitioning to a vacant docking site from the replacement pool (r), and replacement pool replenishment (s) (**Fig 2.6A** and Methods). Using the previously optimized parameters for the simulated LPP-DG synapse (see Methods in (Quintanilla *et al.*, 2022), we searched for changes that generated the LPP-CA3 responses to 50Hz input. Decreasing net release probability, p (i.e., product of δp_v), from 0.33 to 0.25, 0.20 or 0.15 caused a progressive increase in the initial facilitation and a reduction in the subsequent suppression of responses during the train (**Fig 2.6B**). The 0.25 value changed the simulated LPP-DG pattern into one that approximated the recorded 50Hz curve for LPP-CA3 synapses. Further optimization of p by selectively manipulating δ and p_v generated output curves that aligned well with the electrophysiological data recorded from intact slices as well as those lacking the MF connection (i.e., MF cut. **Fig 2.6C, D**; intact: SE = 0.030, MF cut: SE = 0.035). The similarity between the simulated MF-cut and intact frequency curves adds support to the conclusion that recruitment of the MF input to CA3 is unlikely to contribute significantly to the output profile recorded from the LPP-CA3 synapse.

Next, we modified the model so that the relationship between δ and p_v was unconstrained (Methods) and tested how the composition of the overall p (i.e., relative

contribution of δ and p_v) influences the simulated output profile. When the release dynamics (i.e., δp_v) in the model were configured in two ways to produce a p of 0.22 (δ=0.4, p_v=0.55 and δ=0.55, p_v=0.4), the simulated output curves were noticeably different (**Fig 2.6E**). This suggests that subtle manipulations of vesicle docking, or the release probability of docked vesicles can differentially influence the operations at a given synapse. Specifically, decreasing δ produces a significantly larger initial facilitation, a clear difference between the terminals of two branches of the LPP. We then tested how reliably the model recapitulated the experimental data when the overall p was reduced by selectively decreasing δ. A parameter optimization revealed that selectively decreasing δ could reliably reproduce the empirical output curves when the probability of replacement pool replenishment (i.e., s) was additionally increased from 0.4 to 0.5 (**Fig 2.6F**). In all, the modeling work suggests that the different output profiles expressed by the two branches of the LPP result from surprisingly modest differences in release dynamics and vesicle recycling.

Discussion

The present results address a basic and largely unexplored question regarding memory related synaptic plasticity: does the pre- or post- synaptic side of a contact determine the locus of expression and stabilization. Prior studies showed that the pyramidal to pyramidal cell synapses formed by the CA3 to CA1 projection uses a postsynaptic form of LTP (Kauer *et al.*, 1988; Muller & Lynch, 1988; Manabe & Nicoll, 1994; Rex *et al.*, 2009; Granger & Nicoll, 2014). However, the somewhat different fan cells in the lateral entorhinal cortex generate a presynaptic variant at their LPP connections with DG granule cells. If the postsynaptic cell type dictates the form of potentiation, then we would expect the CA3 (pyramidal cell) branch of the LPP to express a postsynaptic LTP variant. On the other hand, it is possible that the presynaptic element imposes the form of potentiation independent of the target cell type, in which case the LPP-CA3 projection would have the same presynaptic LTP as the LPP-DG synapses. The

results indicate that LTP in the CA3 branch belongs to the CA1 category, meaning pre- and post-synaptic forms of LTP are expressed by the same axon in the DG and CA3, respectively.

It follows from the above conclusion that spines on hippocampal pyramidal neurons have competencies that are missing from those on the granule cells. LTP in both systems is blocked by NMDAR antagonists and by buffering of intracellular calcium (Barrionuevo & Brown, 1983; McMahon & Barrionuevo, 2002; Wang *et al.*, 2016; Wang *et al.*, 2018b), which indicates that the initial triggering steps for the two forms of potentiation are located in spines. There is however evidence pointing to substantial differences in the stabilization events. Specifically, experiments using genomic manipulations, toxins, peptide antagonists, and imaging have shown that a subgroup of matrix adhesion receptors belonging to the integrin family is located in the postsynaptic density of CA1 spines and required for LTP consolidation (Chan *et al.*, 2006; Kramar *et al.*, 2006; Babayan *et al.*, 2012). CA1 and CA3 have the same general pattern of integrin expression but DG granule cells produce a very unusual (for brain) α4β7 subunit combination (Pinkstaff *et al.*, 1999). Integrins regulate the cytoskeleton and CA1-LTP requires integrin-driven actin polymerization in spines. Intracellular application of Lat-A, that blocks the latter effect, disrupts LTP in CA1 (Kramar *et al.*, 2006; Rex *et al.*, 2007) and, as shown here, in CA3. The same treatment applied to granule cells had no effect on potentiation in LPP-DG synapses (Wang *et al.*, 2016). These observations raise the possibility that the α4β7 integrin found in granule neurons (Pinkstaff *et al.*, 1999) is either not engaged by HFS afferent activity or is incapable of supporting the spine cytoskeletal reorganization required for postsynaptic LTP. In this scenario, the LPP projections to CA3 have access to integrins similar to those present in CA1 and thus are able to trigger the postsynaptic version of LTP. An implication of this argument is that LTP in the medial perforant path and commissural/associational projections to the DG would be expected to express presynaptic versions of LTP. The pre- vs. post-synaptic locus of potentiation has not been resolved for the first of these pathways but a detailed series

of studies by Castillo and colleagues indicate that expression is presynaptic for the second (Hashimotodani *et al.*, 2017; Jensen *et al.*, 2021).

Conversely, the LPP-CA3 contacts appear to lack most, if not all, of the capability for generating presynaptic LTP. As noted, available evidence indicates that the enhanced release that underlies potentiation in the LPP-DG connection is triggered by on-demand endocannabinoid synthesis in granule cells followed by atypical signaling by cannabinoid receptors located on LPP terminals (Wang *et al.*, 2016; Wang *et al.*, 2018b). The CB1 receptors generate a more conventional depression of release in CA1. CB1R antagonists had no effect on LTP in the CA3 branch of the LPP, which is consistent with the lack of evidence for presynaptic expression of potentiation. However, as with the DG, CB1R agonists failed to produce the expected depression of LPP-CA3 responses, suggesting that in the LPP the CB1Rs produce atypical signaling properties in both terminal fields. Why then didn't patterned afferent stimulation generate the robust, endocannabinoid-dependent enhancement of release found in the DG? One possibility is that the brief periods of activation used to induce LTP fail to generate as robust a surge of postsynaptic endocannabinoid synthesis in CA3 as occurs in the DG. In this hypothesis, the terminals in CA3 possess the machinery for expression of presynaptic LTP but the activation signal arriving from target spines is insufficient. Alternatively, target specification by pyramidal cell spines could reduce one or more of the (presynaptic) signaling steps used by the cannabinoid receptors to produce a lasting increase in evoked release. The clear difference in frequency facilitation curves between the two LPP branches points to local regulation of terminal properties and it is not unreasonable to suggest that this extends to the status of CB1R-initiated signaling cascades. It may be possible to distinguish between the 'weak input' vs. 'disrupted effector' models by testing if cannabinoid receptor agonists activate LTP critical signaling steps in LPP terminals at CA3 to the same extent reported for DG contacts.

The use of distinctly different forms of plasticity by the same afferent innervating two hippocampal subfields will likely have important effects on the encoding of information by the hippocampus. The much discussed 'synaptic tagging' effect constitutes an important example (Frey & Morris, 1997; Redondo & Morris, 2011). Tagging as recorded in CA1 involves a delayed input promoting LTP, due to the delivery of plasticity-related proteins to different contacts that had been stimulated at an earlier time point. The effect therefore requires intra-dendritic transfer of material from one set of synapses to another and accordingly would be operational only in cells that use postsynaptic LTP. It follows from this that tagging between cortical inputs to hippocampus will occur in CA3 pyramidal neurons but not in DG granule cells. Relatedly, recent studies have linked interactions between neighboring spines to a LTP 'spaced trials effect' in which a second TBS train doubles the magnitude of CA1-LTP produced by a first train when the two stimulation episodes are separated by one hour (Kramar *et al.*, 2012). The studies further indicated that synapses in the hippocampus can have low or high plasticity thresholds and that induction of LTP in the former primes the latter for induction of the potentiated state, with protein transfer between spines being the requisite exchange process. The possible production of a spaced trials effect for LTP – which has been linked to learning (Seese *et al.*, 2014) – in the LPP would accordingly be expected to be much greater in CA3 than in the DG.

The functional consequences of two forms of LTP will likely be affected by the sizeable differences in frequency facilitation between the two LPP branches. The latter findings constitute the first evidence that information carried by single cortical axons will be preferentially routed to CA3 via direct (LPP-CA3) as opposed to indirect (LPP-DG-CA3) connections. An appreciation of those aspects of release dynamics that account for differences between the two sites could be an important step towards specifying the spine to terminal specification mechanism. Simulation results identified likely candidates for the kinetic features that differed between the two LPP termination sites, but a more precise description is possible. Specifically, recent studies

have reported that expanding the two-step vesicle release model (e.g., (Miki *et al.*, 2016)) to incorporate two reversible vesicle priming states, termed tightly- and loosely-docked (TS and LS, respectively), enabled the simulated output to reliably recapitulate experimentally derived output curves recorded from the Calyx of Held (Lin *et al.*, 2022). The relative proportion of docked synaptic vesicles occupying the primed, TS state has been postulated as a critical determinant in frequency-dependent operations occurring at a given synapse (Neher & Brose, 2018; Lin *et al.*, 2022). As such, synapses containing a high proportion of TS vesicles typically have a high initial *p*, displaying short term depression of responses following high frequency activation whilst those synapses comprised primarily of LS vesicles exhibit a low *p* and frequency facilitation (Neher & Brose, 2018 ; Aldahabi *et al.*, 2022; Lin *et al.*, 2022). Indeed, it has recently been proposed that different vesicle priming states underpin postsynaptic target-cell differences in synaptic efficacy associated with CA1 pyramidal cell innervation of specific interneuron subtypes (Aldahabi *et al.*, 2022). Consistent with this notion, selectively reducing the probability of vesicles being docked (δ), a feature analogous to the tightly-docked state, in our two-step model, and modestly increasing the recycling of vesicles to the replacement pool (s) transformed the simulated output from the LPP-DG synapse to one more comparable to the output of the LPP-CA3 terminal. This suggests that relatively subtle differences in vesicle priming, and subsequent recycling may explain the functional differences in synaptic transmission evident at the two LPP terminal fields. Synaptotagmin 3 is a Ca^{2+} sensing protein postulated to promote frequency facilitation by driving the transition of synaptic vesicles to their primed state as well as by increasing replenishment of the readily releasable pool (Weingarten *et al.*, 2022). As such it is an attractive candidate for the presynaptic element differentially regulated by granule vs. pyramidal cells.

References

Aldahabi M, Balint F, Holderith N, Lorincz A, Reva M & Nusser Z. (2022). Different priming states of synaptic vesicles underlie distinct release probabilities at hippocampal excitatory synapses. *Neuron*.

Amani M, Lauterborn JC, Le AA, Cox BM, Wang W, Quintanilla J, Cox CD, Gall CM & Lynch G. (2021). Rapid Aging in the Perforant Path Projections to the Rodent Dentate Gyrus. *J Neurosci* **41,** 2301-2312.

Amaral DG. (1993). Emerging principles of intrinsic hippocampal organization. *Curr Opin Neurobiol* **3,** 225-229.

Amaral DG, Ishizuka N & Claiborne B. (1990). Neurons, numbers and the hippocampal network. *Prog Brain Res* **83,** 1-11.

Babayan AH, Kramar EA, Barrett RM, Jafari M, Haettig J, Chen LY, Rex CS, Lauterborn JC, Wood MA, Gall CM & Lynch G. (2012). Integrin dynamics produce a delayed stage of long-term potentiation and memory consolidation. *J Neurosci* **32,** 12854-12861.

Bao J, Reim K & Sakaba T. (2010). Target-dependent feedforward inhibition mediated by short-term synaptic plasticity in the cerebellum. *J Neurosci* **30,** 8171-8179.

Barrionuevo G & Brown TH. (1983). Associative long-term potentiation in hippocampal slices. *Proc Natl Acad Sci U S A* **80,** 7347-7351.

Berzhanskaya J, Urban NN & Barrionuevo G. (1998). Electrophysiological and pharmacological characterization of the direct perforant path input to hippocampal area CA3. *J Neurophysiol* **79,** 2111-2118.

Castillo PE, Younts TJ, Chavez AE & Hashimotodani Y. (2012). Endocannabinoid signaling and synaptic function. *Neuron* **76,** 70-81.

Chan CS, Weeber EJ, Zong L, Fuchs E, Sweatt JD & Davis RL. (2006). Beta 1-integrins are required for hippocampal AMPA receptor-dependent synaptic transmission, synaptic plasticity, and working memory. *J Neurosci* **26,** 223-232.

Chen LY, Rex CS, Casale MS, Gall CM & Lynch G. (2007). Changes in synaptic morphology accompany actin signaling during LTP. *J Neurosci* **27,** 5363-5372.

Chiu CQ & Castillo PE. (2008). Input-specific plasticity at excitatory synapses mediated by endocannabinoids in the dentate gyrus. *Neuropharmacology* **54,** 68-78.

Christie BR & Abraham WC. (1994). Differential regulation of paired-pulse plasticity following LTP in the dentate gyrus. *Neuroreport* **5,** 385-388.

Cox BM, Cox CD, Gunn BG, Le AA, Inshishian VC, Gall CM & Lynch G. (2019). Acquisition of temporal order requires an intact CA3 commissural/associational (C/A) feedback system in mice. *Commun Biol* **2,** 251.

Del Castillo J & Katz B. (1954). Statistical factors involved in neuromuscular facilitation and depression. *J Physiol* **124,** 574-585.

Eichenbaum H & Fortin NJ. (2005). Bridging the gap between brain and behavior: cognitive and neural mechanisms of episodic memory. *J Exp Anal Behav* **84,** 619-629.

Eichenbaum H, Sauvage M, Fortin N, Komorowski R & Lipton P. (2012). Towards a functional organization of episodic memory in the medial temporal lobe. *Neurosci Biobehav Rev* **36,** 1597-1608.

Frey U & Morris RG. (1997). Synaptic tagging and long-term potentiation. *Nature* **385,** 533-536.

Granger AJ & Nicoll RA. (2014). Expression mechanisms underlying long-term potentiation: a postsynaptic view, 10 years on. *Philos Trans R Soc Lond B Biol Sci* **369,** 20130136.

Gunn BG, Cox CD, Chen Y, Frotscher M, Gall CM, Baram TZ & Lynch G. (2017). The Endogenous Stress Hormone CRH Modulates Excitatory Transmission and Network Physiology in Hippocampus. *Cereb Cortex* **27,** 4182-4198.

Hargreaves EL, Rao G, Lee I & Knierim JJ. (2005). Major dissociation between medial and lateral entorhinal input to dorsal hippocampus. *Science* **308,** 1792-1794.

Hashimotodani Y, Nasrallah K, Jensen KR, Chavez AE, Carrera D & Castillo PE. (2017). LTP at Hilar Mossy Cell-Dentate Granule Cell Synapses Modulates Dentate Gyrus Output by Increasing Excitation/Inhibition Balance. *Neuron* **95,** 928-943 e923.

Henze DA, Wittner L & Buzsaki G. (2002). Single granule cells reliably discharge targets in the hippocampal CA3 network in vivo. *Nat Neurosci* **5,** 790-795.

Hunsaker MR, Chen V, Tran GT & Kesner RP. (2013). The medial and lateral entorhinal cortex both contribute to contextual and item recognition memory: a test of the binding of items and context model. *Hippocampus* **23,** 380-391.

Jackman SL & Regehr WG. (2017). The Mechanisms and Functions of Synaptic Facilitation. *Neuron* **94,** 447-464.

Jensen KR, Berthoux C, Nasrallah K & Castillo PE. (2021). Multiple cannabinoid signaling cascades powerfully suppress recurrent excitation in the hippocampus. *Proc Natl Acad Sci U S A* **118**.

Kano M, Ohno-Shosaku T, Hashimotodani Y, Uchigashima M & Watanabe M. (2009). Endocannabinoid-mediated control of synaptic transmission. *Physiol Rev* **89,** 309-380.

Katona I, Urban GM, Wallace M, Ledent C, Jung KM, Piomelli D, Mackie K & Freund TF. (2006). Molecular composition of the endocannabinoid system at glutamatergic synapses. *J Neurosci* **26,** 5628-5637.

Kauer JA, Malenka RC & Nicoll RA. (1988). A persistent postsynaptic modification mediates long-term potentiation in the hippocampus. *Neuron* **1,** 911-917.

Kim CH & Lisman JE. (1999). A role of actin filament in synaptic transmission and long-term potentiation. *J Neurosci* **19,** 4314-4324.

Kramar EA, Babayan AH, Gavin CF, Cox CD, Jafari M, Gall CM, Rumbaugh G & Lynch G. (2012). Synaptic evidence for the efficacy of spaced learning. *Proc Natl Acad Sci U S A* **109,** 5121-5126.

Kramar EA, Lin B, Rex CS, Gall CM & Lynch G. (2006). Integrin-driven actin polymerization consolidates long-term potentiation. *Proc Natl Acad Sci U S A* **103,** 5579-5584.

Krucker T, Siggins GR & Halpain S. (2000). Dynamic actin filaments are required for stable long-term potentiation (LTP) in area CA1 of the hippocampus. *Proc Natl Acad Sci U S A* **97,** 6856-6861.

Lauterborn JC, Kramar EA, Rice JD, Babayan AH, Cox CD, Karsten CA, Gall CM & Lynch G. (2017). Cofilin Activation Is Temporally Associated with the Cessation of Growth in the Developing Hippocampus. *Cereb Cortex* **27,** 2640-2651.

Lawrence JJ, Grinspan ZM & McBain CJ. (2004). Quantal transmission at mossy fibre targets in the CA3 region of the rat hippocampus. *J Physiol* **554,** 175-193.

Lawrence JJ & McBain CJ. (2003). Interneuron diversity series: containing the detonation--feedforward inhibition in the CA3 hippocampus. *Trends Neurosci* **26,** 631-640.

Le AA, Quintanilla J, Amani M, Piomelli D, Lynch G & Gall CM. (2022). Persistent sexually dimorphic effects of adolescent THC exposure on hippocampal synaptic plasticity and episodic memory in rodents. *Neurobiol Dis* **162,** 105565.

Lin KH, Taschenberger H & Neher E. (2022). A sequential two-step priming scheme reproduces diversity in synaptic strength and short-term plasticity. *Proc Natl Acad Sci U S A* **119,** e2207987119.

Manabe T & Nicoll RA. (1994). Long-term potentiation: evidence against an increase in transmitter release probability in the CA1 region of the hippocampus. *Science* **265,** 1888-1892.

McMahon DB & Barrionuevo G. (2002). Short- and long-term plasticity of the perforant path synapse in hippocampal area CA3. *J Neurophysiol* **88,** 528-533.

McNaughton BL. (1980). Evidence for two physiologically distinct perforant pathways to the fascia dentata. *Brain Res* **199,** 1-19.

Miki T, Malagon G, Pulido C, Llano I, Neher E & Marty A. (2016). Actin- and Myosin-Dependent Vesicle Loading of Presynaptic Docking Sites Prior to Exocytosis. *Neuron* **91,** 808-823.

Milior G, Di Castro MA, Sciarria LP, Garofalo S, Branchi I, Ragozzino D, Limatola C & Maggi L. (2016). Electrophysiological Properties of CA1 Pyramidal Neurons along the Longitudinal Axis of the Mouse Hippocampus. *Sci Rep* **6,** 38242.

Muller D & Lynch G. (1988). Long-term potentiation differentially affects two components of synaptic responses in hippocampus. *Proc Natl Acad Sci U S A* **85,** 9346-9350.

Muller D & Lynch G. (1989). Evidence that changes in presynaptic calcium currents are not responsible for long-term potentiation in hippocampus. *Brain Res* **479,** 290-299.

Neher E & Brose N. (2018). Dynamically Primed Synaptic Vesicle States: Key to Understand Synaptic Short-Term Plasticity. *Neuron* **100,** 1283-1291.

Nicoll RA & Schmitz D. (2005). Synaptic plasticity at hippocampal mossy fibre synapses. *Nat Rev Neurosci* **6,** 863-876.

Petersen RP, Moradpour F, Eadie BD, Shin JD, Kannangara TS, Delaney KR & Christie BR. (2013). Electrophysiological identification of medial and lateral perforant path inputs to the dentate gyrus. *Neuroscience* **252,** 154-168.

Piette C, Cui Y, Gervasi N & Venance L. (2020). Lights on Endocannabinoid-Mediated Synaptic Potentiation. *Front Mol Neurosci* **13,** 132.

Pinkstaff JK, Detterich J, Lynch G & Gall C. (1999). Integrin subunit gene expression is regionally differentiated in adult brain. *J Neurosci* **19,** 1541-1556.

Quintanilla J, Jia Y, Lauterborn JC, Pruess BS, Le AA, Cox CD, Gall CM, Lynch G & Gunn BG. (2022). Novel types of frequency filtering in the lateral perforant path projections to dentate gyrus. *J Physiol* **600,** 3865-3896.

Reagh ZM & Yassa MA. (2014). Object and spatial mnemonic interference differentially engage lateral and medial entorhinal cortex in humans. *Proc Natl Acad Sci U S A* **111,** E4264-4273.

Rebola N, Carta M & Mulle C. (2017). Operation and plasticity of hippocampal CA3 circuits: implications for memory encoding. *Nat Rev Neurosci* **18,** 208-220.

Redondo RL & Morris RG. (2011). Making memories last: the synaptic tagging and capture hypothesis. *Nat Rev Neurosci* **12,** 17-30.

Rex CS, Chen LY, Sharma A, Liu J, Babayan AH, Gall CM & Lynch G. (2009). Different Rho GTPase-dependent signaling pathways initiate sequential steps in the consolidation of long-term potentiation. *J Cell Biol* **186,** 85-97.

Rex CS, Lin CY, Kramar EA, Chen LY, Gall CM & Lynch G. (2007). Brain-derived neurotrophic factor promotes long-term potentiation-related cytoskeletal changes in adult hippocampus. *J Neurosci* **27,** 3017-3029.

Reyes A, Lujan R, Rozov A, Burnashev N, Somogyi P & Sakmann B. (1998). Target-cell-specific facilitation and depression in neocortical circuits. *Nat Neurosci* **1,** 279-285.

Rollenhagen A, Satzler K, Rodriguez EP, Jonas P, Frotscher M & Lubke JH. (2007). Structural determinants of transmission at large hippocampal mossy fiber synapses. *J Neurosci* **27,** 10434-10444.

Rozov A, Burnashev N, Sakmann B & Neher E. (2001). Transmitter release modulation by intracellular Ca2+ buffers in facilitating and depressing nerve terminals of pyramidal cells

in layer 2/3 of the rat neocortex indicates a target cell-specific difference in presynaptic calcium dynamics. *J Physiol* **531,** 807-826.

Salin PA, Scanziani M, Malenka RC & Nicoll RA. (1996). Distinct short-term plasticity at two excitatory synapses in the hippocampus. *Proc Natl Acad Sci U S A* **93,** 13304-13309.

Scanziani M, Gahwiler BH & Charpak S. (1998). Target cell-specific modulation of transmitter release at terminals from a single axon. *Proc Natl Acad Sci U S A* **95,** 12004-12009.

Seese RR, Wang K, Yao YQ, Lynch G & Gall CM. (2014). Spaced training rescues memory and ERK1/2 signaling in fragile X syndrome model mice. *Proc Natl Acad Sci U S A* **111,** 16907-16912.

Sun HY, Lyons SA & Dobrunz LE. (2005). Mechanisms of target-cell specific short-term plasticity at Schaffer collateral synapses onto interneurones versus pyramidal cells in juvenile rats. *J Physiol* **568,** 815-840.

Tamamaki N & Nojyo Y. (1993). Projection of the entorhinal layer II neurons in the rat as revealed by intracellular pressure-injection of neurobiotin. *Hippocampus* **3,** 471-480.

Toth K, Suares G, Lawrence JJ, Philips-Tansey E & McBain CJ. (2000). Differential mechanisms of transmission at three types of mossy fiber synapse. *J Neurosci* **20,** 8279-8289.

Trieu BH, Kramar EA, Cox CD, Jia Y, Wang W, Gall CM & Lynch G. (2015). Pronounced differences in signal processing and synaptic plasticity between piriform-hippocampal network stages: a prominent role for adenosine. *J Physiol* **593,** 2889-2907.

Wang W, Cox BM, Jia Y, Le AA, Cox CD, Jung KM, Hou B, Piomelli D, Gall CM & Lynch G. (2018a). Treating a novel plasticity defect rescues episodic memory in Fragile X model mice. *Mol Psychiatry* **23,** 1798-1806.

Wang W, Jia Y, Pham DT, Palmer LC, Jung KM, Cox CD, Rumbaugh G, Piomelli D, Gall CM & Lynch G. (2018b). Atypical Endocannabinoid Signaling Initiates a New Form of Memory-Related Plasticity at a Cortical Input to Hippocampus. *Cereb Cortex* **28,** 2253-2266.

Wang W, Trieu BH, Palmer LC, Jia Y, Pham DT, Jung KM, Karsten CA, Merrill CB, Mackie K, Gall CM, Piomelli D & Lynch G. (2016). A Primary Cortical Input to Hippocampus Expresses a Pathway-Specific and Endocannabinoid-Dependent Form of Long-Term Potentiation. *Eneuro* **3**.

Weingarten DJ, Shrestha A, Juda-Nelson K, Kissiwaa SA, Spruston E & Jackman SL. (2022). Fast resupply of synaptic vesicles requires synaptotagmin-3. *Nature* **611,** 320-325.

Witter MP. (1993). Organization of the entorhinal-hippocampal system: a review of current anatomical data. *Hippocampus* **3 Spec No,** 33-44.

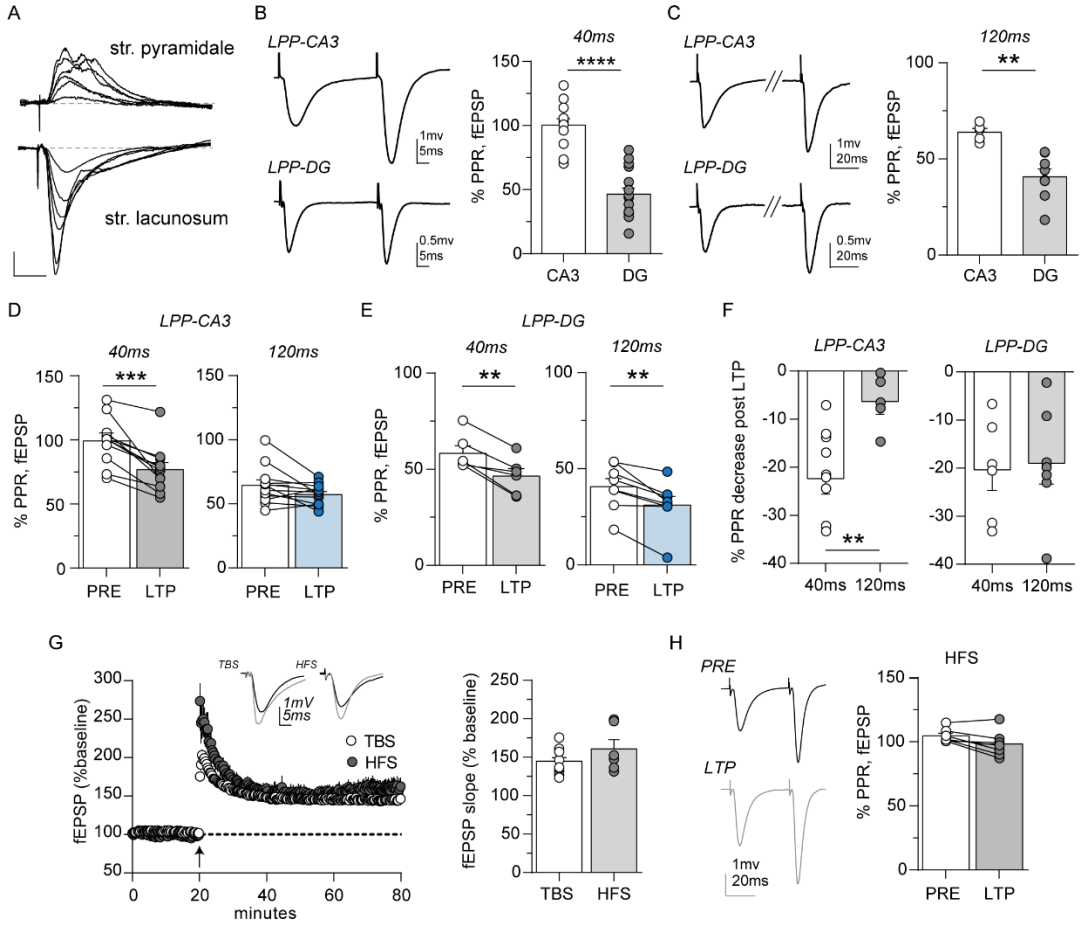

Figure 2.1. Long-term potentiation (LTP) induced by theta burst stimulation (TBS) or high frequency stimulation (HFS) differentially influences the paired-pulse (PP) responses at LPP-CA3 synapses. A. Representative LPP-evoked fEPSP responses recorded from str. pyramidale (top) and str. lacunosum (bottom) of CA3 across a range of stimulation intensities. **B, C.** Representative responses to PP stimulation recorded from LPP-CA3 and LPP-DG with inter-pulse intervals of 40ms (B, *left*) and 120ms (C, *left*). Bar graphs summarizing the PPR magnitude for LPP-CA3 and LPP-DG synapses reveal significant difference between the regions for interpulse intervals of 40ms (****p< 0.0001; **B**, *right*) and 120ms (**p=0.002; **C**, *right*). **D, E.** Bar graphs show that with induction of LTP the PPR is reduced with 40ms but not 120 ms intervals for LPP-CA3 (**D**) and at both latencies for LPP-DG (**E**); ***p<0.001, **p< 0.01 paired Student's t-test. **F.** Plot shows that the percent decrease in PPRs measured after LTP induction differed for 40ms and 120ms interpulse intervals for LPP-CA3 synapses but not for LPP-DG synapses (**p<0.01, unpaired Student's t-test). **G**. *Left.* LTP was induced (arrow) in the LPP-CA3 synapses using TBS or HFS. Representative traces show LPP-evoked responses before (black) and 60-mins after (grey) TBS or HFS. *Right.* The magnitude of TBS- and HFS-induced LTP is shown at right. **H.** Representative traces recorded from LPP-CA3 (*left*) in response to PP stimulation (40ms interval) before (*PRE*) and 60-mins after HFS-induced LTP. Summary graph reveals no effect of LTP on the mean PPR in response to PP stimulation (40ms).

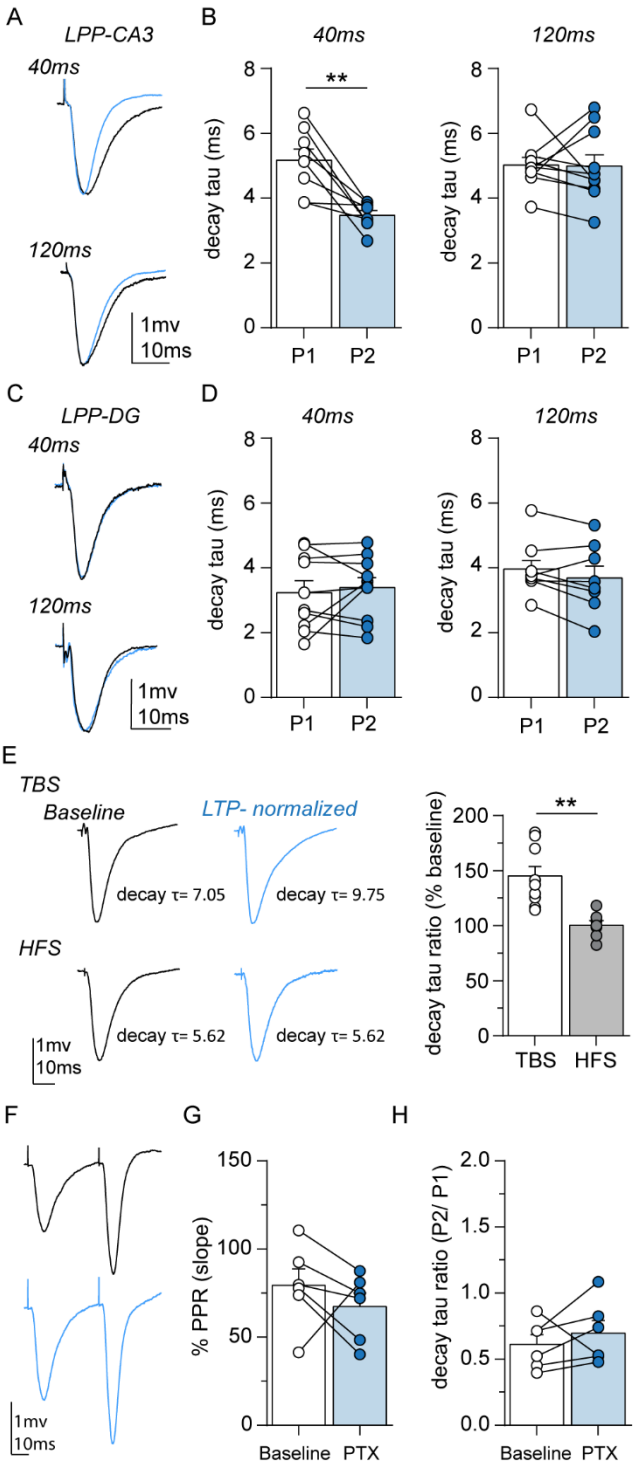

Figure 2.2. The decay time of LPP-evoked fEPSPs is prolonged following TBS-induced LTP. Superimposed normalized first (black) and second (blue) responses recorded from LPP-CA3 (**A**) and LPP-DG (**C**) following paired-pulse stimulation with 40ms (top) and 120ms (bottom) inter-pulse intervals. Graphs summarizing the mean decay τ of the first (P1) and second (P2) responses recorded from LPP-CA3 (**B**) and LPP-DG (**D**) after paired-pulse stimulation with 40ms and 120ms inter-pulse intervals. **p<0.01 paired Student's t test. **E**. *Left:* Normalized representative traces recorded from LPP-CA3 before (black) and 60-mins after (blue) LTP induction with TBS (top) and HFS (bottom). Note the clear prolongation of the fEPSP decay τ following TBS-induced LTP. *Right:* Graph summarizing the effect of TBS- and HFS-induced LTP on the decay □ of fEPSPs. **p<0.01 unpaired Student's t test. **F**. Representative traces recorded from LPP-CA3 after paired pulse stimulation (40ms interval) before (black) and 40-min after PTX (1μM) infusion (blue). Graphs summarize the effect of PTX on the mean PPR (**G**) and decay τ ratio (**H**).

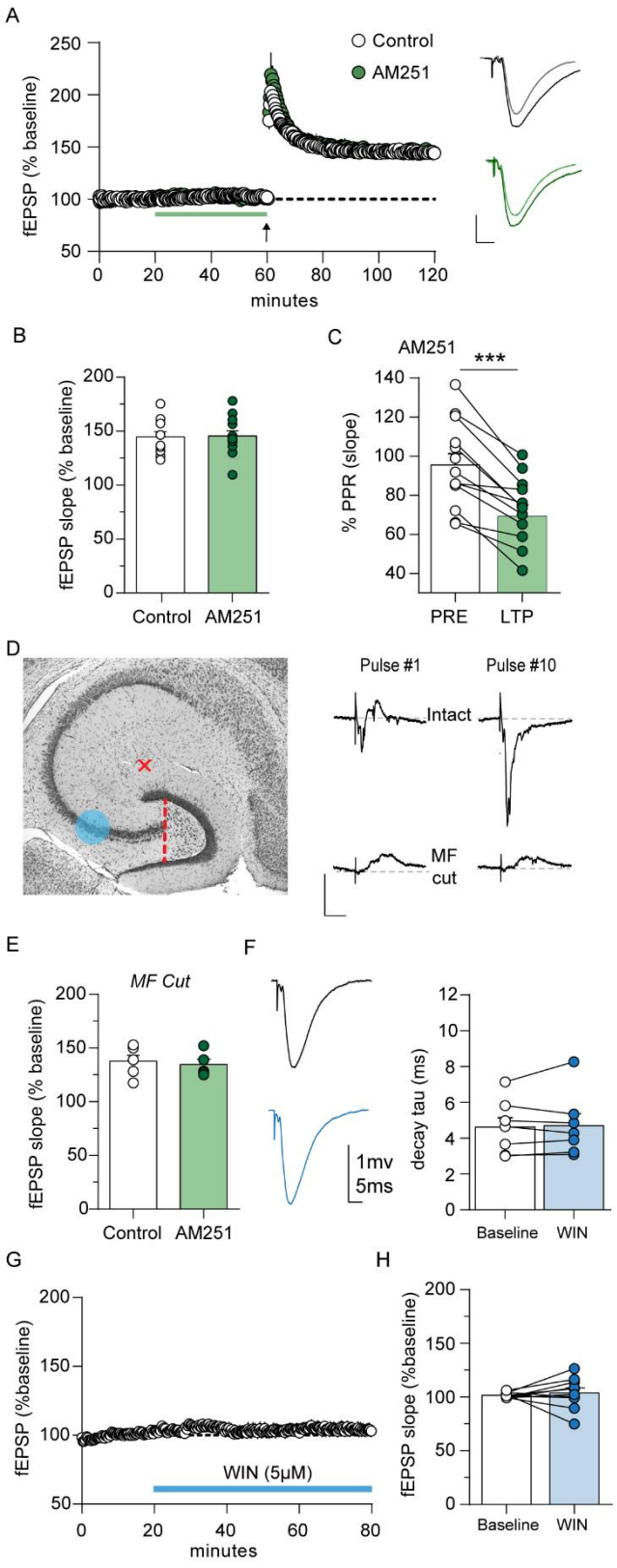

Figure 2.3. LTP at LPP-CA3 synapses does not require endocannabinoid signaling. A. LTP induced at LPP-CA3 synapses using TBS (arrow) was unaffected by 40-min infusion of CB1R inverse agonist, AM251 (5μM). Representative traces show LPP-evoked responses before (light) and 60 mins after TBS (dark), in the absence (top) and presence of AM251 (bottom). **B, C.** AM251 did not influence the magnitude of LTP (fEPSP slope) (**B**) but did significantly reduce the PPR (***p< 0.001; paired Student's t-test) (**C**) as assessed 60 min post-TBS. **D**. *Left:* Nissl-stained cross section of temporal hippocampus illustrates location of the cut through the mossy fibers (red line) and the position of the recording pipette (blue) and stimulating electrode. *Right:* Representative traces recorded from the mossy fiber (MF) -CA3 synapse in response to a 10 pulse 20Hz stimulation train in an intact slice (top) and those lacking the MF connection (bottom). **E.** Cutting the MFs had no effect on the magnitude of LTP or AM251 effect. **F**. *Left:* Representative LPP-evoked responses in the absence (black) and presence (blue) of CB1R agonist WIN55 (5μM). *Right:* Graph showing the mean fEPSP decay τ was unaffected by WIN55 infusion. **G, H.** Graphs show WIN55 infusion did not influence the slope of LPP-evoked fEPSPs as assessed over time (G) and for the final 5-min (55-60 min) post infusion (H).

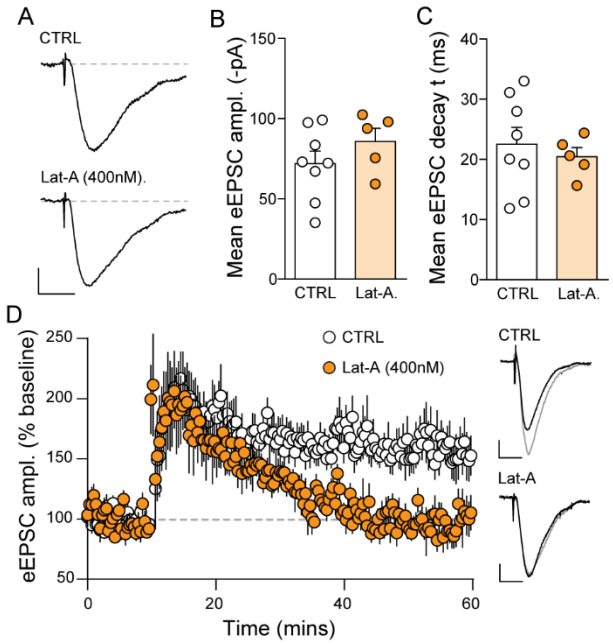

Figure 2.4. Postsynaptic latrunculin-A (Lat-A) prevents stabilization of LPP-CA3 LTP without effect on baseline transmission. A. Ensemble averages of LPP-eEPSCs recorded from representative CA3 pyramidal cells in the absence (top) and presence (bottom) of intracellular Lat-A (scale bars: y=20pA; x=20ms). Intracellular administration of Lat-A has no effect on the amplitude (**B**) or decay time (**C**) of LPP-eEPSCs. **D**. The presence of postsynaptic Lat-A prevented TBS-induced LTP at LPP-CA3 synapses. Traces at right show ensemble average eEPSCs recorded from CA3 pyramidal cells before (black) and after LTP induction (grey) in the absence (top) and presence (bottom) of Lat-A (scale bars: y=20pA; x=20ms).

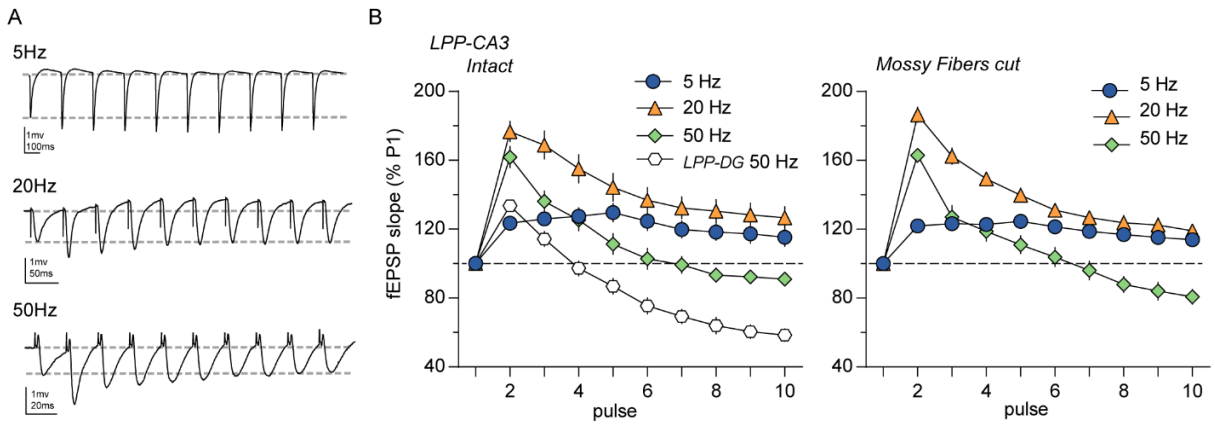

Figure 2.5. LPP-CA3 responses are frequency-dependent. A. Representative traces recorded from CA3 str. lacunosum in response to LPP stimulation (10 pulses) at 5Hz, 20Hz and 50Hz. **B.** Graph summarizing the within train facilitation of the LPP-CA3 fEPSP slope for each stimulation frequency recorded from intact slices (*left*) and slices lacking mossy fiber (MF) connection (*right*).

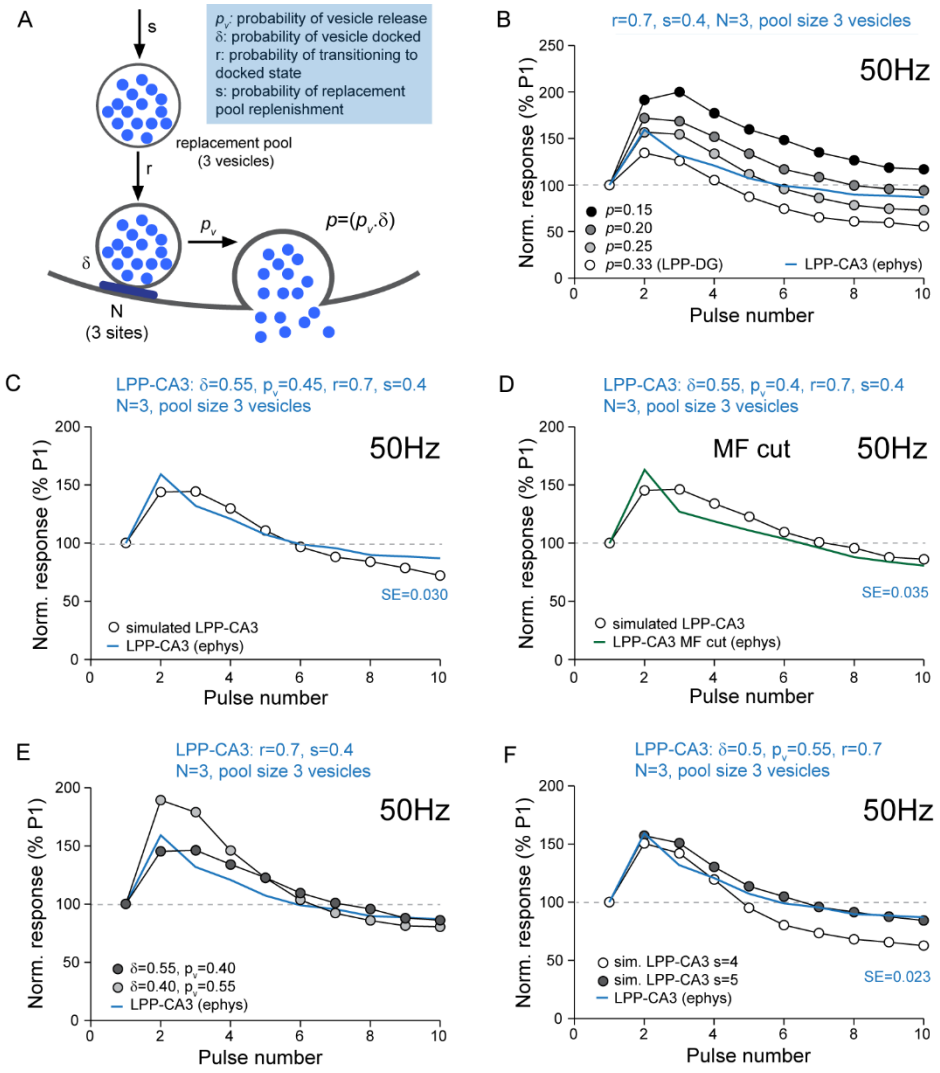

Figure 2.6. Differences in release dynamics may underlie differences in frequency facilitation for the two branches of the LPP. A. Schematic shows the two-step release model, wherein N describes the number of docking sites. **B**. Selectively decreasing *p* in the physiologically constrained two-step release model increased initial facilitation and reduced within-train response suppression in the simulated LPP-DG output curve after 50Hz stimulation. Note: Decreasing *p* to 0.25 crudely recapitulated the empirical LPP-CA3 output profile (blue line). Optimization of the release dynamics, δ and p_v, produced an output curve more analogous to the electrophysiological data recorded from the intact slice (**C**) and those with the MF-cut (**D**). The empirical data for the intact (blue line) and MF-cut (green line) slice are illustrated. **E**. The relative contribution of δ and p_v to the overall *p* is critical for determining the magnitude of the initial facilitation and within-train suppression of the simulated output profile following 50Hz stimulation. **F**. Using a model where δ is selectively reduced, the electrophysiological LPP-CA3 output profile (blue line) can be largely recapitulated by increasing *s*.

CHAPTER 3: Microglia Support an Unusual Form of Synaptic Plasticity and Related Episodic Memory.

Summary

We report here that microglia exert a remarkably discrete but functionally critical influence on the operation of mouse hippocampus. Treatment with the Colony Stimulating Factor-1 receptor antagonist PLX5622 and resultant depletion of microglia did not disturb synaptic transmission at any of four glutamatergic connections in hippocampus. Long-Term Potentiation (LTP) was also intact for three of these sites but the singular LTP variant expressed by the lateral perforant path (LPP) synapses with the dentate gyrus (DG) was severely impaired. The defect was accompanied by failed encoding of three basic elements of episodic memory -- the identities, locations, and temporal order for a collection of cues. Key steps in the endocannabinoid system, including levels of 2-arachidonoylglycerol (2-AG), that initiates LPP-LTP were abnormal in the DG of the microglia deficient animals. Suppression of 2-AG breakdown restored both potentiation and episodic memory. We propose that microglia spatially align the pre- and post-synaptic components of endocannabinoid signaling, thereby enabling a specialized synaptic change required for the encoding of episodes.

Introduction

Initial recognition of microglia as a distinct class of CNS cells was soon followed by the assumption that they constitute a type of macrophage (Aguzzi et al., 2013; Perry and Teeling, 2013). Subsequent work confirmed this idea. In their resting state the cells generate multiple continuously active processes that survey the surrounding tissue for pathological elements or foreign material (Nimmerjahn et al., 2005; Wake et al., 2009; Aguzzi et al., 2013). Detection leads to a rapid transformation into a reactive configuration that favors migration, the release of potent cytokines, engulfment, and phagocytosis. As with most types of macrophages, microglia are competent antigen presenting cells and vigorously respond to inflammatory mediators. They thus qualify as an inflammatory/immune interface for adult brain with the expected capability for eliminating disruptive elements.

There has been considerable speculation about the possibility that microglia -- in addition to their activities under pathological circumstances -- make significant contributions to the normal operations of brain subsystems. The discovery that they play a central role in the pruning of excess connections during development described a role of this type. Other work suggests that microglia via their actions on the extracellular matrix participate in the ‘remodeling’ of synaptic junctions in the adult brain and thus may be needed for experience driven modifications to networks. Whether they also modulate rapid physiological activities in brain remains an open question. Much of the work in this area has involved the induction of long-term potentiation (LTP) and the related acquisition of new memories. It has become clear that factors released by microglia (e.g., interleukin-1ß, matrix metalloproteinase 9) (Cunningham et al., 1996; Schneider et al., 1998; Nagy et al., 2006; Liu and Quan, 2018) potently influence LTP but whether microglial regulation occurs under baseline conditions or is instead only engaged as part of an inflammatory response has yet to be resolved.

The work reported here tested for microglial influences on signal transformation and plasticity at excitatory synapses in hippocampus of young adult rodents. Multiple sites were tested because of increasing evidence for pronounced regional variations in frequency filtering and LTP (Wang et al., 2016; Wang et al., 2018b; Le et al., 2022a; Quintanilla et al., 2022). Accordingly, there may not be a general microglial effect, but instead location-specific actions dependent on the type of mechanism used to adjust synaptic strength. An effect at one or more sites could alter the essential hippocampal contributions to the acquisition and use of episodic memory. Such a result would suggest a link between the inflammatory events that potently affect microglia and the routine encoding of daily experience. We therefore examined three basic elements of episodic memory following elimination of the glial cells.

Materials and Methods

Studies used male C57/BL/6N mice (Charles River) at 2-4 months of age. Mice were group-housed (3-5 per cage) with access to food and water *ad libitum* and maintained on a 12 h light/dark cycle with lights on at 6:30 AM. Electrophysiological experiments were initiated from 8-10 AM. All procedures were conducted in accordance with NIH guidelines for the Care and Use of Laboratory Animals and Protocols and institutional approved protocols.

In-vivo PLX5622 treatment. Young adult (2-4 mo old) mice were provided either normal chow (controls) or chow containing PLX5622 (PLX; 1200 ppm)(Cayman Chemical Company, Ann Arbor, MI, USA), an antagonist of the colony stimulating factor-1 receptor (CSF1R) which is critical for microglial survival (Green et al., 2020; Liu et al., 2021); poloxamine was included in the PLX chow formulation to prevent recrystallization (Kuntsche et al., 2010). Animals were maintained on the experimental diet and water *ad libitum* for a minimum of 10-21 days until experimental use which entailed preparation of hippocampal slices or tissue harvest for endocannabinoid measures; for some cohorts, behavioral analysis was followed by slice preparation (**Fig 3.1A**). In all cases animals were maintained on the experimental diet until

sacrifice. There were no differences in food consumption or body weights between the control and PLX groups over the treatment period.

Slice preparation and recording procedures. Hippocampal slices were prepared for field recordings as previously described (Cox et al., 2019; Le et al., 2022a; Quintanilla et al., 2022). Mice were anesthetized with isoflurane and euthanized by decapitation. Brains were placed in ice-cold oxygenated (95% O_2/ 5% CO_2) high Mg^{2+} artificial cerebrospinal fluid (aCSF) containing (in mM): 87 NaCl, 26 $NaHCO_3$, 25 glucose, 75 sucrose, 2.5 KCl, 1.25 NaH_2PO_4, 0.5 $CaCl_2$, 7 $MgCl_2$, (320-335mOsm) and then sectioned (horizontal, 360 µm) on the Leica vibrating tissue slicer (model, VT1000s, Leica) for DG recordings or perpendicular to the hippocampal long axis on a McIllwain chopper (360µm) for CA1 recordings; sections were collected into ice-cold aCSF. Slices were immediately transferred to an interface recording chamber with a constant perfusion of oxygenated aCSF (31±1°C, 95% O_2/ 5% CO_2) containing the following (in mM): 124 NaCl, 3 KCl, 1.25 KH_2PO_4, 1.5 $MgSO_4$, 26 $NaHCO_3$, 2.5 $CaCl_2$, and 10 dextrose at a rate of 60-70ml/h. Experiments were initiated ~1.5 h after slices were placed in the recording chamber. For all studies, stimulation was adjusted to elicit a field excitatory post-synaptic potential (fEPSP) of amplitude approximately 50% of the maximum population-spike free response. The fEPSPs were elicited using a bipolar stimulating electrode (twisted 65 µm nichrome wire) and recorded using a drawn glass pipette electrode containing 2M NaCl (2-3 MΩ). fEPSP slopes were collected using NACGather 2.0 (Theta Burst Corp., Irvine, CA, USA). For all slices, input-output curves were assessed, as were responses to a ten pulse 40 Hz stimulation train. Afterwards, stable baseline responses were collected for at least 20 min prior to induction of LTP as described below.

Lateral Perforant Path (LPP) - DG. For LPP-DG experiments, stimulating and recording electrodes were placed in the outer third of the DG molecular layer (internal blade). Proper electrode placement was confirmed using paired-pulse stimulation (40ms interval), which elicits

response facilitation in the LPP but not medial perforant path (Christie and Abraham, 1994; Wang et al., 2016). For LPP-LTP experiments, stable baseline responses were collected for at least 20 min at 0.05 Hz and then potentiation was induced by applying 1s of 100 Hz, high-frequency stimulation (HFS) with pulse duration doubled and intensity increased x1.5 relative to baseline parameters; 0.05Hz stimulation resumed immediately after HFS and continued for at least 60 minutes.

Medial Perforant Path (MPP) - DG. For MPP-DG analyses, recordings were performed in the presence of 1µM picrotoxin which was infused into the aCSF bath continuously for 40 min prior to experimentation (Amani et al., 2021). Stimulating and glass recording electrodes were placed in the middle third of the DG molecular layer. Electrode placement was verified by the presence of paired-pulse depression in response to a paired stimuli (40ms interval) as described (McNaughton, 1980; Christie and Abraham, 1994). After recording a stable 20 min baseline at 0.05 Hz, LTP was induced using three HFS trains (100Hz, 500ms each, 20 sec intervals) with pulses at 2x duration and 1.5x intensity, relative to baseline. Recording responses to 0.05 Hz stimulation then resumed for an additional hour.

Schaffer-Commissural (SC) - CA1. For the SC innervation of CA1 stratum (str.) radiatum, a stimulating electrode was placed in CA1c and the recording electrode was positioned in CA1b; both electrodes were located in str. radiatum at the same distance from str. pyramidale (Wang et al., 2018a). For LTP induction, a single five-burst train of theta burst stimulation (TBS; 4 pulses at 100Hz per burst, 200 ms between bursts) (Le et al., 2022a) and 0.05 Hz stimulation resumed for one hour thereafter.

Infusion of experimental agents into hippocampal slices. Stock solutions for the cannabinoid receptor types 1 and 2 (CB1 and CB2, respectively) agonists CP 55940 and WIN 55,212-2 mesylate (WIN), the selective monoacylglycerol lipase (MAGL) inhibitor JZL184 (JZL), and the CSFR1 antagonist PLX5622 were prepared in DMSO (10 mM) and on the day of use diluted

into aCSF to obtain a final bath concentration of 1 µM (final DMSO concentration <0.01%). Vehicle solutions did not include these reagents. After recording steady baseline activity, the test reagent (or vehicle) was applied via a secondary infusion line using a syringe pump (6mL/hr) for 40-60 minutes.

Immunofluorescence. To verify microglial depletion with PLX5622 treatment, hippocampal slices (from groups prepared for electrophysiology) were immersion fixed in 4% paraformaldehyde at the time of slice preparation. The slices were sub-sectioned at a thickness of 25µm, mounted onto microscope slices, and processed for immunofluorescence (Rex et al., 2009; Seese et al., 2012; Wang et al., 2018a) using rabbit antisera to the microglial protein Iba1 (1:1000; Fujifilm Wako Pure Chemical Corp) and AlexaFluor Donkey anti-rabbit 594 (1:1000; Millipore). Slides were cover slipped with Vectashield containing DAPI (Vector laboratories). Iba1-immunoreactive (ir) cells were quantified within the full field of view (685 µm x 580 µm) at 20X objective magnification; this field extended from the DG granule cell layer (internal blade) to the hippocampal pyramidal cell layer at the CA1/subicular border (**Fig 1a**); immunoreactive somata were counted from digital images.

Endocannabinoid/Lipid Assay. To assess effects of microglial depletion levels of endocannabinoids and related lipids, we used the recently developed liquid chromatography/tandem mass spectrometry assay (Ahmed et al., 2022) to simultaneously measure concentrations of 2-AG, anandamide (AEA), oleoylethanolamide (OEA) and palmitoylethanolamide (PEA) in punch samples collected from the DG and, for comparison purposes, medial frontal cortex. Single punches were collected from the DG and medial frontal cortex on each hemisphere, and for a given region samples from the two hemispheres were pooled for each of 5 control and 5 PLX-treated mice assessed 3 weeks after PLX treatment onset. Briefly, frozen punch samples were homogenized in acetonitrile containing 1% formic acid and internal standards, using Precellys homogenizer (Bertin technologies, Montigny-le-

Bretonneux, France). Then, lipids were purified using Captiva-Enhanced Matrix Removal (EMR)-Lipid cartridges (Agilent technologies, Santa Clara, CA), dried under nitrogen stream, and reconstituted in methanol with 0.1% formic acid. LC separation was carried out using an Eclipse PAH C18, polymeric bonded phase (1.8 µm, 2.1×50 mm; Agilent technologies). The mobile phase consisted of water containing 0.1% formic acid as solvent A and methanol containing 0.1% formic acid as solvent B. The flow rate was kept at 0.3 mL/min. The gradient conditions were as follows: starting 70% B to 80% B in 10.0 min, changed to 95% B at 10.01 min, and maintained till 2.5 min to remove any strongly retained materials from the column. Equilibration time was 2.5 min. Total analysis time, including re-equilibrium, was 15 min. Column temperature was maintained at experimentally determined optimal 40°C, and the autosampler at 9°C. Injection volume was 1.0 µL. For the MS^n analysis, the mass spectrometric detector (MSD) was operated in the positive ESI mode and analytes were quantified by dynamic multiple reaction monitoring (dMRM). Replicate analyses were performed to determine the average retention times of analytes for use under dMRM conditions. The scan time (ΔT) for each analyte was experimentally determined to ensure complete integration of the peaks, approximately twice their peak widths obtained under MRM. Acquisition parameters were optimized for each analyte using the Agilent MassHunter Optimizer software (Agilent technologies). Source parameters were also optimized using the Agilent MassHunter. Nebulizer and sheath gas temperatures were each set at 300°C with flow rates of 9.0 and 12.0 L/min, respectively. Nebulizer pressure was 50 psi. Capillary and nozzle voltages were set at 3000 and 1900 V, respectively. The MassHunter software was used for instrument control, data acquisition, and analysis.

Behavioral Tasks. Tests involving olfactory cues were used to assess spatial, object location memory and acquisition of elements of episodic memory (i.e., What, Where, and When) in tests

using multiple olfactory cues (Cox et al., 2019; Quintanilla et al., 2021; Le et al., 2022b; Le et al., 2022a). Individual mice were used for no more than two tasks.

General procedures for olfactory cue studies. All odorants (Table 1) were prepared 10-min before use; 100µL of a single odorant was pipetted onto a filter paper that rested at the bottom of a glass jar (5.25 cm diam x 5 cm high), with a perforated lid. All odors were verified to have equal salience and no preferences were observed (Cox et al., 2019; Quintanilla et al., 2021; Le et al., 2022a). Testing arenas and odor cups were wiped clean with 70% ethanol between subjects. Mice were considered to be exploring a cup when their nose was directly above the lid and directed toward the odor hole. Cases where mice sat on top of the cups were not scored. Additionally, animals were excluded from analysis if they did not sniff any cup for at least 1 sec.

Serial 'What' Task. Mice were placed in a test chamber (Plexiglass 30x25x21.5 cm; with distinct spatial cues on adjacent walls) with two unscented, habituation cups, placed in opposite corners, for 2 min. Habituation cups were then removed with the mouse remaining in the chamber. After a 3 min period, the first set of scented odor cups (A:A) was placed in the arena in the same corners as the removed habituation cups. Mice were allowed to sample the odor set for 3 min, after which the cups were removed. After a 3 min delay, the second set of odor cups (B:B) were placed in the arena for a 3 min sampling period. This process was repeated for odor pair C:C. The testing session began 3 min after the removal of cups C:C, and mice were exposed to two different odor cups including the previously sampled odor A and a novel odor D. The time spent with odor D versus odor A was used as a measure of retention. In a separate set of animals, the effects of treatment with MAGL inhibitor JZL184 (8 mg/kg in 80% polyethylene glycol 400 / 20% Tween-80) or vehicle were tested on microglia depleted mice during the 'What' task. Both JZL and vehicle compounds were made fresh the morning of experimentation and were injected intraperitoneal 4 hrs before experimental use (remained in home cage). The animals then performed the serial 'What' task as described above.

'When' Task. Similar to the 'What' task, odor pairs were given in pairs at 3 min intervals (3 min with each), with the addition of a fourth odor pair D:D after set C:C. After the 4 odor sets, the testing period compared the time spent with two previously sampled odors (B:C). Mice that retained the temporal order of cue exposure sampled the odor that was presented earlier (e.g., odor B more than odor C) (Cox et al 2019).

'Where' Task. A separate group of mice were placed in a large testing arena (60x60x30 cm; with spatial cues on adjacent walls) that contained 4 different odor cups (A:B:C:D) with one in each corner (~1 in from each wall). Mice were allowed to sample the cups for 5 min timed from their first interaction with any cup. Mice were then returned to their home cage. For testing 24 hrs later, mice were returned to the same test arena with the location of two diagonal odor cups swapped. Testing lasted 5 min after initial cup interaction. The time spent with the two swapped cups was compared to the time spent with the unmoved cups.

'Two-odor Discrimination' Task. As a control for odor identification, mice were placed in the plexiglass chamber used for the Serial '*What'* Task. After a set of habituation cups (3 min, unscented), mice were presented with odor pair E:E for 3 min. Cups were then removed and after a 15 min delay (timing corresponds to time between familiar pair and testing pair in Serial '*What*'), were tested with odor pairs E:F. The time spent exploring the novel odor F was compared to the time spent exploring familiar odor E.

Object Location Memory Task. Mice were placed in the Serial 'What' arena containing two identical objects (clear glass funnels), which were located near adjacent corners. Mice were allowed to explore the objects for 5 min from their first interaction with an object. Testing occurred 24 hrs later, with one object moved toward the center of the arena. Video recordings were analyzed for the 5 min after first interaction to assess the time interacting with the displaced vs the stationary object.

Results

Cells immunolabeled for ionized calcium binding adaptor molecule 1 (IBA1), a marker of microglia, were evenly distributed across hippocampal subfields in mice receiving the control chow diet (controls) (**Fig 3.1B**). The cells were highly ramified with a meshwork of fine immunolabeled processes (**Fig 3.1B',C**) and no obvious differences in morphology across the major hippocampal subdivisions (DG, CA3, CA1). There was a near complete elimination of IBA1-immunoreactive (ir) microglia in all hippocampal subfields In mice given chow containing the colony stimulating factor 1 receptor (CSF1R) antagonist PLX5622 (PLX) for 10-21 days, in accord with previous reports (Huang et al., 2018; Spangenberg et al., 2019; Liu et al., 2021; Basilico et al., 2022) (**Fig 3.1D**). Quantitative analyses for a sample field that included segments of the DG and CA1 (**Fig. 3,1D**) confirmed that the treatment produced a profound loss of microglia (PLX: 3.48 ± 2.03 cells /xxμm^2, Con: 79.3±7.12; mean ± std. dev. for 5 PLX and 4 Con mice; $p<0.000001$; 2-tailed unpaired t-test).

3.2 Depletion selectively disrupts plasticity in the LPP projections to the DG

The hippocampus receives the great majority of its excitatory input from the medial and lateral subdivisions of the entorhinal cortex (Amaral and Lavenex, 2007). The medial division conveys spatial information to the DG and field CA3 via the MPP whereas lateral entorhinal uses the LPP to relay data relating to cue identity to the two subfields (Dickerson and Eichenbaum, 2010; Eichenbaum et al., 2012; Stensola and Moser, 2016; Cox et al., 2019). MPP and LPP terminal fields form contiguous but non-overlapping lamina in both CA3 and the DG with the LPP occupying the distal most dendrites in each instance. Microglial depletion had no evident effect on the waveform of baseline LPP fEPSPs evoked by single pulse stimulation recorded in the DG outer molecular layer (**Fig 3.2A**). Moreover, input / output (I/O) curves (stimulation current vs. initial slope of the response) were not detectably different between the two groups (**Fig 3.2B**), indicating that microglial depletion did not affect the relationship between

number of axons activated and the resultant magnitude of dendritic depolarization. Next, we examined the manner in which input arriving at the frequency of the gamma rhythm (~40Hz) is transformed by LPP synapses. Gamma trains produce a robust facilitation of responses (frequency facilitation) at most types of synapses, an effect that involves transient adjustments to the machinery controlling release probability (Del Castillo and Katz, 1954; Atwood and Karunanithi, 2002; Abbott and Regehr, 2004). There are also sites at which EPSCs progressively decrease during repetitive activation – it is generally agreed that depression vs. facilitation reflect the initial release probability of the synapse (Del Castillo and Katz, 1954; Atluri and Regehr, 1996; Jackman and Regehr, 2017). LPP contacts are unusual in that they express both effects during a single gamma train: fEPSPs (or EPSCs) facilitate for the first two or three pulses and then become progressively smaller as the train continues (Le et al., 2022a; Quintanilla et al., 2022). This complex pattern was intact in slices from PLX-treated mice and not detectably different from that seen in controls ($F_{9, 135}$=0.37, p=0.95; PLX n=10, Con n=7, two-way RM-ANOVA for PLX vs. control) (**Fig 3.2C**). In all, near complete microglial depletion did not significantly affect signal transformation across LPP-DG synapses.

There was however a dramatic change in the LTP induced by a single, one-second train of high frequency stimulation (HFS; 100 Hz). The first response after HFS was enhanced in the PLX group to about the same degree as in controls, but potentiation rapidly decayed to near baseline values (PLX: 115.8± 6.1, Con: 147.7± 6.8, t_{16}=3.51, p<0.003; PLX n= 9, Con n=9 at 60 min post-HFS; two-tailed unpaired t-test) (**Fig 3.2D-F**). Given that potentiation of the first response after the high frequency train is dependent upon NMDARs (Hanse and Gustafsson, 1992; Wang et al., 2016), it would appear that the microglial contribution to potentiation begins shortly after the initial expression of potentiation.

Further analyses on the LPP-LTP were conducted because of the marked effect of microglial depletion on plasticity in this system. We assessed the effects of acute administration

of the compound PLX at a concentration that blocks CSF1R in untreated mice. Infusion of 1 μM PLX for 60-90 minutes had no evident effect on the waveform of LPP fEPSPs in slices from naïve mice. We used the responses recorded during the 10 minutes immediately prior to HFS, and at least 50 minutes after the start of vehicle or PLX infusion, as a baseline for calculating the magnitude of LPP-LTP. The percent potentiation at 60 minutes post-HFS was 156.0 ± 11.8% in the vehicle group and 155.5 ± 14.5% for PLX-treated slices n= 8/group, t_{14}=0.028, p=0.98; two-tailed unpaired t-test) (**Fig 3.S1A,B**).

PLX effects on LPP projections to field CA3.

LPP axons extend from the DG outer molecular layer to generate a dense terminal field in the most distal dendrites of field CA3 (i.e., distal str. moleculare) (Amaral and Lavenex, 2007) (**Fig 3.2G**). If microglia promote LTP via an action on LPP terminals, then depletion should block potentiation in the CA3 component of the projection. Single pulse stimulation of the LPP produced a large fEPSP in the outermost lamina of apical CA3 accompanied by a smaller positive going wave in str. pyramidale. Microglial elimination had no detectable effect on the waveform of dendritic response and failed to produce a measurable change in magnitude of LPP-CA3 LTP (t_{12}=1.43, p=0.17, n= 7/group; two-tailed unpaired t-test) (**Fig 3.2H,I**). This result further narrows the site of action for microglia by showing that removing the cells affects plasticity in one (DG) but not the other (CA3) LPP terminal field.

3.3 PLX does not affect a neighboring input to the DG.

The MPP terminates immediately below the distal dendritic field innervated by the LPP (middle vs. outer molecular layer of the DG) (**Fig 3.3A**). If microglial depletion disrupts potentiation in the LPP-DG system through global effects on the target granule cells, then changes comparable to those recorded in the LPP should be present in the MPP. Field EPSPs elicited by MPP stimulation in the middle molecular layer were not discernably different in

control vs. PLX cases and I/O curves were comparable between groups (**Fig 3.3B**). MPP synapses fall into the category in which repetitive stimulation produces within-train reduction of postsynaptic responses (McNaughton, 1980; Christie and Abraham, 1994). MPP-evoked responses exhibited similar depression in control and PLX groups across a 10-pulse 40Hz, gamma train ($F_{9, 108}$=1.09, p=0.38; Con n=5, PLX n=9, two-way R-M ANOVA) (**Fig 3.3C**).

In contrast to the LTP results obtained for LPP-DG, microglial depletion did not impair LTP in the MPP input to the DG (t_{11}=1.14 p=0.28, PLX n=7, Con n=6, two-tailed unpaired t-test) (**Fig 3.3D, E**). The percent potentiation recorded 55-60 minutes after HFS was 162.2 ± 9.7% and 148.2 ± 6.9% for slices from PLX- and control mice, respectively. Pertinent to this, we have shown that the substrates for LTP are markedly different in the MPP and LPP. The LPP uses metabotropic glutamate receptors and retrograde, spine to terminal endocannabinoid signaling to produce a stable increase in evoked transmitter release (Wang et al., 2016; Wang et al., 2018b). Much less is known about the substrates for MPP-LTP but it is clear that these do not include the endocannabinoid-triggered presynaptic mechanisms that express and stabilize LPP-LTP (Wang et al., 2016). Thus, two adjacent populations of perforant path synapses on the same dendritic tree employ different forms of plasticity and only one of these is dependent on microglia. Together the results for the three connections (LPP-CA3, LPP-DG, MPP-DG) strongly suggest that the microglial influence on normal physiology is restricted to a plasticity-related interaction between LPP terminals and granule cell dendrites.

3.4 Schaffer-commissural (SC) projections from CA3 to CA1.

Finally, we tested the effects of microglial depletion on synapses formed by the SC projections from field CA3 to the proximal apical dendrites of field CA1 in slices from the middle third of the septotemporal hippocampal axis (**Fig 3.4A**). These well-studied CA3-CA1 contacts exhibit an uncomplicated frequency facilitation during repetitive activation (Wang et al., 2016; Le et al., 2022a) and a low threshold LTP that is induced, expressed, and consolidated in the

postsynaptic compartment (Lynch et al., 1983; Muller and Lynch, 1988; Granger and Nicoll, 2014). The SC system thus has operating characteristics that are distinct from those in the LPP or the MPP. Synaptic responses elicited by single pulse stimulation of the SC fibers were not significantly changed by microglial depletion. As was the case for the DG afferents, I/O curves were nearly identical in control and PLX groups (**Fig 3.4B**). The conventional frequency facilitation effect to short (10 pulse) trains of 40 Hz stimulation was intact in PLX-treated cases ($F_{9,99}$= 0.30, p=0.97; two-way R-M ANOVA) (**Fig 3.4C**). LTP was induced using a train of five theta bursts. The sizes (area) of composite theta burst responses were not measurably changed by microglial depletion ($F_{4,52}$=0.081, p=0.99) (**Fig 3.4D**). This is informative because the burst response profile is strongly modulated by feedforward GABAergic input (Larson and Lynch, 1986; Larson and Munkacsy, 2015; Le et al., 2022b) and includes a sizeable NMDAR-gated component (Chen et al., 2010). It appears that these variables were unaffected by microglial depletion.

For the SC system there were no evident effects of microglial depletion on the initial facilitation that follows TBS or the plateau level of potentiation recorded 15 min later. The magnitude of LTP assessed at 60 minutes post-TBS was comparable in control and PLX groups (PLX: 140.8±3.2% n=7, Con: 148.0±5.2% n=9, p=0.24; two-tailed unpaired t-test) (**Fig 3.4E**). In summary, microglial depletion did not substantially affect throughput, burst responses, or plasticity in the CA3-CA1 link of the primary hippocampal circuit.

3.5 & 3.6 Effects of microglial depletion on the endocannabinoid system

Induction of LTP in LPP-DG synapses requires activation of NMDA and metabotropic glutamate (mGluR5) receptors, an increase in postsynaptic calcium, and activation of the postsynaptic enzyme diacylglycerol lipase (DGL-α) (Wang et al., 2016). DGL-α hydrolyses diacylglycerol to generate the endocannabinoid 2-acylglycerol (2-AG) which diffuses from the spine to cannabinoid type 1 receptors (CB1Rs) located on LPP terminals. The resulting

signaling leads to a stable increase in evoked glutamate release (i.e., LPP-DG LTP) (Wang et al., 2016; Wang et al., 2018b). We used our recently developed liquid chromatography/tandem mass spectrometry method (Ahmed et al., 2022) to simultaneously measure concentrations of 2-AG, AEA, and related lipids OEA, and PEA, in punch samples collected from the DG (Con n=5, PLX n=5) and, for comparison purposes, medial frontal cortex (Con n=5; PLX n=4**) (Fig 3.5A)**. Measures of DG samples detected a robust (>3-fold) increase in 2-AG levels (t_8=4.005; p=0.0039) **(Fig 3.5B)** and a more modest but significant decrease in AEA (t_8=4.144; p=0.0032) and OEA (t_8=2.620; p=0.0307) levels in PLX-treated as compared to control mice **(Fig 3.5C,D)**. In contrast levels of all 4 lipids in the medial frontal cortex, and PEA in the DG, were not affected by PLX treatment **(Fig 3.5E)** (CTX 2-AG: t_7=0.5463, p=0.6018; CTX AEA: t_7=0.3557, p=0.7325; CTX OEA: t_7=0.1316, p=0.8990; CTX PEA: t_7=0.4598, p=0.6596; DG PEA: t_8=0.2063; p=0.8417). The supramolecular signalosome complex responsible for activity induced 2-AG production at excitatory synapses has been localized to the perisynaptic region of the dendritic spine, proximal to the presynaptic CB1Rs (Jung et al., 2012). The above results suggest that active maintenance of these arrangements in the DG, but not elsewhere in the cortex, requires the presence of microglia.

Next, we used Fluorescence Deconvolution Tomography (FDT) (Rex et al., 2009; Chen et al., 2010; Wang et al., 2018b) to test if microglial depletion disrupts postsynaptic concentrations of proteins that form the 2-AG signalosome. The technique measures relative concentrations of target proteins at large numbers of individually reconstructed 3-D postsynaptic densities within the dendritic lamina innervated by a projection of interest. We compared results for the outer molecular layer of the DG with those for the CA1 zone innervated by SC projections (str. radiatum) of CA3. The density value for mGluR5 labeling co-localized with a 3-D reconstructed PSD95 was placed in one of a series of ascending bins and the total number observations that fell within a given density bin expressed as a percentage of all doubled

labeled contacts. The resultant frequency-density curve for mGluR5 labeling in the DG of the depleted mice was right skewed towards higher values in the PLX group relative to the control curve (n=11/group; $F_{(22, 440)}$= 7.824, p<0.0001). There was no effect of the PLX treatment in CA1 (n=11/group; $F_{(22, 462)}$= 0.105, p>0.99) (**Fig 3.5F**). Levels of DAGL co-localized with PSD95 in the experimental cases were unchanged from those for the control group (**Fig 3.5G**). Counts of PSD95 positive profiles with co-localized with measurable levels of DAGL or mGluR5 were comparable in the PLX and control groups in both sample fields (CA1: n=21/group; $F_{(22, 880)}$= 0.978, p=0.49; DG: n=21/group; $F_{(22, 902)}$= 0.984, p=0.98).

Finally, we investigated the possibility that the elevated levels of 2-AG produced by microglia elimination are accompanied by adjustments to the CB1Rs that initiate the presynaptic sequence leading to LTP in the LPP. Synaptophysin was used as a marker for axon terminals. There was a clear rightward shift towards higher per terminal levels of CB1Rs phosphorylated within the DG outer molecular layer (n=21/group; p<0.001), associated with a desensitization type loss of function, without evident adjustments in the str, radiatum of CA1 (**Fig 3.5H**).

The latter results raise the possibility that, despite elevated baseline values, on-demand production and diffusion of 2-AG during high frequency stimulation are not adequate in PLX-treated mice to engage the presynaptic events required to shift LPP terminals into their potentiated condition. We therefore tested if blocking the presynaptic 2-AG degradative enzyme monoacylglycerol lipase (MAGL) offsets the effects of microglial depletion on potentiation of LPP-DG synapses. Slices from the same PLX-treated mice were treated with vehicle or MAGL inhibitor JZL184 (1μM) for 30 min prior to HFS. Consistent with results described above, LTP was absent in slices treated with vehicle (% LTP at 55-60 min post-induction: +5.7±3.1%; n=4) but infusion of JZL restored LPP potentiation to values found in slices from control mice (+50.3±3.6%; n=6, p<0.01; PLX+Veh vs PLX+JZL184) (**Fig 3.6A**).

The potent effects of JZL184 strongly suggest that microglial removal does not lead to distorted CB1R signaling within the LPP. Terminals generated by the pathway are unusual in that agonists do not depress baseline transmitter release (Wang et al., 2016). We used the agonist WIN55,212 to test if the loss of microglia shifts CB1R signaling towards a more typical release-depression profile. Infusion of the compound at a concentration that causes a pronounced depression in CA3 projections to CA1 (Wang et al., 2016) had no effect on LPP-DG elicited fEPSPs in the PLX group. This was also the case for the structurally distinct agonist CP55940 (1 µM) (Veh n= 6, Win n= 9; CP55940 n= 11; $F_{2,21}$= 0.05, p=0.95; one-way ANOVA) (**Fig 3.6B**).

3.7 Microglia depletion acquisition episodic and object location memory

People organize the flow of everyday experience into narrative episodes that minimally incorporate the identity of the cues that were encountered, their spatial locations, and the sequence in which they occurred (Tulving, 1984; Dickerson and Eichenbaum, 2010; Eichenbaum et al., 2012). An increasing body of evidence suggests that rodents capture the basic ‘what’, where’, and ‘when’ elements of episodic memory during unsupervised (unrewarded, no practice) interactions with multiple cues (Dere et al., 2005; Eacott and Easton, 2010; Allen et al., 2014; Crystal, 2021). A study using transient Gi-DREADD silencing of specific synaptic populations showed that the LPP-DG system is critical for acquiring the ‘what’ element and as expected from this is also required for acquisition of “where” and “when” (Cox et al., 2019). The possibility thus arises that the microglial contribution to LPP plasticity is critical to the processing multiple facets of a fundamental form of everyday memory.

We first tested if microglial depletion affects detection and discrimination of a single odor. Mice were first habituated to a chamber for 5 min and then exposed to single odorant placed in two identical containers (E:E). They were tested 15 minutes later with familiar odor ‘E’ in one cup and novel odor ‘F’ in the second (E:F). Control mice showed the expected

preferential sampling of odor F and an equivalent focus on the novel odor was present in PLX-treated mice (Control: n= 7, t_6= 5.49, p= 0.002; PLX n= 10, t_9= 4.66, p= 0.001, paired t-test; Between groups: t_{15}= 0.45, p= 0.66, unpaired t-test) (**Fig 3.7A**). We then tested for encoding cues within a multiple odor sequence: mice were presented odor pairs A:A, B:B, and C:C with 3 minute intervals between pairs. This was intended to mimic the serial events that are routinely encoded into an episode. The retention trial involved a presentation of familiar odor A vs. novel odor D (A:D). Controls showed a clear preference for 'D' (as in prior work (Wang et al., 2018c; Cox et al., 2019); n= 10, t_9= 3.30, p= 0.009; time with A vs D,) but this effect was absent with microglial depletion (n= 10, t_9= 0.82, p=0.43, A vs D paired t-test; Between groups: t_{18}= 2.83, p= 0.01, Con vs PLX, unpaired t-test; **Fig 3.7B**).

We tested episodic 'where' by habituating mice to a larger chamber and then giving them 5 min access to four identical odor cups, each containing a different odorant (A:B:C:D). A retention test was given 24 hours later in which the positions of two of the odors were switched. It will be noted that the animal is required to deal with multiple cues and multiple locations in order to detect a change in position. Control mice spent more time investigating the two relocated odors than the cues left in their original positions (Con: n=10, t_9=5.70, p< 0.001, paired t-test). This preference was not evident in mice with microglial depletion (n=12, t_{11}=1.26, p=0.23, paired t-test; Between groups: t_{20}=2.16, p=0.043, unpaired t-test; **Fig 3.7C**). Next, we assessed retention of the order of cue sampling (i.e., episodic 'when'). As in the 'what' task the mice were exposed to an odor pair series A:A, B:B, C:C, D:D but the retention trial entailed presentation of two odors from the prior sequence (B:C). In accord with prior results (Cox et al., 2019), control mice spent more time sampling the least recently encountered odor (n= 10, t_9= 4.42, p= 0.002, paired t-test) but this preference was not evident in the PLX-treatment group (n= 9, t_8= 1.42 p= 0.195, paired t-test; Between groups: t_{17}= 2.31, p= 0.34, unpaired t-test; **Fig 3.7D**). Finally, we tested if the loss of microglia affects spatial learning in the absence of the

multiple cue feature of an episode. The widely used Object Location Memory paradigm involves free exploration of two identical objects on day one followed a day later with a test in which one of these is moved to a new location. Rodents spend more time investigating the novel-location cue, indicating that they had learned the original locations. OLM is dependent upon hippocampal field CA1 (Barrett et al., 2011; Babayan et al., 2012). The OLM retention scores did not differ between the control and PLX-treated groups (n=9/group, t_{16}= 1.25, p= 0.230, unpaired t-test; **Fig 3.7E**). Thus, the loss of microglia produced significant disturbances in tasks involving multiple, distinct cues but not for learning the identity or location of a single object.

Knowing episodic 'what' encoding depends on the LPP, and that JZL-184 rescued LPP-DG potentiation in microglia depleted rats, we tested the effects of JZL184 on performance in the serial 'What' task. In this new cohort, performance was impaired in PLX mice that were given a vehicle prior to the behavioral session but was rescued PLX-mice given JZL184 (n= 9/ group, t_{16}=3.03, p=0.008; unpaired t-test; **Fig 3.7F**). Together these findings indicate that eliminating microglia disrupted acquisition of the three basic elements of episodic memory without interfering with simpler forms of memory and that despite microglial depletion, episodic encoding was rescued by a compound (JZL) that increases synaptic 2-AG signaling.

Discussion

The present studies show that microglial depletion has surprisingly selective effects on synaptic *physiology*. There were no changes in waveforms, input/output relationships, or responses to short trains of gamma frequency input at any of four synaptic links. The frequency results are particularly informative because within-train changes vary considerably across the target projection systems largely due to differences in presynaptic variables that control release dynamics (Katz and Miledi, 1968; Edwards, 2007; Trieu et al., 2015; Jackman and Regehr, 2017; Le et al., 2022a; Quintanilla et al., 2022). There was accordingly a range of parameters against which the experimental treatment might have exerted an effect. However, depletion of

microglial cells did produce a severe impairment in LTP but only at one site: the LPP contacts with the DG. This defect did not appear to be due to an effect on LPP axons and terminals themselves because LTP in the CA3 branch of the LPP projection was intact. Moreover, the impairment to LTP likely did not arise from a disturbance of granule cell function because LTP in the MPP synapses, which innervate the dendritic field subjacent to the LPP, was not affected by PLX treatment. Rather, the results point to the conclusion that microglia regulate conditions needed for the unusual, LTP- related interaction that occurs between LPP terminals and granule cell dendrites.

Different types of analysis converged on the endocannabinoid signalosome as being the DG system regulated by microglia. Levels of 2-AG were dramatically elevated above control values in the DG of microglia depleted mice but appeared to be unchanged in the frontal cortex. Quantitative dual immunolabeling indicated that concentrations of mGluR5 at granule cell, but not CA1 pyramidal neuron, synapses were also increased in the experimental animals. These results are plausibly related because stimulation of mGluR5 is known to increase 2-AG levels via activation of DAGL-α (Jung et al., 2005; Katona et al., 2006; Jung et al., 2007). It thus appears that microglia tonically depress baseline activity in the signalosome, possibly to restrict retrograde endocannabinoid signaling to the infrequent arrival of high frequency input. As noted, such signaling can lead to lasting modifications of LPP terminals and there is accordingly a need for tight regulation. Moreover, we found that the postsynaptic consequences of eliminating microglia were accompanied by a possibly critical presynaptic effect: excessive phosphorylation of CB1Rs at a site that has been linked to desensitization of receptor function. This is not unexpected consequence of tonically elevated levels of an agonist (2-AG) that freely diffuses to a binding pocket on the receptor. The CB1R effect provides a first explanation for why removal of microglia causes severe impairments to LTP in the LPP but not elsewhere in hippocampus. That is, pharmacological and genomic studies showed that stabilization of potentiation in the

LPP-DG synapses, but not in the other tested connections, requires activity-driven stimulation of CB1Rs by 2-AG. Chronic desensitization of the receptors would reduce their response to a 2-AG pulse elicited by a burst of high frequency afferent activity.

The above proposals imply that microglial depletion disrupts LTP by causing a relatively discrete adjustment to the endocannabinoid system such as a change in the production or trafficking of mGluR5. But there are reasons to suspect that the pertinent disturbances occur at a supra-molecular level are involved. The signalosome complex responsible for activity induced 2-AG production at excitatory synapses has been localized to the perisynaptic region of the dendritic spine, proximal to the presynaptic CB1Rs (Jung et al., 2012). It is possible that active maintenance of these arrangements requires the presence of microglia. There is increasing evidence that microglia regulate synaptic organization by sculpting the extracellular matrix (Crapser et al., 2021) via release of proteinases (del Zoppo et al., 2007; Könnecke and Bechmann, 2013; Crapser et al., 2021). Such an action would alter the activities of the matrix adhesion receptors that organize the submembrane actin network and the micro domains it creates. Tonic microglial activities could be required to maintain an unusually precise alignment between spine signalosome and the complex, CB1R driven machinery that expresses presynaptic LTP. It is noteworthy in this regard that granule cells express a matrix adhesion receptor belonging to the integrin family not found elsewhere in the forebrain (Pinkstaff et al., 1999). This observation is consistent with the idea of a specialized junctional organization and in addition predicts that protracted blockade of the adhesion receptor will reproduce the loss of LTP -- but not of frequency filtering -- in the microglia depleted LPP.

The hypothesis that removal of a microglial brake on tonic endocannabinoid signaling depresses acute activation of the system and thereby disrupts LPP-LTP raises the question of whether acute enhancement of signaling could rescue potentiation. We tested this by blocking 2-AG breakdown during high frequency activation of the LPP and obtained a complete

restoration of LTP. It follows from this that the atypical actions of CB1R are not subject to tonic control by microglia, an observation that adds further support to the conclusion that the cells exert their primary effect on the endocannabinoid system. But as described there was no evidence of such a microglial action outside the DG. There is considerable evidence for different microglial categories that are distinguishable by functional, as well as morphological, characteristics (Stratoulias et al., 2019). It is thus possible the outer molecular layer population is atypical in that it releases factors that affect endocannabinoid production and actions. Alternatively, LPP terminals could release factors that produce uncommon responses by local microglia. The projection expresses singularly high levels of the opioid enkephalin (Fredens et al., 1984; Gall et al., 1984), a neuroactive peptide that modulates a number of microglial properties including membrane polarization and release of signaling molecules (Das et al., 1995; Xu et al., 2016). Enkephalin is released in an activity dependent manner from the LPP and diffuses sufficiently far to reach interneuron terminals on granule cells and thus will be available in an activity dependent manner to microglia.

The LPP conveys information about the identity of cues and events from entorhinal cortex to the hippocampus. As expected from this, transient silencing of the LPP eliminates the ability of mice to encode any of the three basic aspects of an episode (“what’, ‘where’, ‘when’). This broad effect stands in contrast to the selective defects produced by blocking the MPP (episodic ‘where’) or a segment of hippocampal field CA3 (‘when’) (Cox et al., 2019). The present findings extend these analyses by showing that blocking plasticity but not throughput in the LPP also produces a severe defect in each of the three basic elements of an episode. This leads to the conclusion that strengthening of LPP-DG synapses is a necessary condition for high capacity, unsupervised storage of everyday experience. One effect of LTP would be to increase the likelihood that the cues in a previously encountered sequence will trigger granule cell spiking and activation of the potent mossy fiber projections to field CA3. LTP in this case

would significantly increase the probability that the signal would activate the full extent of the primary hippocampal circuit and thereby cause discharges from the CA1 output station.

Episodic memory not only provides means for retrievable storage of vast amounts of everyday experience but as well is foundational to cognitive operations including inferential thinking and imagination (Crane and Goddard, 2008; Gaigg et al., 2014). The present findings point to the surprising conclusion that these complex aspects of psychology are dependent on microglial influence on a circumscribed and unusual set of synapses. But we can assume that the cells in the LPP terminal field retain their functions as macrophages, which helps explain why invasive elements can so quickly interfere with orderly thought.

References

Abbott LF, Regehr WG (2004) Synaptic computation. Nature 431:796-803.

Aguzzi A, Barres BA, Bennett ML (2013) Microglia: scapegoat, saboteur, or something else? Science 339:156-161.

Ahmed F, Torrens A, Mahler SV, Ferlenghi F, Huestis MA, Piomelli D (2022) A Sensitive Ultrahigh-Performance Liquid Chromatography/Tandem Mass Spectrometry Method for the Simultaneous Analysis of Phytocannabinoids and Endocannabinoids in Plasma and Brain. Cannabis Cannabinoid Res.

Allen TA, Morris AM, Mattfeld AT, Stark CE, Fortin NJ (2014) A Sequence of events model of episodic memory shows parallels in rats and humans. Hippocampus 24:1178-1188.

Amani M, Lauterborn JC, Le AA, Cox BM, Wang W, Quintanilla J, Cox CD, Gall CM, Lynch G (2021) Rapid Aging in the Perforant Path Projections to the Rodent Dentate Gyrus. J Neurosci 41:2301-2312.

Amaral D, Lavenex P (2007) Hippocampal Neuroanatomy. In: The Hippocampus Book (Andersen P, Morris RG, Amaral D, Bliss TV, O'Keefe J, eds), pp 37-114. New York: Oxford University Press.

Atluri PP, Regehr WG (1996) Determinants of the time course of facilitation at the granule cell to Purkinje cell synapse. J Neurosci 16:5661-5671.

Atwood HL, Karunanithi S (2002) Diversification of synaptic strength: presynaptic elements. Nat Rev Neurosci 3:497-516.

Babayan AH, Kramar EA, Barrett RM, Jafari M, Haettig J, Chen LY, Rex CS, Lauterborn JC, Wood MA, Gall CM, Lynch G (2012) Integrin dynamics produce a delayed stage of long-term potentiation and memory consolidation. J Neurosci 32:12854-12861.

Barrett RM, Malvaez M, Kramar E, Matheos DP, Arrizon A, Cabrera SM, Lynch G, Greene RW, Wood MA (2011) Hippocampal focal knockout of CBP affects specific histone modifications, long-term potentiation, and long-term memory. Neuropsychopharmacology 36:1545-1556.

Basilico B et al. (2022) Microglia control glutamatergic synapses in the adult mouse hippocampus. Glia 70:173-195.

Chen LY, Rex CS, Sanaiha Y, Lynch G, Gall CM (2010) Learning induces neurotrophin signaling at hippocampal synapses. Proc Natl Acad Sci U S A 107:7030-7035.

Christie BR, Abraham WC (1994) Differential regulation of paired-pulse plasticity following LTP in the dentate gyrus. Neuroreport 5:385-388.

Cox BM, Cox CD, Gunn BG, Le AA, Inshishian VC, Gall CM, Lynch G (2019) Acquisition of temporal order requires an intact CA3 commissural/associational (C/A) feedback system in mice. Commun Biol 2:251.

Crane L, Goddard L (2008) Episodic and semantic autobiographical memory in adults with autism spectrum disorders. J Autism Dev Disord 38:498-506.

Crapser JD, Arreola MA, Tsourmas KI, Green KN (2021) Microglia as hackers of the matrix: sculpting synapses and the extracellular space. Cell Mol Immunol 18:2472-2488.

Crystal JD (2021) Evaluating evidence from animal models of episodic memory. J Exp Psychol Anim Learn Cogn 47:337-356.

Cunningham AJ, Murray CA, O'Neill LA, Lynch MA, O'Connor JJ (1996) Interleukin-1 beta (IL-1 beta) and tumour necrosis factor (TNF) inhibit long-term potentiation in the rat dentate gyrus in vitro. Neurosci Lett 203:17-20.

Das KP, McMillian MK, Bing G, Hong JS (1995) Modulatory effects of [Met5]-enkephalin on interleukin-1 beta secretion from microglia in mixed brain cell cultures. J Neuroimmunol 62:9-17.

Del Castillo J, Katz B (1954) Quantal components of the end-plate potential. J Physiol 124:560-573.

del Zoppo GJ, Milner R, Mabuchi T, Hung S, Wang X, Berg GI, Koziol JA (2007) Microglial activation and matrix protease generation during focal cerebral ischemia. Stroke 38:646-651.
Dere E, Huston JP, De Souza Silva MA (2005) Integrated memory for objects, places, and temporal order: evidence for episodic-like memory in mice. Neurobiol Learn Mem 84:214-221.
Dickerson BC, Eichenbaum H (2010) The episodic memory system: neurocircuitry and disorders. Neuropsychopharm 35:86-104.
Eacott MJ, Easton A (2010) Episodic memory in animals: remembering which occasion. Neuropsychologia 48:2273-2280.
Edwards RH (2007) The neurotransmitter cycle and quantal size. Neuron 55:835-858.
Eichenbaum H, Sauvage M, Fortin N, Komorowski R, Lipton P (2012) Towards a functional organization of episodic memory in the medial temporal lobe. Neurosci Biobehav Rev 36:1597-1608.
Fredens K, Stengaard-Pedersen K, Larsson LI (1984) Localization of enkephalin and cholecystokinin immunoreactivities in the perforant path terminal fields of the rat hippocampal formation. Brain Res 304:255-263.
Gaigg SB, Bowler DM, Gardiner JM (2014) Episodic but not semantic order memory difficulties in autism spectrum disorder: evidence from the Historical Figures Task. Memory 22:669-678.
Gall C, Brecha N, Chang KJ, Karten HJ (1984) Ontogeny of enkephalin-like immunoreactivity in the rat hippocampus. Neuroscience 11:359-379.
Granger AJ, Nicoll RA (2014) Expression mechanisms underlying long-term potentiation: a postsynaptic view, 10 years on. Philos Trans R Soc Lond B Biol Sci 369:20130136.
Green KN, Crapser JD, Hohsfield LA (2020) To Kill a Microglia: A Case for CSF1R Inhibitors. Trends Immunol 41:771-784.
Hanse E, Gustafsson B (1992) Postsynaptic, but not presynaptic, activity controls the early time course of long-term potentiation in the dentate gyrus. J Neurosci 12:3226-3240.
Huang Y, Xu Z, Xiong S, Sun F, Qin G, Hu G, Wang J, Zhao L, Liang YX, Wu T, Lu Z, Humayun MS, So KF, Pan Y, Li N, Yuan TF, Rao Y, Peng B (2018) Repopulated microglia are solely derived from the proliferation of residual microglia after acute depletion. Nat Neurosci 21:530-540.
Jackman SL, Regehr WG (2017) The Mechanisms and Functions of Synaptic Facilitation. Neuron 94:447-464.
Jung KM, Astarita G, Zhu C, Wallace M, Mackie K, Piomelli D (2007) A key role for diacylglycerol lipase-alpha in metabotropic glutamate receptor-dependent endocannabinoid mobilization. Mol Pharmacol 72:612-621.
Jung KM, Mangieri R, Stapleton C, Kim J, Fegley D, Wallace M, Mackie K, Piomelli D (2005) Stimulation of endocannabinoid formation in brain slice cultures through activation of group I metabotropic glutamate receptors. Mol Pharmacol 68:1196-1202.
Jung KM, Sepers M, Henstridge CM, Lassalle O, Neuhofer D, Martin H, Ginger M, Frick A, DiPatrizio NV, Mackie K, Katona I, Piomelli D, Manzoni OJ (2012) Uncoupling of the endocannabinoid signalling complex in a mouse model of fragile X syndrome. Nat Commun 3:1080.
Katona I, Urban GM, Wallace M, Ledent C, Jung KM, Piomelli D, Mackie K, Freund TF (2006) Molecular composition of the endocannabinoid system at glutamatergic synapses. J Neurosci 26:5628-5637.
Katz B, Miledi R (1968) The role of calcium in neuromuscular facilitation. J Physiol 195:481-492.
Könnecke H, Bechmann I (2013) The role of microglia and matrix metalloproteinases involvement in neuroinflammation and gliomas. Clin Dev Immunol 2013:914104.

Kuntsche J, Koch MH, Steiniger F, Bunjes H (2010) Influence of stabilizer systems on the properties and phase behavior of supercooled smectic nanoparticles. J Colloid Interface Sci 350:229-239.
Larson J, Lynch G (1986) Induction of synaptic potentiation in hippocampus by patterned stimulation involves two events. Science 232:985-988.
Larson J, Munkacsy E (2015) Theta-burst LTP. Brain Res 1621:38-50.
Le AA, Quintanilla J, Amani M, Piomelli D, Lynch G, Gall CM (2022a) Persistent sexually dimorphic effects of adolescent THC exposure on hippocampal synaptic plasticity and episodic memory in rodents. Neurobiol Dis 162:105565.
Le AA, Lauterborn JC, Jia Y, Wang W, Cox CD, Gall CM, Lynch G (2022b) Prepubescent female rodents have enhanced hippocampal LTP and learning relative to males, reversing in adulthood as inhibition increases. Nat Neurosci 25:180-190.
Liu X, Quan N (2018) Microglia and CNS Interleukin-1: Beyond Immunological Concepts. Front Neurol 9:8.
Liu YJ, Spangenberg EE, Tang B, Holmes TC, Green KN, Xu X (2021) Microglia Elimination Increases Neural Circuit Connectivity and Activity in Adult Mouse Cortex. J Neurosci 41:1274-1287.
Lynch G, Larson J, Kelso S, Barrionuevo G, Schottler F (1983) Intracellular injections of EGTA block induction of hippocampal long-term potentiation. Nature 305:719-721.
McNaughton BL (1980) Evidence for two physiologically distinct perforant pathways to the fascia dentata. Brain Res 199:1-19.
Muller D, Lynch G (1988) Long-term potentiation differentially affects two components of synaptic responses in hippocampus. Proc Natl Acad Sci U S A 85:9346-9350.
Nagy V, Bozdagi O, Matynia A, Balcerzyk M, Okulski P, Dzwonek J, Costa RM, Silva AJ, Kaczmarek L, Huntley GW (2006) Matrix metalloproteinase-9 is required for hippocampal late-phase long-term potentiation and memory. J Neurosci 26:1923-1934.
Nimmerjahn A, Kirchhoff F, Helmchen F (2005) Resting microglial cells are highly dynamic surveillants of brain parenchyma in vivo. Science 308:1314-1318.
Perry VH, Teeling J (2013) Microglia and macrophages of the central nervous system: the contribution of microglia priming and systemic inflammation to chronic neurodegeneration. Semin Immunopathol 35:601-612.
Pinkstaff JK, Detterich J, Lynch G, Gall C (1999) Integrin subunit gene expression is regionally differentiated in adult brain. J Neurosci 19:1541-1556.
Quintanilla J, Cox BM, Gall CM, Mahler SV, Lynch G (2021) Retrograde enhancement of episodic learning by a postlearning stimulus. Learn Mem 28:82-86.
Quintanilla J, Jia Y, Lauterborn JC, Pruess B, Le AA, Cox CD, Gall CM, Lynch G (2022) Novel types of frequency filtering in the lateral perforant path projections to dentate gyrus. The Journal of Physiology.
Rex CS, Chen LY, Sharma A, Liu J, Babayan AH, Gall CM, Lynch G (2009) Different Rho GTPase-dependent signaling pathways initiate sequential steps in the consolidation of long-term potentiation. J Cell Biol 186:85-97.
Schneider H, Pitossi F, Balschun D, Wagner A, del Rey A, Besedovsky HO (1998) A neuromodulatory role of interleukin-1beta in the hippocampus. Proc Natl Acad Sci U S A 95:7778-7783.
Seese RR, Babayan AH, Katz AM, Cox CD, Lauterborn JC, Lynch G, Gall CM (2012) LTP induction translocates cortactin at distant synapses in wild-type but not Fmr1 knock-out mice. J Neurosci 32:7403-7413.
Spangenberg E et al. (2019) Sustained microglial depletion with CSF1R inhibitor impairs parenchymal plaque development in an Alzheimer's disease model. Nat Commun 10:3758.

Stensola T, Moser EI (2016) Grid Cells and Spatial Maps in Entorhinal Cortex and Hippocampus. In: Micro-, Meso- and Macro-Dynamics of the Brain (Buzsaki G, Christen Y, eds), pp 59-80. Cham (CH).

Stratoulias V, Venero JL, Tremblay ME, Joseph B (2019) Microglial subtypes: diversity within the microglial community. EMBO J 38:e101997.

Trieu BH, Kramar EA, Cox CD, Jia Y, Wang W, Gall CM, Lynch G (2015) Pronounced differences in signal processing and synaptic plasticity between piriform-hippocampal network stages: a prominent role for adenosine. J Physiol 593:2889-2907.

Tulving E (1984) Elements of Episodic Memory: Oxford University Press.

Wake H, Moorhouse AJ, Jinno S, Kohsaka S, Nabekura J (2009) Resting microglia directly monitor the functional state of synapses in vivo and determine the fate of ischemic terminals. J Neurosci 29:3974-3980.

Wang W, Le AA, Hou B, Lauterborn JC, Cox CD, Levin ER, Lynch G, Gall CM (2018a) Memory-Related Synaptic Plasticity Is Sexually Dimorphic in Rodent Hippocampus. J Neurosci 38:7935-7951.

Wang W, Jia Y, Pham DT, Palmer LC, Jung KM, Cox CD, Rumbaugh G, Piomelli D, Gall CM, Lynch G (2018b) Atypical Endocannabinoid Signaling Initiates a New Form of Memory-Related Plasticity at a Cortical Input to Hippocampus. Cereb Cortex 28:2253-2266.

Wang W, Cox BM, Jia Y, Le AA, Cox CD, Jung KM, Hou B, Piomelli D, Gall CM, Lynch G (2018c) Treating a novel plasticity defect rescues episodic memory in Fragile X model mice. Mol Psychiatry 23:1798-1806.

Wang W, Trieu BH, Palmer LC, Jia Y, Pham DT, Jung KM, Karsten CA, Merrill CB, Mackie K, Gall CM, Piomelli D, Lynch G (2016) A Primary Cortical Input to Hippocampus Expresses a Pathway-Specific and Endocannabinoid-Dependent Form of Long-Term Potentiation. Eneuro 3.

Xu X, Gao Y, Wen L, Zhai Z, Zhang S, Shan F, Feng J (2016) Methionine enkephalin regulates microglia polarization and function. Int Immunopharmacol 40:90-97.

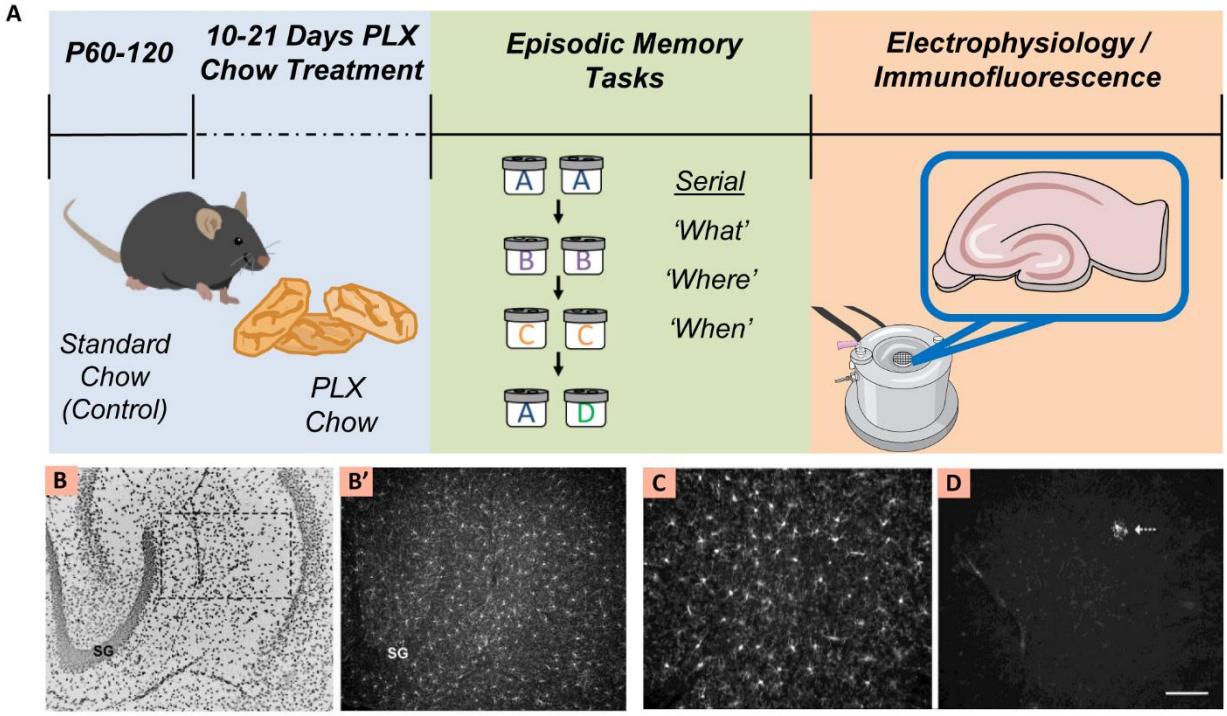

Figure 3.1: Experimental design and microglia depletion. A) Adult C57Bl6 mice (postnatal day, P 60-120) received standard or PLX5622-containing chow for a minimum of 10 days (10 to 21 days across groups) before experimental use. Groups of mice were tested in learning tasks (episodic 'what', 'where', and 'when' acquisition; 2 odor discrimination, object location memory) and then used for electrophysiological measures and verification of microglial depletion. Other groups were processed for electrophysiological analysis and/or biochemical measures alone. **B, B'**) Images of the same hippocampal cross section viewed in different color channels to show DAPI-labeling of cellular nuclei (B, inverse contrast image) and IBA1 immunoreactivity (B') in a slice from a control chow mouse fixed promptly after preparation (SG: dentate gyrus stratum granulosum; CA1 stratum pyramidale at right). Microglia appear white in B'-D. Dashed rectangle in A indicates the placement of the higher magnification images from which the IBA1-immunoreactive (ir) cells were quantified. **C, D)** Representative images of the quantification field showing IBA1-ir cells in slices from control (C) and PLX5622-treated (D) mice: a severe depletion of IBA1-ir cells is evident in the PLX5622 case (arrow in D indicates the single immunolabeled cell in the field). Calibration bar in C indicates 200 µm for B and B', 100 µm for C and D.

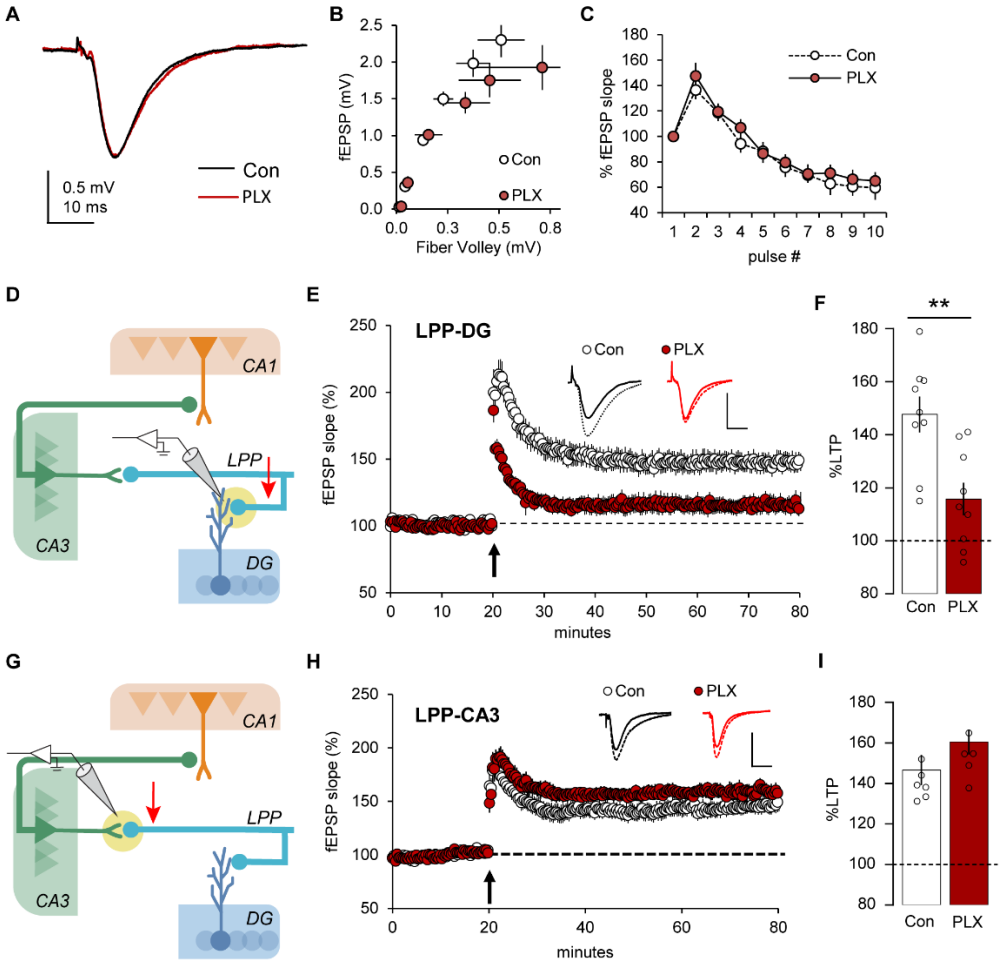

Figure 3.2: Lateral perforant path (LPP) LTP is markedly impaired in microglia depleted mice. A,B) Representative waveforms (A) and input-output curves (**B**) for LPP fEPSP responses in the dentate gyrus (DG) outer molecular layer of control (Con)- and PLX-treated mice (Con n=8, PLX n=5; mean ± SEM shown). **C)** The DG response profile to a ten-pulse, 40 Hz train of LPP stimulation was comparable between Con and PLX groups, both showing response facilitation followed by depression ($F_{9,135}$=0.3653, p=0.9497, Con n=7; PLX n=10; two-way RM ANOVA). **C**) Schematic of stimulation (red arrow) and recording electrode placement for LPP-DG recordings. **D)** After collecting stable baseline responses, a single 100 Hz HFS train applied to the LPP (arrow) elicited an initial potentiation in the DG in Con and PLX groups; in both, responses declined to a stable potentiated plateau over 10-15 mins, but the magnitude of potentiation was markedly lower in PLX- vs Con cases. Traces show representative LPP-DG responses before (solid) and 55 min after (dashed) HFS. Scale bars: x=1 mV, y=10 ms. **E)** The mean LPP-DG potentiation at 55-60 min post-HFS was smaller in slices from PLX-treated vs Con mice (**p=0.0029, n=9/group; two-tailed unpaired t-test). **F)** Schematic showing stimulation (red arrow) and recording electrode placement for LPP-CA3 recordings. **G,H)** With HFS of the LPP-CA3 system both PLX and Con groups exhibited an initial potentiation that was sustained through 60 min post-induction (G). The level of LPP-CA3 potentiation did not differ between Con and PLX groups as assessed 55-60 min post-HFS (H).

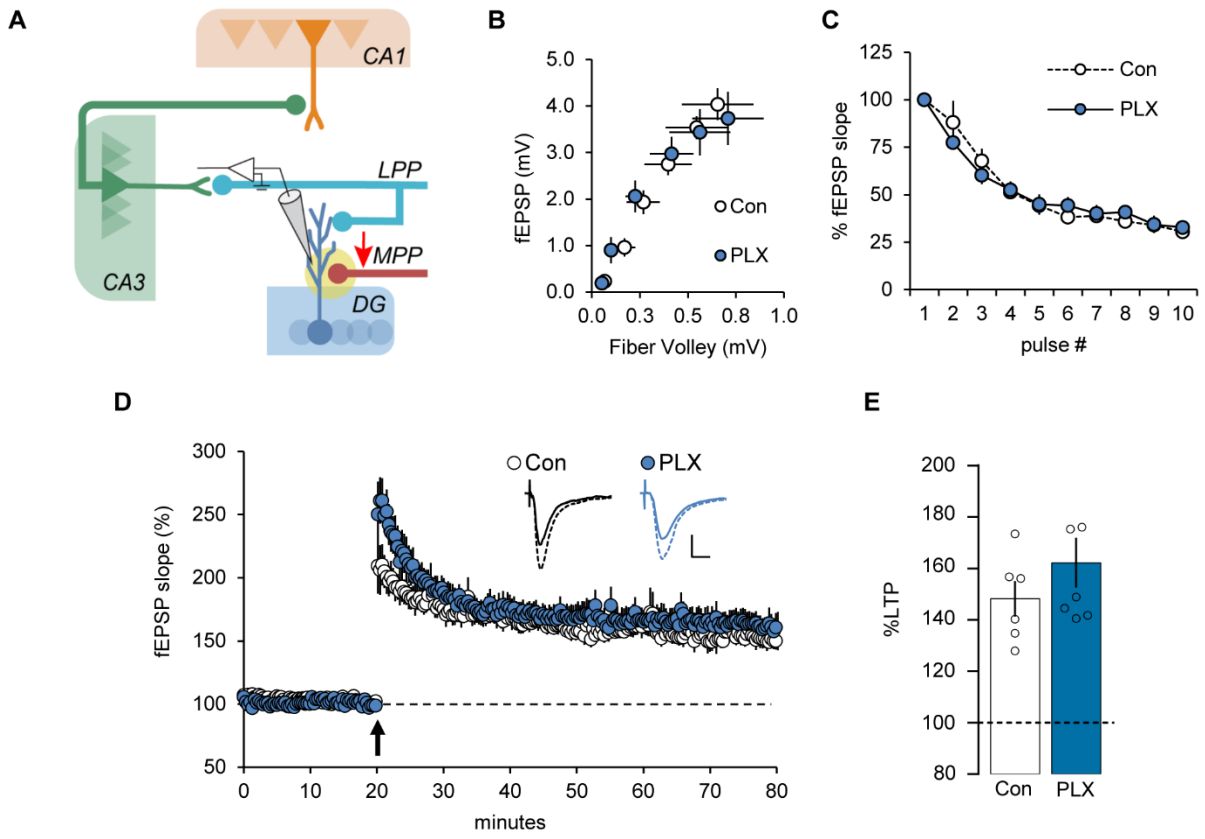

Figure 3.3: Microglial depletion did not affect medial perforant path (MPP) responses. A) Schematic showing stimulation (red arrow) and recording electrode placement for the MPP-DG analysis. **B**) MPP input/output curves were comparable in slices from control (Con-) and PLX-treated mice. **C**) MPP-fEPSP responses to a ten pulse, 40 Hz train were comparable in Con and PLX groups with both being depressed by ~30% over the course of the train ($F_{9,108}$= 1.09, p= 0.379; Con n=5, PLX n=9; two-way RM ANOVA). **D**) After recording stable baseline responses for 20 min, MPP LTP was induced using three, 500ms long 100Hz (HFS) trains separated by 20 sec (arrow): HFS elicited robust and comparable potentiation in both groups (Scale bars: x=1 mV, y=10 ms) **E**) The mean fEPSP response recorded 55-60 min post-HFS did not differ between Con and PLX groups (p=0.2768; Con n=7, PLX n=6; two-tailed unpaired t-test).

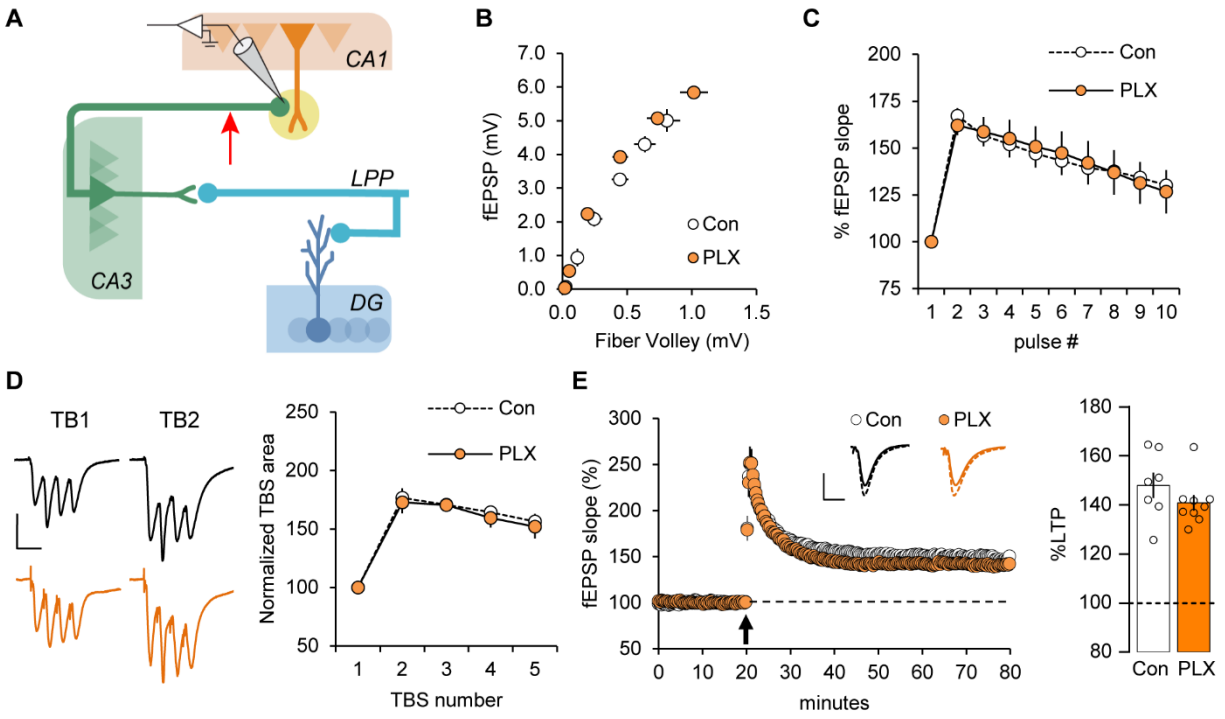

Figure 3.4: Microglial depletion does not influence CA1, Schaffer-commissural (SC) LTP. **A)** Schematic of stimulation (red arrow) and recording placement. **B)** SC input/output curves did not differ between control (Con) and PLX treatment groups. **C)** SC fEPSP responses to a 10 pulse, 40 Hz train (normalized to the first pulse response) were comparable between groups ($F_{9,99}$= 0.3022, p=0.9725; Con=6, PLX n=7; two-way RM ANOVA). **D)** The area of the composite fEPSP response to individual theta bursts used to induce LTP was not influenced by PLX treatment ($F_{4,52}$=0.0812, p=0.988; Con=8, PLX n=7; representative traces shown at left). **E)** *Left.* A single train of 5 theta bursts (at arrow) elicited comparable short and long-term potentiation in slices from Con and PLX-treated mice (mean ± SEM values plotted). Representative traces collected before (solid line) and after (dotted line) TBS shown. *Right.* The mean normalized fEPSP slopes collected 55-60 post-TBS did not differ between groups (p=0.2365; Con n=7, PLX n=9; two-tailed unpaired t-test). Scale bars: x=1 mV, y=10 ms.

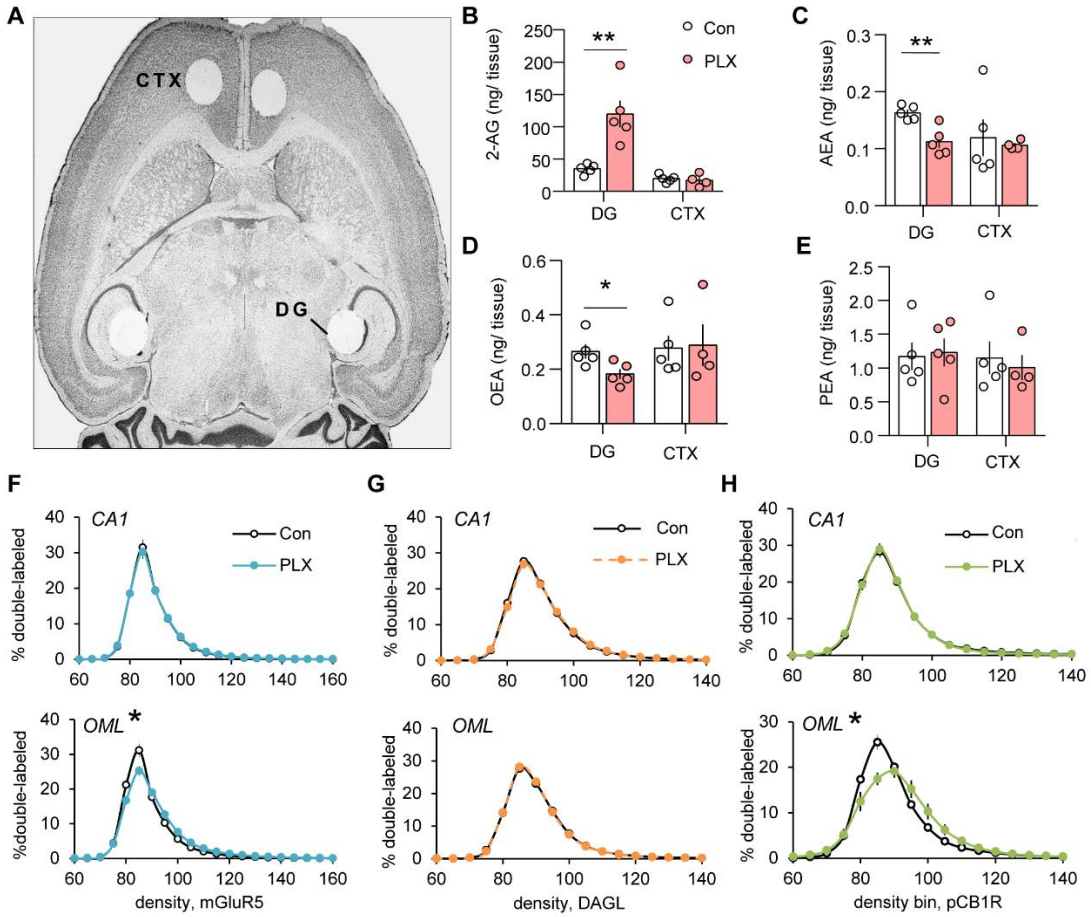

Figure 3.5: Microglial depletion disrupts endocannabinoid levels and their contributions to LTP. A) Image of horizontal section showing placement of tissue punches in dentate gyrus (DG) and frontal cortex (CTX) used for high performance liquid chromatography/tandem mass spectrometry measures of regional endocannabinoid levels. **B**) PLX treatment increased 2-AG levels in the DG (t_8=4.005, p=0.0039; for B-E n=5/group, unpaired 2-tailed t test) but not CTX (t_7=0.5463, p=0.6018). **C,D**) Anandamide (AEA; C) and oleoylethanolamide (OEA; D) levels were reduced in the DG (AEA: t_8=4.144, p=0.0032; OEA: t_8=2.620, p=0.0307) but not CTX (AEA: t_7=0.3557, p=0.7325; OEA: t_7=0.1316; p=0.8990) of PLX-treated vs Con mice. **E**) Palmitoylethanolamide (PEA) levels were not altered by PLX treatment (DG: t_8=0.206; p=0.842; CTX: t_7=0.460, p=0.66). **F**) The density of immunolabeling frequency distributions of mGluR5 within the outer molecular later (OML) of DG (*bottom)* were marked right-shift toward higher densities in PLX mice compared to Con mice (n=11/group; $F_{(22,\ 440)}$= 7.824, p<0.0001); no differences were found in CA1 (*top;* (n=11/group; $F_{(22,\ 462)}$= 0.105, p>0.99) **G**) No differences in density frequency distributions for DAGL-α were found in CA1 or OML between Con and PLX treated mice (CA1: n=21/group; $F_{(22,\ 880)}$= 0.978, p=0.49; DG: n=21/group; $F_{(22,\ 902)}$= 0.984, p=0.98). **H**) Density frequency distributions for phosphorylated CB1R (pCB1R) did not differ between PLX and Con treated mice within CA1. In DG, the higher density frequencies of immunolabeled pCB1R (right-shifted) were found in PLX mice compared to Con mice (n=21/group; p<0.001).

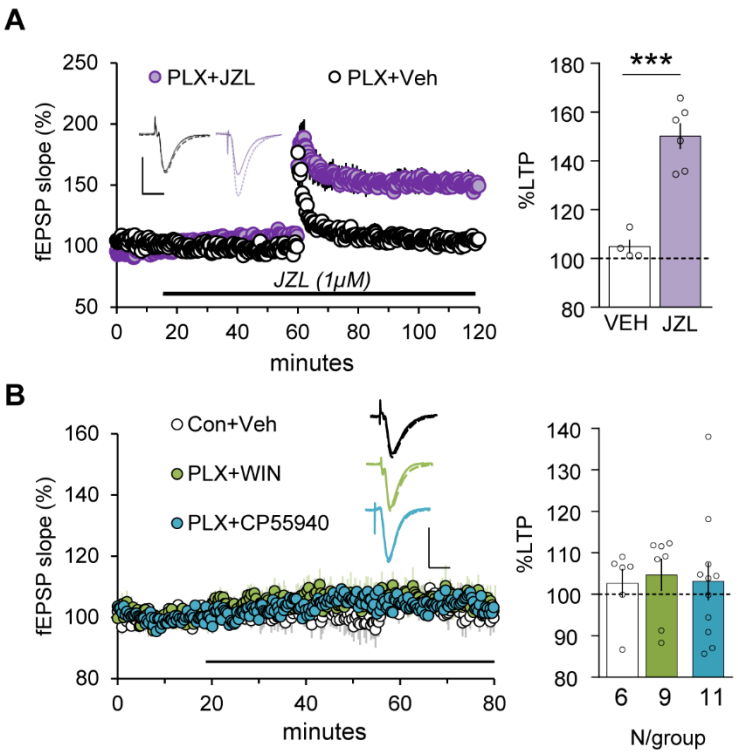

Figure 3.6: Prevention of 2-AG degredation offset PLX induced impairments of LPP-DG LTP. A) In hippocampal slices from PLX-treated mice otherwise impaired LPP-LTP was fully restored with infusion of 1μM JZL184 (JZL) (horizontal bar). Traces show responses before (solid line) and 55 min after (dashed line) HFS. Bar graph shows mean LPP fEPSP slope at 55-60 min post-HFS normalized to baseline values (t_8=6.498, ***p=0.0002; vehicle (Veh) n=6, JZL n=4; two-tailed unpaired t-test). **B**) Infusion (horizontal bar) of WIN 55,212-2 (WIN, 1μM; green), CP55940 (1μM; blue), or Veh did not influence LPP fEPSPs. Right: Mean LPP fEPSP slope over the last 5 min of infusion did not differ from baseline for all three groups ($F_{2,21}$=0.04976, p=0.9516, two-tailed one-way RM ANOVA).

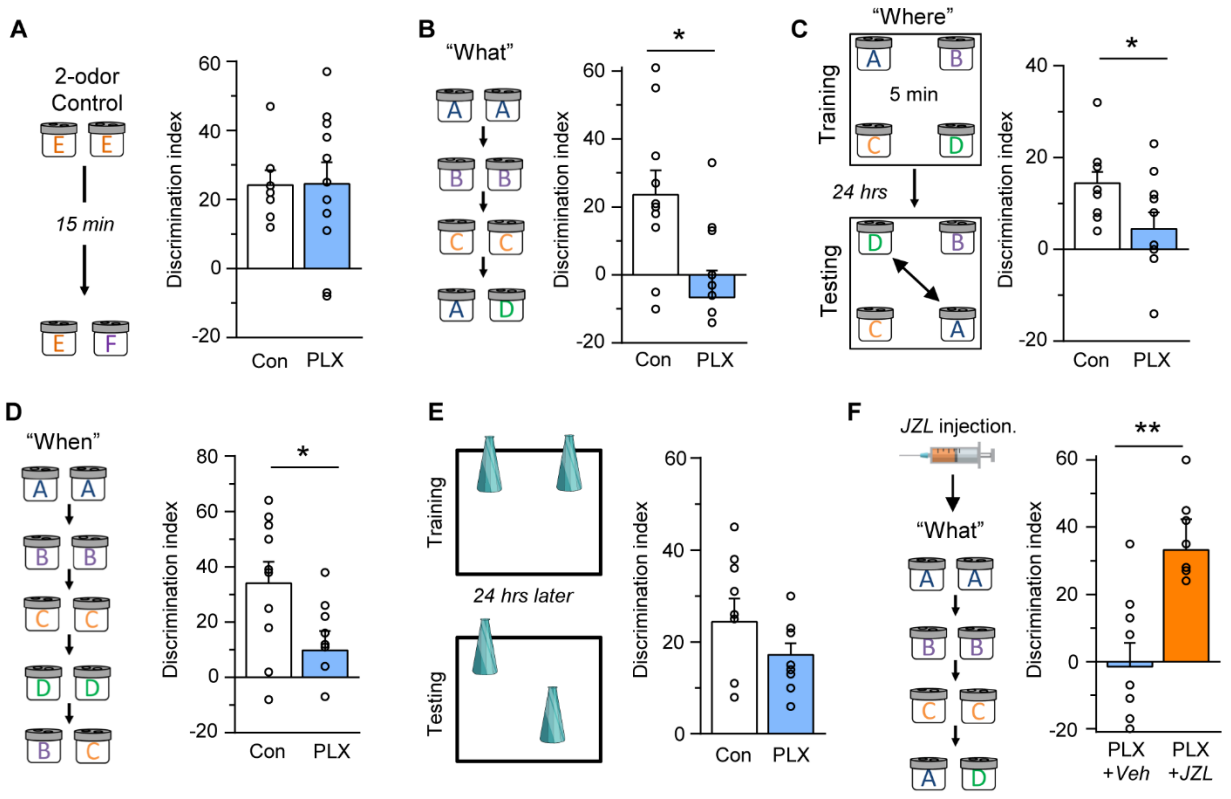

Figure 3.7: Microglia elimination selectively impairs acquiring elements of episodic memory. A) *Left.* Schematic of the 2-Odor control task. *Right.* Both control (Con) and PLX groups sampled novel odor F more than familiar odor E (Con n=7, PLX n= 10; t_{16}= 0.05, p= 0.96; two-tailed, unpaired Students t-test). **B)** *Left.* Schematic of Serial Odor 'What' task. *Right.* Con mice preferentially explored novel odor D vs familiar odor A (Con n=10; t_9= 3.30, **p< 0.01; paired Students t-test), whereas PLX-treated mice did not (PLX n=10, t_9= 0.82, p= 0.43; t_{18}= 2.83, *p=0.01 between groups). **C)** *Left*. Schematic of four odor 'Where' task. *Right.* Con mice preferentially explored the displaced odors at testing (n=10, t_9=5.7, ***p<0.001, paired Student's t-test) whereas PLX-treated mice did not (n=12, t_{11}=1.26, p=0.23; t_{20}= 2.12, *p=0.04, PLX vs Con, unpaired Student's t-test). **D)** *Left.* Schematic of Serial Odor 'When' task. *Right*. Con mice preferentially sampled earlier presented odor B over later presented odor C (Con n=10; t_9= 4.42, **p=0.002;) and did so significantly more than PLX-treated mice (PLX n=10; t_{17}=2.31, *p= 0.03 between groups). **E)** *Left.* Schematic of Object Location Memory Task. *Right.* Con and PLX-treated mice both distinguished the displaced object from the stationary object (Con n=9, PLX n=9; t_{16}=1.25, p=0.23; two-tailed, unpaired Students t-test). **F)** *Left.* PLX-treated mice were given JZL184 (JZL) or vehicle (Veh) 4 hrs prior to serial odor 'What' training. *Right.* PLX-treated mice given Veh failed to discriminate the novel vs familiar odor whereas those given JZL184 showed robust discrimination (Con n=9, PLX n=9, t_{16}= 3.03, **p< 0.008; two-tailed, unpaired Students t-test). Discrimination index: (sampling novel – sampling familiar)/ total cue sampling time.

Table 1. Odorants and dilutions for behavioral studies. All odorants were diluted with mineral oil and then pipetted (100µL) onto filter paper. Scented papers were then placed in odorant cups.

Odorant I.D.	Odorant (name, *company*)	Concentration (odorant : mineral oil)
A	(+) -Limonene (>97% purity, *Sigma- Aldrich*)	1 : 4000
B	Cyclohexyl ethyl acetate (>97%, *International Flavors & Fragrances Inc.*)	1.97 : 4000
C	Citronellal 96% (~96%, *Alfa Aesar*)	1.5 : 4000
D	Octyl aldehyde 99% (~99% *Acros Organics*)	1.5 : 4000
E	Anisole 99% (~99% *Acros Organics*)	0.85 : 4000
F	1-Pentanol 99% (~99% *Acros Organics*)	1.36 : 4000

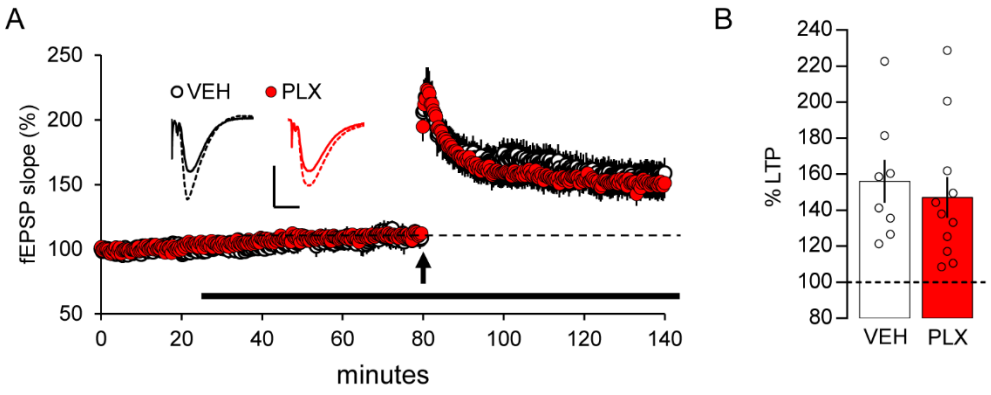

Suppl. Figure 3.1. Acute PLX5622 treatment does not influence LPP-DG fEPSPs. A) Plot shows that in slices from naïve mice, PLX (1µM, red symbols) infusion did not influence LPP-DG fEPSP responses (relative to vehicle (VEH) treated slices during drug-baseline stimulation (25-80 min) or after application of LTP-inducing 100Hz stimulation (at arrow; values normalized to mean pre-drug baseline). B) The potentiated fEPSP response (assessed 55-60 min after HFS) was comparable in PLX- and VEH-treated slices (symbols show individual slice values).

CHAPTER 4: Summary and Discussion

As detailed in *Chapter 1*, frequency facilitation in the LPP-DG segment of the primary hippocampal circuit was unlike that seen in other links. Rather than a typical facilitation, as found in CA1, or depression, as recorded at MPP synapses, the LPP-DG responses expressed both enhancement and depression during repetitive activation. Ten-pulse trains arriving at 5- 20 Hz caused an initial facilitation in fEPSP slope but a return to baseline levels as the train progressed. However, at 50 Hz the initial facilitation became a drastic depression to below baseline levels. Thus, the LPP-DG acts as a low-pass filter where lower frequency inputs are transferred to the granule cells while high frequencies are strongly suppressed. This raised the question of how high frequency information arriving from the entorhinal cortex (Chrobak *et al.*, 2000; Schomburg *et al.*, 2014; Colgin, 2015; Larson & Munkacsy, 2015; Colgin, 2016) initiates DG output. One possibility involved stimulation of the LPP with short bursts of gamma (50-100Hz) activity with the bursts separated by the period of the theta rhythm (~200 msec). This pattern known as theta-gamma coupling (Jensen & Colgin, 2007; Tort *et al.*, 2009; Colgin, 2015) occurs during a variety of behaviors including learning. Theta-gamma activity was transmitted across LPP-DG synapses but a sizeable depression after an initial facilitation was still present. Pharmacological experiments strongly suggested that the filtering did not occur postsynaptically but instead involved adjustments to release probability. In all, the LPP-DG synapse potently filters repetitive signals arriving in the gamma range and thereby imposes a requirement for patterned input signals to transfer high frequency information.

Surprisingly, the above input parameters produced quite different results when applied to the CA3 extension of the LPP. Responses to 5-20 Hz were facilitated throughout the 10-pulse train and 50Hz stimulation did not produce the pronounced depression seen at the DG branch of the LPP. Simulations suggested that these differences between the two sets of terminals can be attributed to the relative proportion of docked synaptic vesicles in the tightly docked vs. loosely docked states. In the LPP-DG, 50 Hz frequency facilitation curves that were generated

in simulations had higher docked vesicles (tightly docked) and a slower replacement pool replenishment (loosely docked) rate relative to those generated for LPP-CA3.

Disparate functional properties by two branches of the same projection were first described in the peripheral nervous system. In the crayfish, parallel paths to phasic muscles produce large initial responses that depress during a train while those to tonic muscles generate small initial responses that facilitate (Hennig & Lomo, 1985; Reid *et al.*, 1999). What might be the functional significance of distinctly different parallel pathways in the hippocampus? Because the LPP-DG acts as a low-pass filter, it is unlikely that repetitive gamma (50 Hz) will enter the hippocampus through the DG without a loss of signal. Instead, high frequencies will be relayed through the LPP-CA3 connection, where responses are maintained across short trains. This suggests that high frequency information entering the hippocampus is preferentially routed to CA3 via the direct projection as opposed to the indirect one (LPP-DG-CA3). Of relevance is that the DG projections to CA3, the mossy fibers, have a massive faciliatory response to repetitive inputs (Nicoll & Schmitz, 2005; Trieu *et al.*, 2015). This would have added consequences as mossy fiber transmission has been described to initiate reverberating activity across the associational system of CA3, lasting for several minutes (Cox *et al.*, 2019). Hence, the low-pass filtering at LPP-DG is possibly acting as a gating mechanism, preventing unchecked facilitation and runaway activity at mossy fiber-CA3 connections. The importance of this becomes clear when taking into account a leading hypothesis, based on computational models, of memory encoding (Treves & Rolls, 1992; Lee & Kesner, 2004). These studies suggest that the granule cells of the DG recruit CA3 pyramidal cells in order to associate entorhinal and recurrent collateral inputs as ensembles. Once ensembles are established, the perforant path inputs can then directly engage the network, without the use of mossy fiber activity, to recall the associated memory (Treves & Rolls, 1992; Tsukamoto *et al.*, 2003; Lee & Kesner, 2004; Zheng *et al.*, 2022). In this case, tightly regulated mossy fiber activation would be needed to avoid saturating the circuit and inadvertently reorganizing established ensembles.

Parallel pathways also enable diversification of incoming signals, thereby generating a higher computational potential -- the same stimulus can produce two clearly different responses (Abbott & Regehr, 2004). However, a major uncertainty surrounds the possibility that an unknown factor(s) enables higher frequency inputs to activate the indirect pathway. Neuromodulators such as dopamine (Kusuki *et al.*, 1997; Swanson-Park *et al.*, 1999; Hamilton *et al.*, 2010; Hansen & Manahan-Vaughan, 2014), acetylcholine (Sawada *et al.*, 1994; Welsby *et al.*, 2006; Luo *et al.*, 2008; Welsby *et al.*, 2009; Ogando *et al.*, 2021), and opioids (Bramham *et al.*, 1988; Do *et al.*, 2002) are all thought to regulate dentate gyrus activity and accordingly are of interest in this regard.

The conclusion that frequency facilitation differs between the two branches of the LPP because of presynaptic variables raised the possibility that LTP discrepancies are also present because the unusual version of the potentiation effect found in the DG is presynaptic in origin. Few studies have looked into LTP mechanisms at the LPP-CA3 synapse, and the issue of pre- vs. post-synaptic expression is unresolved. We found no evidence for pre-synaptic LTP mechanisms in the LPP-CA3 branch. Paired pulse facilitation was unchanged by LTP induction and blocking postsynaptic actin polymerization prevented consolidation of the potentiated state. Crucially, an antagonist of the retrograde endocannabinoid signaling that triggers expression of presynaptic LTP in the LPP-DG synapses had no effect in the CA3 extension. The reasons for this very basic difference in the operation of two sets of synapses generated by the same axons are unclear. The postsynaptic NMDAR-calcium triggering system is used at both sites (Barrionuevo & Brown, 1983; McMahon & Barrionuevo, 2002) but apparently for very different purposes: In LPP-DG contacts it appears to promote the synthesis of the endocannabinoid trigger for presynaptic ppotnetiation, while it is generally agreed that it activates CaMKII and AMPAR receptor movement in pyramidal cell spines. The reasons for the difference in postsynaptic signaling remain to be elucidated but the two types of target cells (LPP-DG vs. LPP-CA3) are characterized by radically different synaptic adhesion receptors belonging to the

integrin family (Pinkstaff *et al.*, 1999). It is thus possible that LPP-DG synapses lack the machinery required to reorganize the postsynaptic density so as to accommodate additional receptors. At the same time, endocannabinoid receptors on LPP terminals within the DG exhibit a very unusual type of signaling and it is possible that this is absent at LPP-CA3 contacts, which therefore lack steps needed to produce lasting changes in release kinetics. However, similar to DG, CB1 receptors agonists did not cause the expected decrease in LPP-CA3 fEPSP responses during baseline activity (Wang *et al.*, 2018). This suggests that although endocannabinoids are not necessary for LPP-CA3 LTP, the atypical signaling properties that allow for presynaptic LTP, found in LPP-DG, are present in CA3. Much like the short-term plasticity, one explanation for the differences at LPP terminals is target specificity. If this is the case, postsynaptic target cells would determine the locus of LTP expression, and thus at LPP-CA3, the endocannabinoid signaling process is disrupted in or by the pyramidal cells of CA3. This situation is not implausible as levels of the 2-AG synthesizing protein (DGL-α) vary between the two terminals of the LPP (Katona *et al.*, 2006). Hence a higher expression of 2-AG at LPP-DG may be responsible for setting in motion the mechanisms needed for presynaptic LTP (i.e., Integrins) while lower levels are unable to do so at LPP-CA3.

The use of two forms of long-term plasticity at two branches of the same input to the hippocampus could play an important role in memory processing. Due to its presynaptic nature LTP induction in the LPP-DG increases release probability and thereby depresses paired-pulse ratio. As described in *Chapter 1*, this translates into a decrease in the frequency facilitation and greater filtering of information across the synapse. This may seem counterintuitive as LTP is typically thought of as a means to increase transmission efficiency. However, within the LPP this may be advantageous as the extension to CA3 is postsynaptic, and thus filtering of information would not be influenced by amplification of the incoming signal. Instead, when potentiation is triggered in both terminals there will be a further prioritization of the flow of subsequent information from one region (DG) to the other (CA3). In this case, the relative strength of the

signal would constitute a type of encoding, minimally denoting that the input has been previously encountered. More importantly, a shift in the balance of strengths would very likely result in a clear difference between the manner in which the input is processed by the two target cell groups for the LPP. In this sense, a learned signal would not only be recognized by the hippocampus but would as well be processed in a significantly different manner than a novel input.

The mechanisms responsible for the specialized nature of LPP-DG synapses – including frequency filtering and presynaptic LTP --- are not well understood. For reasons discussed, the differentiating factors are not likely to be generated by the granule cell dendrites or by the parent axons from entorhinal cortex. An alternative possibility would be that glia cells surrounding the LPP-DG connection interact with the terminals and spines to generate singular forms of filtering and plasticity. *Chapter 3* described a test of this idea with regard to microglia. Mice were systematically depleted of the cells through a PLX-mediated diet and tested for plasticity at four hippocampal connections (LPP-DG, LPP-CA3, MPP-DG, CA3-CA1). In PLX treated mice, we found no differences in baseline transmission or frequency facilitation at any of the sites compared to standard chow controls. LTP in the LPP-DG synapses, but not elsewhere, was severely impaired in the PLX group. As described, this deficit was associated with evident disturbances to the endocannabinoid trigger for potentiation and its CB1R target.

Microglia could potentially regulate plasticity through the release of cytokines (Khairova *et al.*, 2009; del Rey *et al.*, 2013; Bourgognon & Cavanagh, 2020; De Felice *et al.*, 2022). One study demonstrated that mice with a conditional knockout of microglial CB1 receptor expressed a decrease in TNF-α compared to wild types, when exposed to a lipopolysaccharide (Cutando *et al.*, 2013; Scipioni *et al.*, 2022). This specific cytokine, as well as Interleukin 1β (IL-1β) and Interleukin 6 (IL-6), have been implicated in hippocampal dependent acquisition, consolidation, or retrieval of memory (Rachal Pugh *et al.*, 2001; Miller *et al.*, 2013; Bourgognon & Cavanagh, 2020). During inflammatory responses, cytokine levels, produced by microglia, elevate and are

detrimental to the stabilization of LTP. Rather than having a direct effect, cytokines depress LTP by disrupting neurotrophin signaling cascades, such as BDNF in the case of IL-1β (Tong *et al.*, 2012). Interestingly, the suppressive effects are regionally differentiated, with lesser effects found in field CA3 (Tong *et al.*, 2012). In contrast to the well-documented negative effects of cytokines, there is little evidence for enhancement of potentiation by the acute release of such factors.

A particularly surprising aspect of the microglial depletion results was the LPP-DG specific nature of the effects on the endocannabinoid system. Changes in 2-AG levels as seen in the DG were not found in cortex and the increased phosphorylation of CB1R observed for LPP terminals was absent in the *Schaffer-collateral* boutons in CA1. These results strongly suggest that microglial removal had a tonic rather than acute effect on these variables due to an unusual interaction with LPP-DG synapses. This leads us back to the unusual integrin receptors expressed at the junction and a specific hypothesis in which microglial sculpting of an unusual junction produces an equally unusual alignment of post- to pre-synaptic elements for retrograde endocannabinoid signaling. These arrangements allow for a novel form of plasticity. *Chapter 3* results also emphasized the potential importance for microglia- dependent LTP. Elimination of the cells resulted in failed acquisition of the three basic elements (‘what’, ‘where’, and ‘when’) of the episodic memory used to organize the flow of daily experience.

In summary, target specific differences in frequency filtering can be attributed to variations in the presynaptic mechanisms involved in the availability of readily releasable pools of neurotransmitter vesicles. This adds a diversification in signal processing at DG and CA3, where certain frequencies are routed through one region over the other. Meanwhile, as yet incompletely understood, specializations in the LPP-DG synapses produce a very unusual form of LTP that is expressed by an increase in vesicle release. The reasons for these specializations at the head stage of the hippocampal circuit are also obscure but likely relate to the demanding conditions that must be met for the production and use of episodic memories.

Notably, the reliance on endocannabinoids, and as shown by others the opioid encephalin, at LPP-DG is expected to make LTP within this region susceptible to diverse pharmacological influences. In all, the work presented here provides critical information for the development of theories about signal processing across the initial nodes of the hippocampal network.

References

Abbott LF & Regehr WG. (2004). Synaptic computation. *Nature* **431,** 796-803.

Barrionuevo G & Brown TH. (1983). Associative long-term potentiation in hippocampal slices. *Proc Natl Acad Sci U S A* **80,** 7347-7351.

Bourgognon JM & Cavanagh J. (2020). The role of cytokines in modulating learning and memory and brain plasticity. *Brain Neurosci Adv* **4,** 2398212820979802.

Bramham CR, Errington ML & Bliss TV. (1988). Naloxone blocks the induction of long-term potentiation in the lateral but not in the medial perforant pathway in the anesthetized rat. *Brain Res* **449,** 352-356.

Chrobak JJ, Lorincz A & Buzsaki G. (2000). Physiological patterns in the hippocampo-entorhinal cortex system. *Hippocampus* **10,** 457-465.

Colgin LL. (2015). Theta-gamma coupling in the entorhinal-hippocampal system. *Curr Opin Neurobiol* **31,** 45-50.

Colgin LL. (2016). Rhythms of the hippocampal network. *Nat Rev Neurosci* **17,** 239-249.

Cox BM, Cox CD, Gunn BG, Le AA, Inshishian VC, Gall CM & Lynch G. (2019). Acquisition of temporal order requires an intact CA3 commissural/associational (C/A) feedback system in mice. *Commun Biol* **2,** 251.

Cutando L, Busquets-Garcia A, Puighermanal E, Gomis-Gonzalez M, Delgado-Garcia JM, Gruart A, Maldonado R & Ozaita A. (2013). Microglial activation underlies cerebellar deficits produced by repeated cannabis exposure. *J Clin Invest* **123,** 2816-2831.

De Felice E, Goncalves de Andrade E, Golia MT, Gonzalez Ibanez F, Khakpour M, Di Castro MA, Garofalo S, Di Pietro E, Benatti C, Brunello N, Tascedda F, Kaminska B, Limatola C, Ragozzino D, Tremblay ME, Alboni S & Maggi L. (2022). Microglial diversity along the hippocampal longitudinal axis impacts synaptic plasticity in adult male mice under homeostatic conditions. *J Neuroinflammation* **19,** 292.

del Rey A, Balschun D, Wetzel W, Randolf A & Besedovsky HO. (2013). A cytokine network involving brain-borne IL-1beta, IL-1ra, IL-18, IL-6, and TNFalpha operates during long-term potentiation and learning. *Brain Behav Immun* **33,** 15-23.

Do VH, Martinez CO, Martinez JL, Jr. & Derrick BE. (2002). Long-term potentiation in direct perforant path projections to the hippocampal CA3 region in vivo. *J Neurophysiol* **87,** 669-678.

Hamilton TJ, Wheatley BM, Sinclair DB, Bachmann M, Larkum ME & Colmers WF. (2010). Dopamine modulates synaptic plasticity in dendrites of rat and human dentate granule cells. *Proc Natl Acad Sci U S A* **107,** 18185-18190.

Hansen N & Manahan-Vaughan D. (2014). Dopamine D1/D5 receptors mediate informational saliency that promotes persistent hippocampal long-term plasticity. *Cereb Cortex* **24,** 845-858.

Hennig R & Lomo T. (1985). Firing patterns of motor units in normal rats. *Nature* **314,** 164-166.

Jensen O & Colgin LL. (2007). Cross-frequency coupling between neuronal oscillations. *Trends Cogn Sci* **11,** 267-269.

Katona I, Urban GM, Wallace M, Ledent C, Jung KM, Piomelli D, Mackie K & Freund TF. (2006). Molecular composition of the endocannabinoid system at glutamatergic synapses. *J Neurosci* **26,** 5628-5637.

Khairova RA, Machado-Vieira R, Du J & Manji HK. (2009). A potential role for pro-inflammatory cytokines in regulating synaptic plasticity in major depressive disorder. *Int J Neuropsychopharmacol* **12,** 561-578.

Kusuki T, Imahori Y, Ueda S & Inokuchi K. (1997). Dopaminergic modulation of LTP induction in the dentate gyrus of intact brain. *Neuroreport* **8,** 2037-2040.

Larson J & Munkacsy E. (2015). Theta-burst LTP. *Brain Res* **1621,** 38-50.

Lee I & Kesner RP. (2004). Encoding versus retrieval of spatial memory: double dissociation between the dentate gyrus and the perforant path inputs into CA3 in the dorsal hippocampus. *Hippocampus* **14,** 66-76.

Luo L, Chen WH, Wang M, Zhu DM, She JQ & Ruan DY. (2008). Modulation of long-term potentiation by individual subtypes of muscarinic acetylcholine receptor in the rat dentate gyrus. *Hippocampus* **18,** 989-995.

McMahon DB & Barrionuevo G. (2002). Short- and long-term plasticity of the perforant path synapse in hippocampal area CA3. *J Neurophysiol* **88,** 528-533.

Miller AH, Haroon E, Raison CL & Felger JC. (2013). Cytokine targets in the brain: impact on neurotransmitters and neurocircuits. *Depress Anxiety* **30,** 297-306.

Nicoll RA & Schmitz D. (2005). Synaptic plasticity at hippocampal mossy fibre synapses. *Nat Rev Neurosci* **6,** 863-876.

Ogando MB, Pedroncini O, Federman N, Romano SA, Brum LA, Lanuza GM, Refojo D & Marin-Burgin A. (2021). Cholinergic modulation of dentate gyrus processing through dynamic reconfiguration of inhibitory circuits. *Cell Rep* **36,** 109572.

Pinkstaff JK, Detterich J, Lynch G & Gall C. (1999). Integrin subunit gene expression is regionally differentiated in adult brain. *J Neurosci* **19,** 1541-1556.

Rachal Pugh C, Fleshner M, Watkins LR, Maier SF & Rudy JW. (2001). The immune system and memory consolidation: a role for the cytokine IL-1beta. *Neurosci Biobehav Rev* **25,** 29-41.

Reid B, Slater CR & Bewick GS. (1999). Synaptic vesicle dynamics in rat fast and slow motor nerve terminals. *J Neurosci* **19,** 2511-2521.

Sawada S, Yamamoto C & Ohno-Shosaku T. (1994). Long-term potentiation and depression in the dentate gyrus, and effects of nicotine. *Neurosci Res* **20,** 323-329.

Schomburg EW, Fernandez-Ruiz A, Mizuseki K, Berenyi A, Anastassiou CA, Koch C & Buzsaki G. (2014). Theta phase segregation of input-specific gamma patterns in entorhinal-hippocampal networks. *Neuron* **84,** 470-485.

Scipioni L, Ciaramellano F, Carnicelli V, Leuti A, Lizzi AR, De Dominicis N, Oddi S & Maccarrone M. (2022). Microglial Endocannabinoid Signalling in AD. *Cells* **11**.

Swanson-Park JL, Coussens CM, Mason-Parker SE, Raymond CR, Hargreaves EL, Dragunow M, Cohen AS & Abraham WC. (1999). A double dissociation within the hippocampus of dopamine D1/D5 receptor and beta-adrenergic receptor contributions to the persistence of long-term potentiation. *Neuroscience* **92,** 485-497.

Tong L, Prieto GA, Kramar EA, Smith ED, Cribbs DH, Lynch G & Cotman CW. (2012). Brain-derived neurotrophic factor-dependent synaptic plasticity is suppressed by interleukin-1beta via p38 mitogen-activated protein kinase. *J Neurosci* **32,** 17714-17724.

Tort AB, Komorowski RW, Manns JR, Kopell NJ & Eichenbaum H. (2009). Theta-gamma coupling increases during the learning of item-context associations. *Proc Natl Acad Sci U S A* **106,** 20942-20947.

Treves A & Rolls ET. (1992). Computational constraints suggest the need for two distinct input systems to the hippocampal CA3 network. *Hippocampus* **2,** 189-199.

Trieu BH, Kramar EA, Cox CD, Jia Y, Wang W, Gall CM & Lynch G. (2015). Pronounced differences in signal processing and synaptic plasticity between piriform-hippocampal network stages: a prominent role for adenosine. *J Physiol* **593,** 2889-2907.

Tsukamoto M, Yasui T, Yamada MK, Nishiyama N, Matsuki N & Ikegaya Y. (2003). Mossy fibre synaptic NMDA receptors trigger non-Hebbian long-term potentiation at entorhino-CA3 synapses in the rat. *J Physiol* **546,** 665-675.

Wang W, Jia Y, Pham DT, Palmer LC, Jung KM, Cox CD, Rumbaugh G, Piomelli D, Gall CM & Lynch G. (2018). Atypical Endocannabinoid Signaling Initiates a New Form of Memory-Related Plasticity at a Cortical Input to Hippocampus. *Cereb Cortex* **28,** 2253-2266.

Welsby P, Rowan M & Anwyl R. (2006). Nicotinic receptor-mediated enhancement of long-term potentiation involves activation of metabotropic glutamate receptors and ryanodine-sensitive calcium stores in the dentate gyrus. *Eur J Neurosci* **24,** 3109-3118.

Welsby PJ, Rowan MJ & Anwyl R. (2009). Intracellular mechanisms underlying the nicotinic enhancement of LTP in the rat dentate gyrus. *Eur J Neurosci* **29,** 65-75.

Zheng Y, Liu XL, Nishiyama S, Ranganath C & O'Reilly RC. (2022). Correcting the hebbian mistake: Toward a fully error-driven hippocampus. *PLoS Comput Biol* **18,** e1010589.